

NASA CR - 165602  
LYC NO. 82-15



(NASA-CR-165602) SMALL AXIAL TURBINE STATOR  
TECHNOLOGY PROGRAM Final Report (Avco  
Lycoming Div.) 89 p HC A05/MF A01 CSCL 21B

N82-32367

Unclas  
G3/07 27792

## FINAL REPORT

# SMALL AXIAL TURBINE STATOR TECHNOLOGY PROGRAM

by

Walter Brockett and Andrew Kozak



AVCO LYCOMING DIVISION  
550 South Main Street  
Stratford, Connecticut 06497

Prepared for

NATIONAL AERONAUTICS AND SPACE ADMINISTRATION

APRIL 1982

Contract NAS 3-22109

NASA Lewis Research Center  
Cleveland, Ohio 44135

**ORIGINAL PAGE IS  
OF POOR QUALITY**

1. Report No. NASA-CR-165602		2. Government Accession No.		3. Recipient's Catalog No.	
4. Title and Subtitle  SMALL AXIAL TURBINE STATOR TECHNOLOGY PROGRAM.				5. Report Date April 1982	
				6. Performing Organization Code	
7. Author(s) W. BROCKETT A. KOZAK				8. Performing Organization Report No. LYC 82-15	
				10. Work Unit No.	
9. Performing Organization Name and Address AVCO LYCOMING DIVISION 550 SOUTH MAIN STREET STRATFORD, CT 06497				11. Contract or Grant No. NAS-3-22109	
				13. Type of Report and Period Covered Contractor Report	
12. Sponsoring Agency Name and Address National Aeronautics and Space Administration Washington, D. C. 20546 U.S. Army Research and Technology Laboratories (AVRADCOM) Propulsion Laboratory, Cleveland, Ohio 44135				14. Sponsoring Agency Code 505-32-2B IL 162209 AH 76	
15. Supplementary Notes Project Manager, Jeffrey E. Haas, U.S. Army Research and Technology Laboratories (AVRADCOM), Propulsion Laboratory, Lewis Research Center, Cleveland, Ohio.					
16. Abstract  An experimental investigation was conducted to determine the effects of surface finish, fillet radius, inlet boundary layer thickness, and free-stream inlet turbulence level on the aerodynamic performance of a small axial flow turbine stator. The principal objective of this program was to help understand why large turbine efficiency is not maintained when a large turbine is scaled to a smaller size. The stator used in this program was a one-sixth scale of a 762 mm (30 in.) diameter stator design with 50 vanes having a vane height of 17 mm (0.666 in.) and an aspect ratio of 1.77. A comprehensive overall test matrix was used to provide a complete engineering understanding of the effects of each variable over the full range of all the other variables. The range of each variable investigated was as follows: surface finish 0.1 $\mu$ m (4 $\mu$ in.) to 2.4 $\mu$ m (95 $\mu$ in.); boundary layer thickness 2 to 25 percent of channel height at each wall; fillet radius 0 mm (0 in.) to 1.0 mm (.040 in.) and turbulence 2 to 12 percent.					
17. Key Words (Suggested by Author(s))  TURBINE STATOR SCALING SURFACE FINISH, FILLET RADIUS TURBULENCE BOUNDARY LAYER			18. Distribution Statement  Unclassified STAR Category 07		
19. Security Classif. (of this report) UNCLASSIFIED		20. Security Classif. (of this page) UNCLASSIFIED		21. No. of Pages	
				22. Price*	

\* For sale by the National Technical Information Service, Springfield, Virginia 22161

# FOREWORD

The investigation described herein was conducted by the Avco Lycoming Division, Stratford, Connecticut. Program management was directed by the Lewis Research Center of the National Aeronautics and Space Administration under Contract NAS3 - 22109.

The Avco Lycoming Program Manager was Mr. Walter Brockett. Mr. Andrew Kozak was the principal investigator. The authors wish to acknowledge guidance and support from Mr. Jeffrey Haas, NASA Project Manager.

PRECEDING PAGE BLANK NOT FILMED

## TABLE OF CONTENTS

	<u>Page</u>
FOREWORD .....	iii
LIST OF ILLUSTRATIONS .....	vii
LIST OF TABLES .....	ix
1.0 SUMMARY .....	1
2.0 INTRODUCTION .....	2
3.0 TEST APPARATUS PROCEDURE .....	3
3.1 TEST RIG .....	3
3.2 TEST VARIABLES .....	15
3.2.1 Boundary Layer .....	15
3.2.2 Free-Stream Turbulence .....	15
3.2.3 Surface Finish .....	15
3.2.4 Fillet Radius .....	15
3.3 INSTRUMENTATION .....	20
3.4 DATA ACQUISITION .....	24
3.5 TEST PROCEDURE .....	25
4.0 DATA REDUCTION .....	27
5.0 RESULTS AND DISCUSSIONS .....	30
5.1 TABULATED TEST DATA .....	30
5.2 DIRECT EFFECTS .....	30
5.2.1 Pressure Ratio .....	45
5.2.2 Fillet Radius .....	45
5.2.3 Free-Stream Turbulence .....	47
5.2.4 Boundary Layer .....	47

PRECEDING PAGE BLANK NOT FILMED

## TABLE OF CONTENTS

	<u>Page</u>
5.2.5 Surface Finish .....	48
5.3 INTERACTION EFFECTS .....	49
5.4 COMPARISON WITH FULL SCALE RESULTS .....	71
5.5 STATISTICAL ANALYSIS .....	74
6.0 CONCLUSIONS .....	77
7.0 RECOMMENDATIONS .....	79
8.0 REFERENCES .....	80
APPENDIX - List of Symbols .....	81
DISTRIBUTION LIST.....	82

## LIST OF ILLUSTRATIONS

<u>Figure</u>		<u>Page</u>
1	Stator Test Rig Cross Section Schematic .....	4
2	Test Facility Schematic .....	5
3	Forward Module .....	6
4	Rear View, Forward Module with 25 Percent Boundary Layer Rings Installed .....	7
5	Exploded View, Forward and Aft Module Components .....	8
6	Stator Assembly .....	9
7	Stator with Vane Clamping Ring and Labyrinth Seal .....	10
8	Labyrinth Seal, Stator Assembly .....	12
9	Labyrinth Seal Detail .....	13
10	Exhaust Casing Assembly with Seal Buffer Air and Bypass Air Holes .....	14
11	Two Inlet Duct Configurations - Turbulence Generator, and Boundary Layer Ring Locations .....	15
12	Turbulence Generators .....	17
13	Stator Details Showing Surface Finish and Fillet Radius .....	18
14	Stator Assembly with Fillet Radius Applied .....	19
15	Test Rig Instrumentation Locations .....	21
16	Hot-Film and Boundary Layer Pressure Probes .....	23
17	Boundary Layer Pressure Profiles (1.7 Pressure Ratio) .....	26
18	Average Stator Efficiency Versus Pressure Ratio .....	43
19	Efficiency Versus Each Variable at Constant Pressure Ratio ..	44
20	Efficiency Versus Pressure Ratio Showing Effects of Each Variable .....	46
21	Example of Variable Interactions .....	50

# LIST OF ILLUSTRATIONS

<u>Figure</u>		<u>Page</u>
22	Efficiency Versus Fillet Radius at 1.2 Pressure Ratio .....	51
23	Efficiency Versus Fillet Radius at 1.4 Pressure Ratio .....	52
24	Efficiency Versus Fillet Radius at 1.7 Pressure Ratio .....	53
25	Efficiency Versus Fillet Radius at 2.1 Pressure Ratio .....	54
26	Efficiency Versus Turbulence at 1.2 Pressure Ratio .....	55
27	Efficiency Versus Turbulence at 1.4 Pressure Ratio .....	56
28	Efficiency Versus Turbulence at 1.7 Pressure Ratio .....	57
29	Efficiency Versus Turbulence at 2.1 Pressure Ratio .....	58
30	Efficiency Versus Boundary Layer at 1.2 Pressure Ratio .....	59
31	Efficiency Versus Boundary Layer at 1.4 Pressure Ratio .....	60
32	Efficiency Versus Boundary Layer at 1.7 Pressure Ratio .....	61
33	Efficiency Versus Boundary Layer at 2.1 Pressure Ratio .....	62
34	Efficiency Versus Surface Finish at 1.2 Pressure Ratio .....	63
35	Efficiency Versus Surface Finish at 1.4 Pressure Ratio .....	64
36	Efficiency Versus Surface Finish at 1.7 Pressure Ratio .....	65
37	Efficiency Versus Surface Finish at 2.1 Pressure Ratio .....	66
38	Plot of Turbulence and Fillet Radius Interaction .....	67
39	Plot of Fillet Radius and Surface Finish Interaction .....	69
40	Plot of Turbulence and Surface Finish Interaction .....	70
41	Kinetic Energy Loss Coefficient Versus Critical Velocity Ratio for Full-Scale and One-Sixth Scale Test .....	72
42	Equivalent Weight Flow Versus Pressure Ratio for Full- Scale and Scaled Stators .....	73

# LIST OF TABLES

<u>Table</u>		<u>Page</u>
I	Vane Coordinates, One-Sixth Scale .....	11
II	Test Rig Instrumentation Summary .....	22
III	Influence Coefficients .....	29
IV	Test Results 0.1 $\mu$ m Surface Finish 0.0 mm Fillet Radius ....	31
V	Test Results 0.1 $\mu$ m Surface Finish 0.5 mm Fillet Radius ....	32
VI	Test Results 0.1 $\mu$ m Surface Finish 1.0 mm Fillet Radius ....	33
VII	Test Results 0.6 $\mu$ m Surface Finish 0.0 mm Fillet Radius ....	34
VIII	Test Results 0.6 $\mu$ m Surface Finish 1.0 mm Fillet Radius ....	35
IX	Test Results 2.4 $\mu$ m Surface Finish 0.0 mm Fillet Radius ....	36
X	Test Results 2.4 $\mu$ m Surface Finish 0.5 mm Fillet Radius ....	37
XI	Test Results 2.4 $\mu$ m Surface Finish 1.0 mm Fillet Radius ....	38
XII	Test Matrix 1.2 Pressure Ratio .....	39
XIII	Test Matrix 1.4 Pressure Ratio .....	40
XIV	Test Matrix 1.7 Pressure Ratio .....	41
XV	Test Matrix 2.1 Pressure Ratio .....	42
XVI	Statistical Results .....	75



## 1.0 SUMMARY

An experimental investigation was conducted to determine the effects of surface finish, fillet radius, inlet boundary layer thickness and free-stream inlet turbulence level on the aerodynamic performance of a small axial flow turbine stator. The principal objective of this program was to help understand why large turbine efficiency is not maintained when a large turbine is scaled to a small size. The stator used in this program was a one-sixth scale of a 762 mm (30-inch) diameter stator design with 50 vanes having a vane height of 17 mm (0.666 inch) and an aspect ratio of 1.77.

The results of the investigation can be summarized as follows: Large levels of turbulence induced up to 2 percent drops in efficiencies. An optimum fillet radius was found to exist that increased the stator efficiency level by 1.4 percent. A very small inlet boundary layer showed a 1.5 percent increase in efficiency over the larger boundary layers. Rougher surface finish showed up to a 0.5 percent increase in efficiency over the smooth finish. A significant first order interaction was found to exist between turbulence and fillet radius.

A comparison was made between the full scale and one-sixth scale stator performance. Good agreement in stator efficiency was obtained when a Reynolds Number correction was made to the full-scale stator data. The mass flow for the scaled stator matched the scaled flow of the full-scale stator.

## 2.0 INTRODUCTION

The efficiency levels demonstrated in large turbines have not been achieved generally in smaller scale since, in practice, surface finish, fillet radius, turbulence, and boundary layer thickness - in addition to Reynolds number, manufacturing tolerances, and other parameters - may not be practically scaled. This experimental program was conducted to establish the performance effects of the first four variables on a one-sixth scale of a previously tested turbine nozzle design. The results are designed to quantify the effects of each parameter and establish each parameter's sensitivity to scaling. This is intended to provide the turbine designer with the performance compromises expected for a small-scale design. The potential benefits from this program are to design more efficient small turbine components and permit development testing to be performed on small-scale hardware by establishing scaling effects.

The program was designed to systematically evaluate the effects of vane surface finish, fillet radius, inlet turbulence level, and inlet boundary layer thickness on small turbine stator performance. A one-sixth scale of a 762 mm (30-inch) tip diameter high-pressure turbine stator (Reference 1) was used for the investigation with levels of each variable independently varied over the full range of interest based on current gas turbine manufacturing technology and measured experience. The test matrix was designed to generate data for engineering analysis and also to perform a statistical regression analysis where the entire body of collected data is used to quantify the effects of each variable.

The range of each variable was selected as follows:

	Minimum	Maximum
Surface Finish	0.1 $\mu$ m (4 $\mu$ in.)	2.4 $\mu$ m (95 $\mu$ in.)
Fillet Radius	0	1.0 mm (.040 in.) (nearly overlapping at throat)
Turbulence	2 percent	12 percent
Boundary layer thickness (at each wall)	2 percent	25 percent of channel height

In addition, for each variable, the pressure ratio was varied to produce Mach numbers from 0.5 to 1.0 at the throat. Data were taken at more than 300 test conditions by directly measuring the reaction torque of the nozzle with a strain-gauged torque element and limited fixed instrumentation to establish the gross cascade performance.

### 3.0 TEST APPARATUS AND PROCEDURE

#### 3.1 TEST RIG

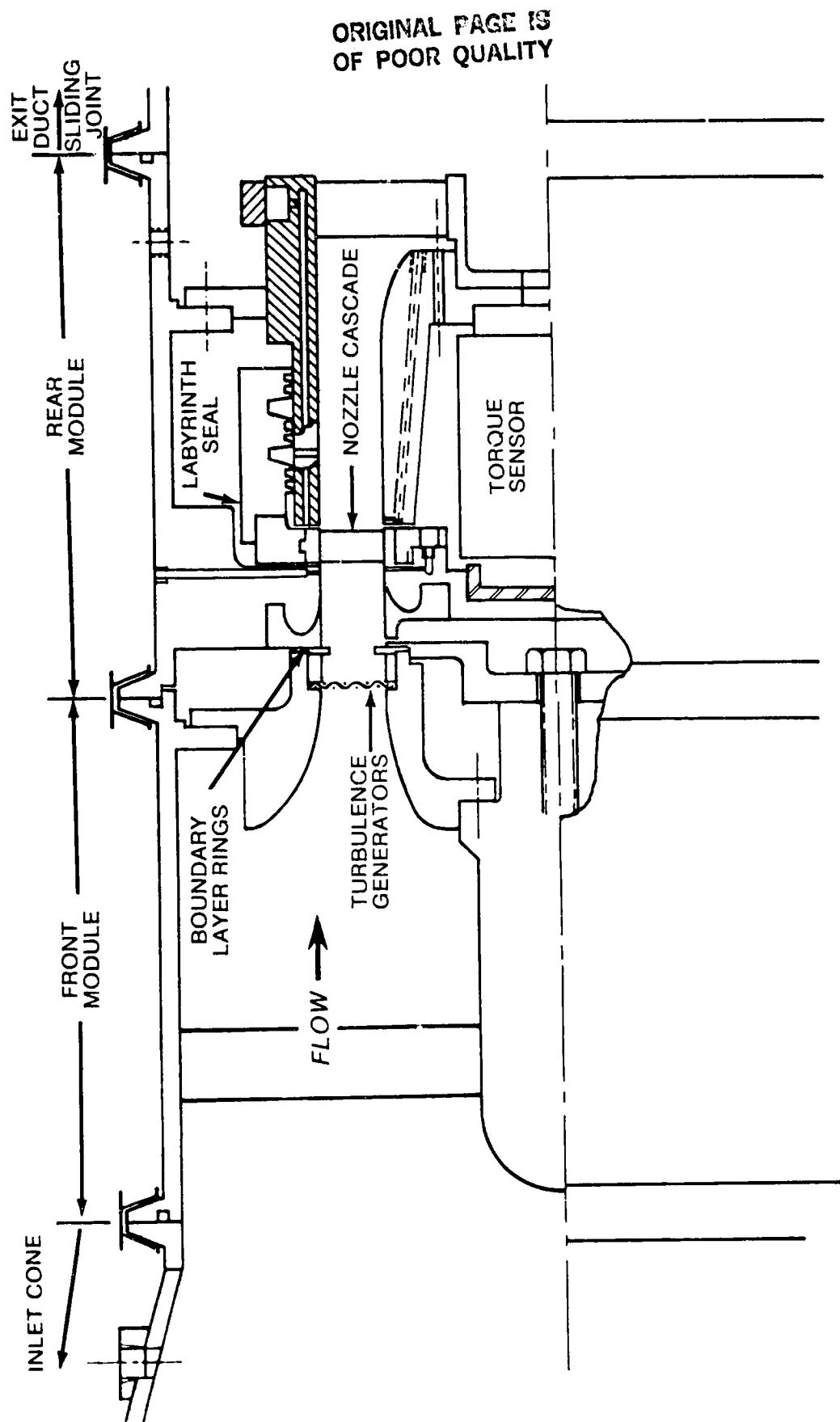
The cascade test rig (Figure 1) was designed and fabricated as part of the program for use in an existing testway (Figure 2). The test rig comprised four major sections: an inlet cone, an exit duct with a sliding joint, and two core modules. The forward or lower core module contains the front portion of the inlet duct where the turbulence generators and boundary layer rings are located. The aft module contains the nozzle cascade mounted on a torque sensor and the exhaust duct. The inlet cone mounts directly on a test facility inlet plenum chamber and the exit duct is connected to facility piping.

The forward module (Figure 3) is easily removable to accommodate a large number of boundary layer and turbulence combinations. Removal of two flange clamps allows the forward module to be withdrawn from the remainder of the test rig. No instrumentation is disturbed when the forward module is removed. Rubber "O-ring" seals prevent leakage at the flanges. The inner flow path is supported from the outer case through four welded struts located in a low-velocity inlet section to minimize wakes. Final machining of the welded assembly assured inner and outer flow path concentricity. Removal of a single bolt allows the inner boundary layer ring (Figure 4) to be removed. The outer boundary layer ring is trapped by the aft module. The boundary layer rings are also brazed onto spacer rings.

The aft core module contains the turbine cascade mounted directly on the reaction torque sensor (Figure 5). The vanes, fit into contoured slots machined in both the inner and outer shrouds shown in Figure 6. The vanes butt against a ring in the inner shroud. A two-piece ring contoured to the shape of the outer shroud and vane tips, restrains the vanes radially. (See Figure 7.) The same set of vanes was used throughout all of the testing except for a repeat test of the baseline  $0.1 \mu\text{m}$  ( $4 \mu\text{in.}$ ) surface finish test. Stator blade coordinates are given in Table I. The manufacturing tolerance permitted on surface coordinates was  $\pm .05 \text{ mm}$  (.002 inch) from the true surface providing the contour was smooth and did not deviate with respect to the true contour more than  $0.1 \text{ mm}$  (.004 inch) per  $2.5 \text{ mm}$  (0.10 inch) of surface length. The total throat area of the stator was within  $\pm 2$  percent of the scaled value, and the variation in individual throat areas did not exceed  $\pm 2$  percent. The allowed variation in stagger angle was  $\pm 0^\circ 30'$ .

The labyrinth seal is supported by the outer shroud ring (Figure 8). Buffer air is used to eliminate leakage past the forward face of the outer shroud, while bypass air holes reduce the leakage past the rear face of the outer shroud to about 0.4 percent of the inlet flow (Figures 9 and 10). High lateral stiffness of the torque sensor insures no contact between the electrically isolated cascade components and stationary rig parts. An electronic contact monitor between the cascade and stationary hardware verifies the seal clearance. The cascade mounted on the torque sensor permits direct measurement of the torque less any tare loadings. Only the inner wall static pressure teflon lines and the electrical lead wire could produce any tare loadings on the torque sensor. The torque sensor was calibrated in the rig with all the instrumentation lines attached. No significant difference with previous calibrations was found. All remaining instrumentation was mounted on stationary part

ORIGINAL PAGE IS  
OF POOR QUALITY



BF1125

Figure 1. Stator Test Rig Cross Section Schematic

ORIGINAL PAGE IS  
OF POOR QUALITY

BF1128

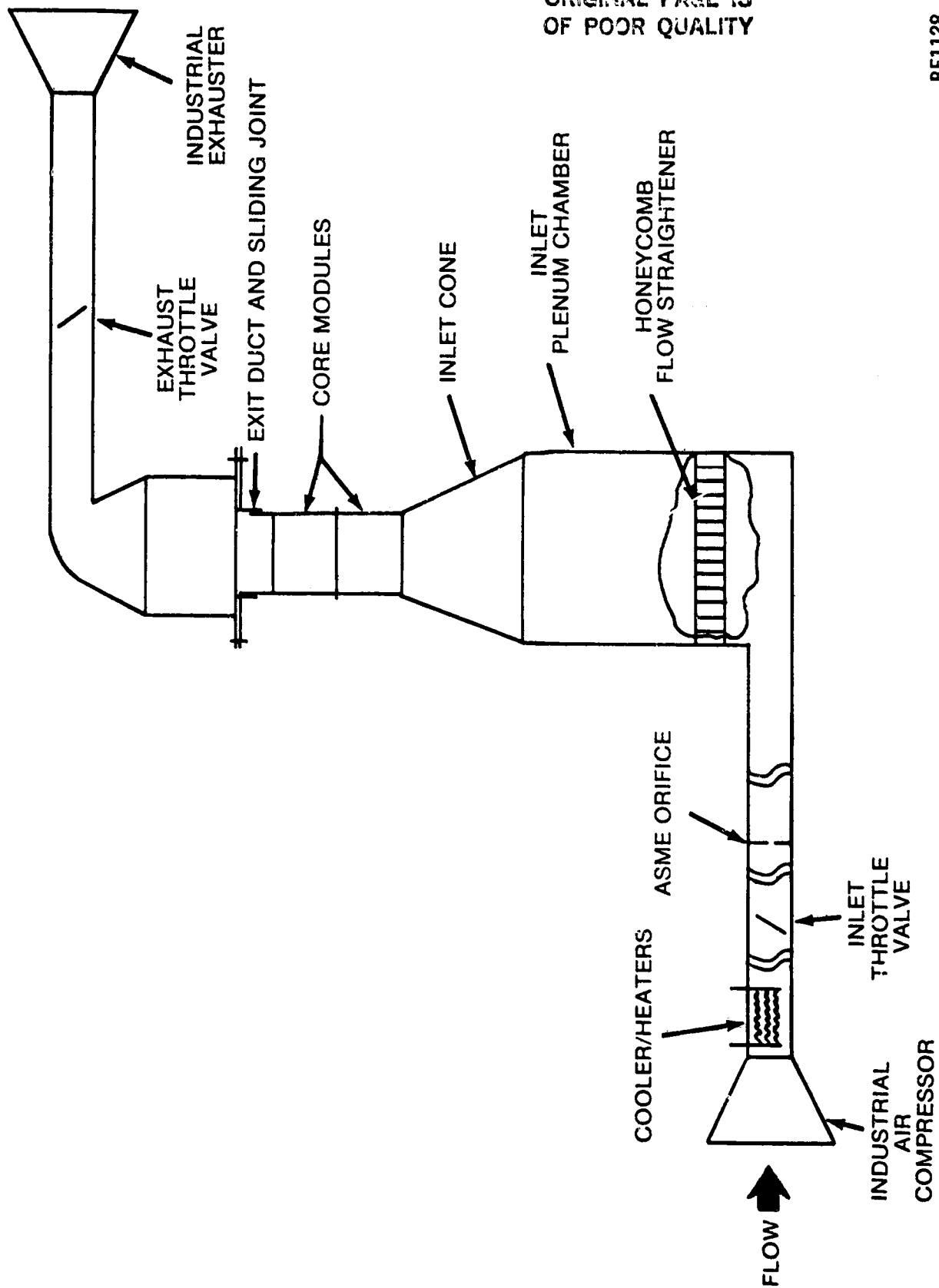
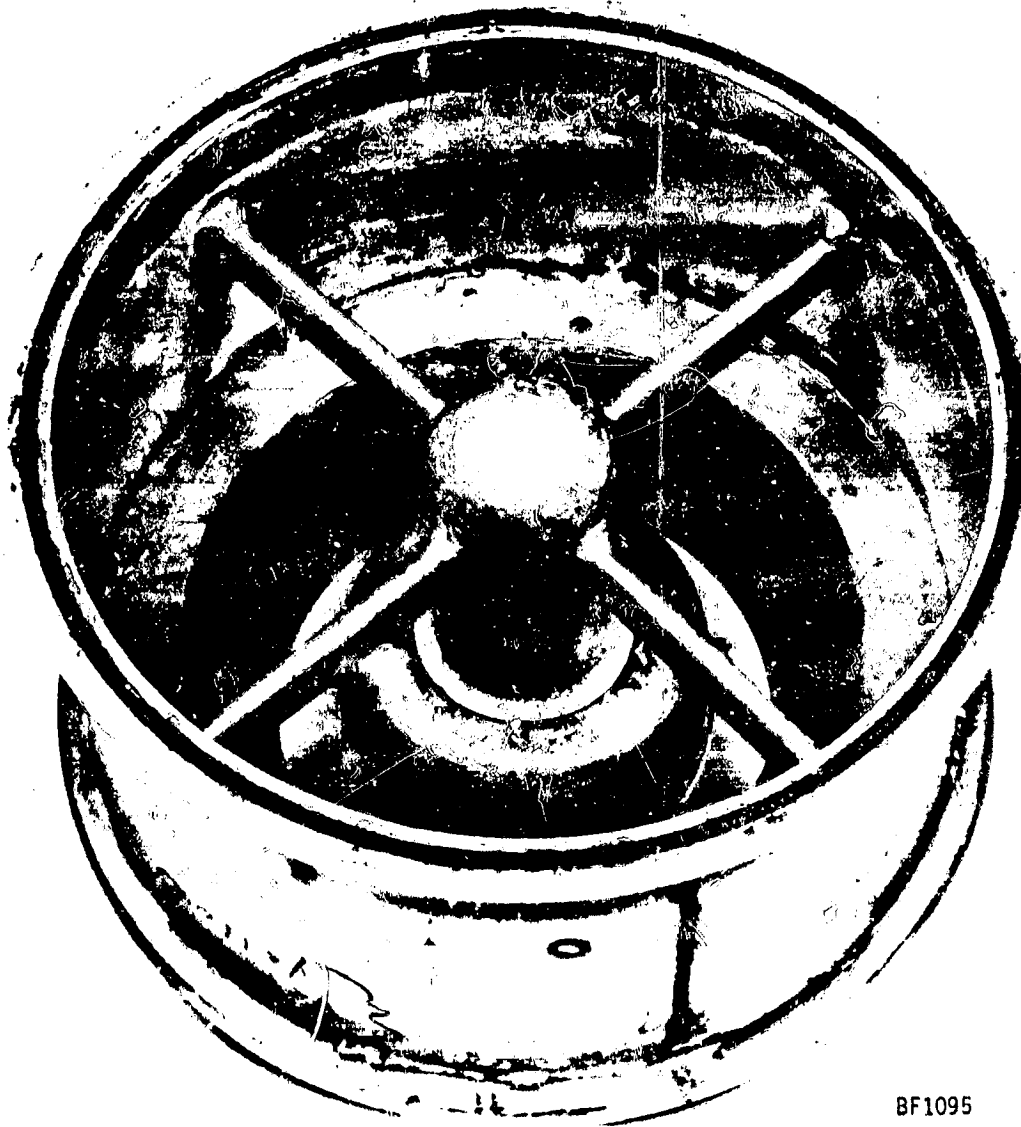


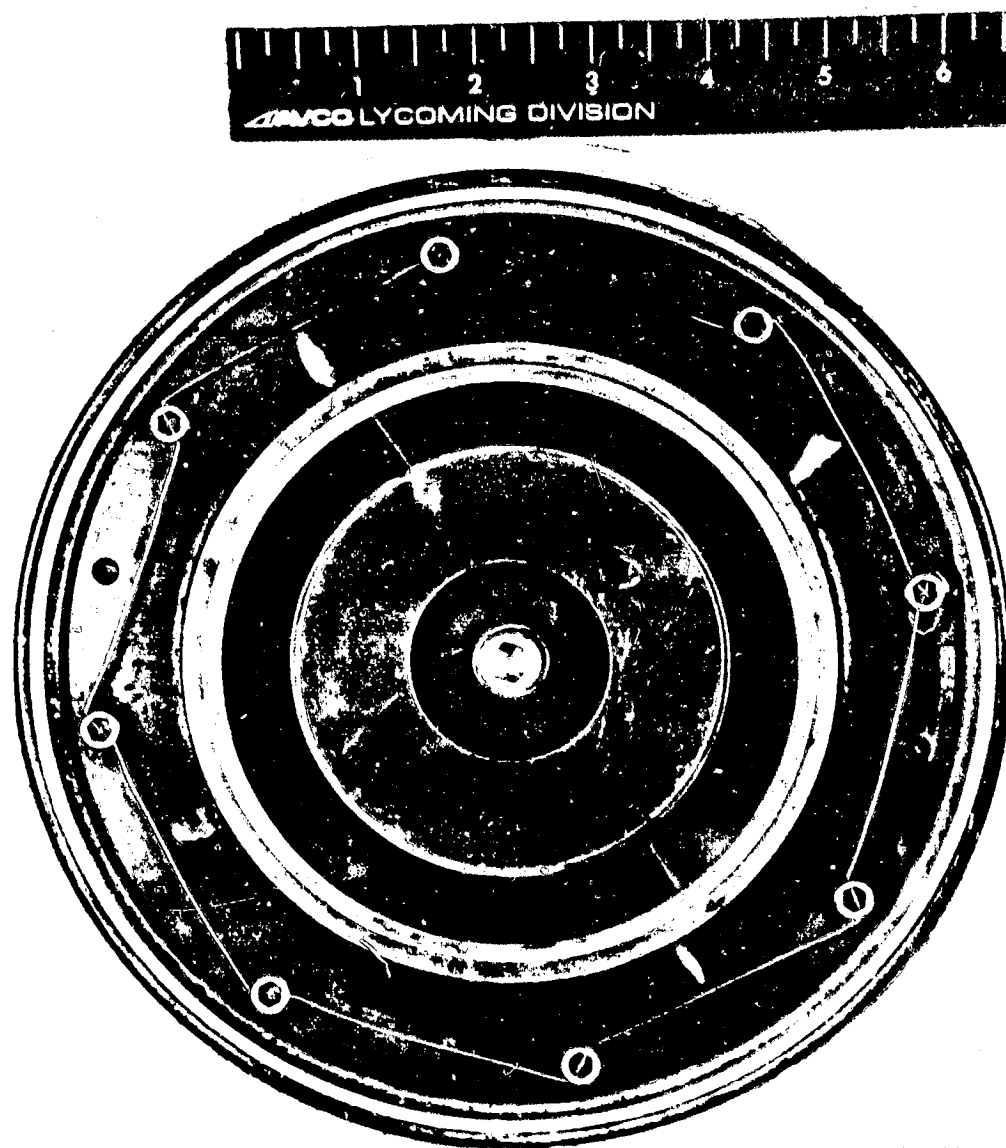
Figure 2. Test Facility Schematic

ORIGINAL PAGE IS  
OF POOR QUALITY



BF1095

Figure 3. Forward Module

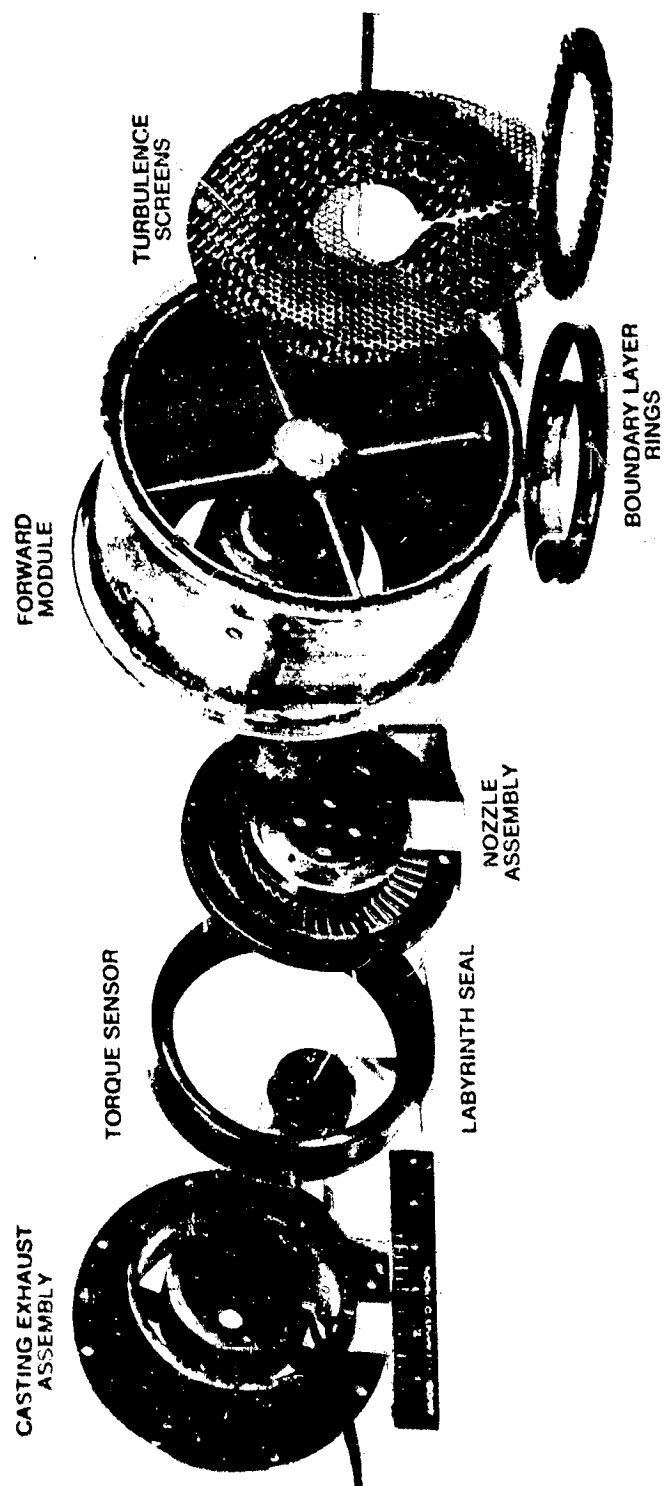


BF1096

Figure 4. Rear View, Forward Module with 25 Percent Boundary Layer Rings  
Installed

ORIGINAL PAGE IS  
OF POOR QUALITY

ORIGINAL PAGE  
BLACK AND WHITE PHOTOGRAPH



BF1099

Figure 5. Exploded View, Forward and Aft Module Components



ORIGINAL PAGE  
BLACK AND WHITE PHOTOGRAPH



BF1094

Figure 6. Stator Assembly

ORIGINAL PAGE  
BLACK AND WHITE PHOTOGRAPH

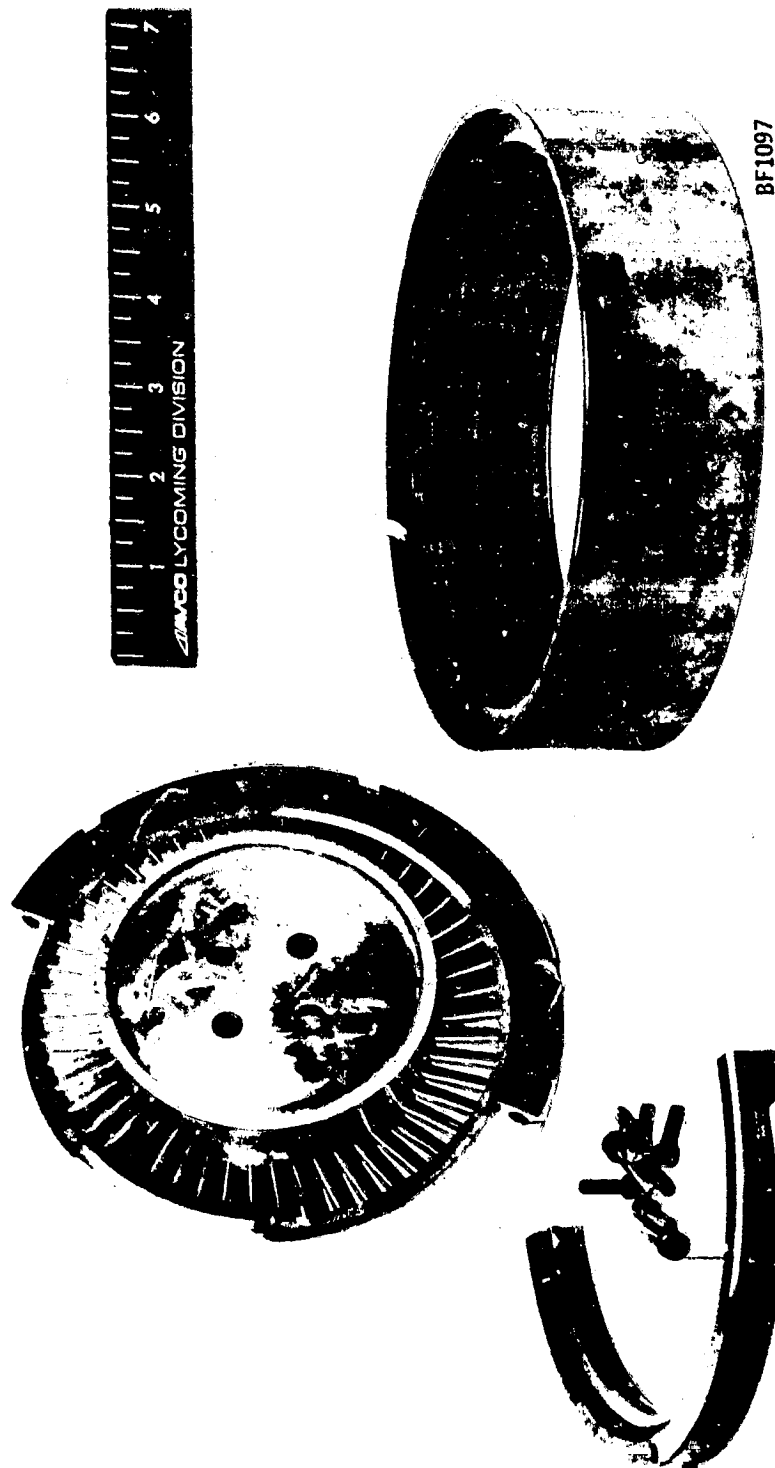
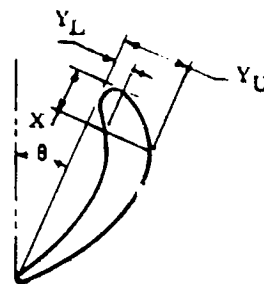


Figure 7. Stator with Vane Clamping Ring and Labyrinth Seal

U.S. GOVERNMENT PRINTING OFFICE  
1964 O - 350-000

TABLE I. VANE COORDINATES, ONE-SIXTH SCALE



BLADE COORDINATES - FULL SIZE (MM)						
X	HUB		MEAN		TIP	
	42° 26'		41° 2'		39° 40'	
	Y <sub>L</sub>	Y <sub>U</sub>	Y <sub>L</sub>	Y <sub>U</sub>	Y <sub>L</sub>	Y <sub>U</sub>
.0000	.6350	.6350	.6350	.6350	.6350	.6350
.2117	-----	1.2404	-----	1.2827	-----	1.4112
.4233	-----	1.5875	-----	1.6673	-----	1.8076
.6350	-----	1.8500	-----	1.9588	-----	2.0997
.8467	-----	2.0574	-----	2.1759	-----	2.3283
1.0583	.1439	2.2267	.1482	2.3495	.1482	2.4934
1.2700	.2540	2.3622	.2582	2.4392	.2667	2.6289
1.4817	.3514	2.4680	.3598	2.6035	.3683	2.7347
1.6933	.4445	2.5527	.4487	2.6924	.4699	2.8152
1.9050	.5292	2.6204	.5376	2.7644	.5545	2.8744
2.1167	.6054	2.6670	.6138	2.8152	.6265	2.9125
2.3283	.6731	2.6966	.6773	2.8448	.6943	2.9422
2.5400	.7366	2.7220	.7366	2.8617	.7578	2.9664
2.7517	.7874	2.7463	.7874	2.8660	.8128	2.9422
2.9633	.8340	2.7620	.8297	2.8575	.8594	2.9210
3.1750	.8763	2.7693	.8636	2.8363	.8932	2.8914
3.3867	.9059	2.6882	.8890	2.8067	.9186	2.8575
3.5983	.9398	2.6543	.9102	2.7728	.9440	2.8067
3.8100	.9667	2.6162	.9271	2.7263	.9610	2.7559
4.0217	.9894	2.5696	.9398	2.6755	.9737	2.6966
4.2333	.9937	2.5188	.9440	2.6204	.9779	2.6458
4.4450	.9937	2.4680	-----	-----	-----	-----
4.6567	.9652	2.4130	.9386	2.4977	.9694	2.5273
4.8683	.9440	2.2902	.9102	2.3707	.9440	2.3918
5.0800	.8974	2.1505	.8618	2.2310	.9059	2.2648
5.2917	.8297	2.0023	.8086	2.0828	.8467	2.1167
5.5033	.7408	1.8330	.7408	1.9135	.7747	1.9558
5.7150	.6477	1.6572	.6467	1.7357	.6900	1.7865
5.9267	.5419	1.4605	.5433	1.5452	.5927	1.6087
6.1383	.4360	1.2488	.4699	1.3504	.4963	1.4182
6.3500	.3315	1.0245	.3641	1.1503	.4022	1.2150
6.5617	.2394	.8074	.2540	.9059	.2963	1.0033
6.7733	.1577	.6122	.1697	.6946	.1995	.8037
6.9850	.1482	.4857	.0217	.4604	.0889	.5803
7.1967	-----	-----	.1482	.1482	-----	-----
7.4083	-----	-----	-----	-----	.1482	.1482

ORIGINAL PAGE  
BLACK AND WHITE PHOTOGRAPH

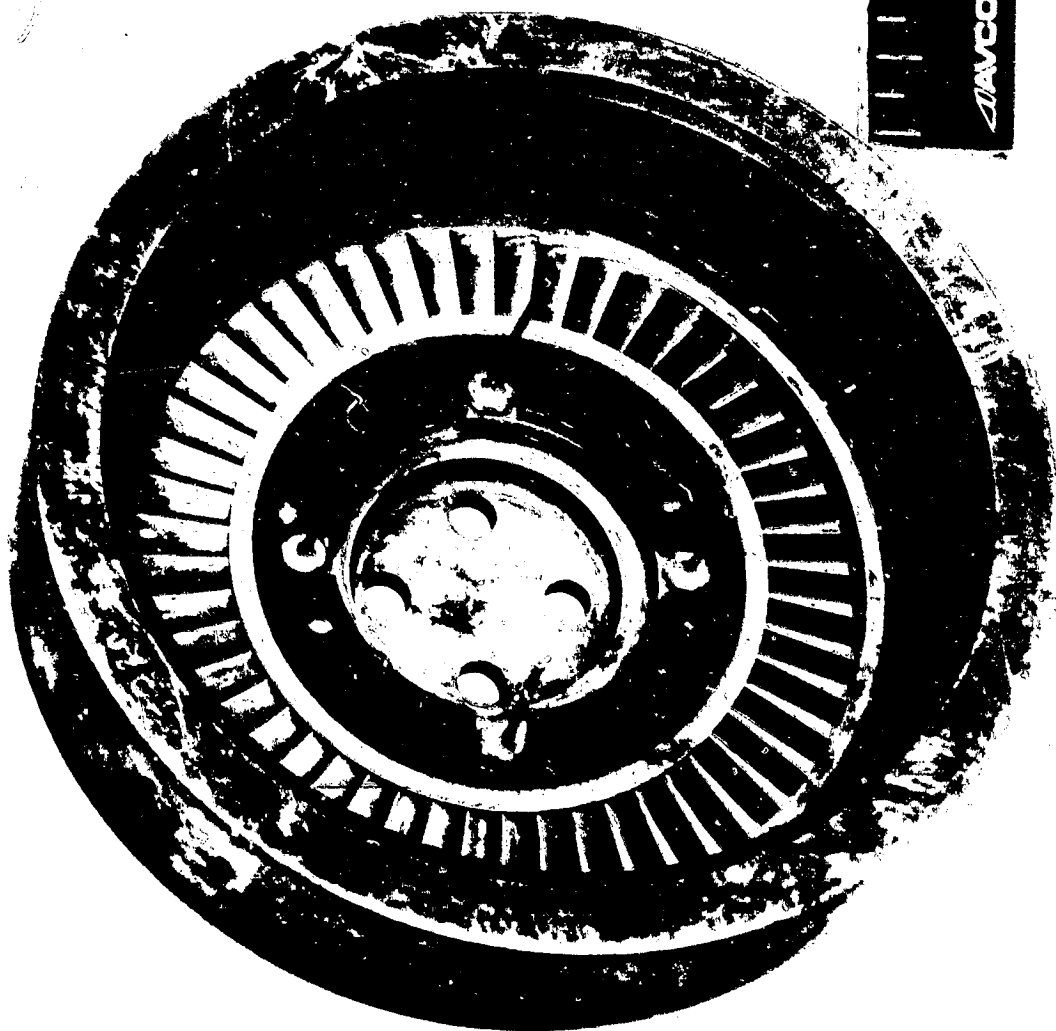


Figure 8. Labyrinth Seal, Stator Assembly

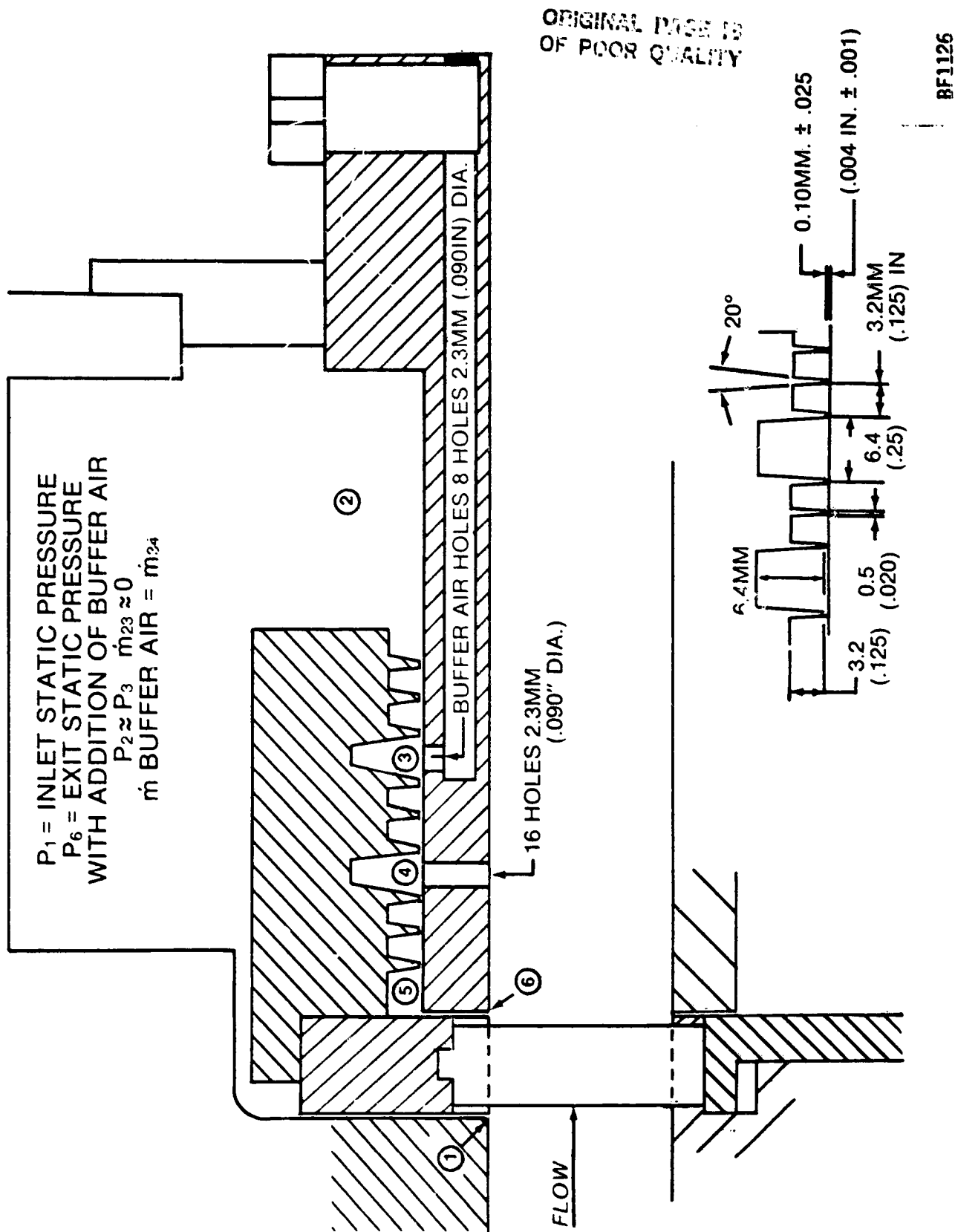


Figure 9. Labyrinth Seal Detail

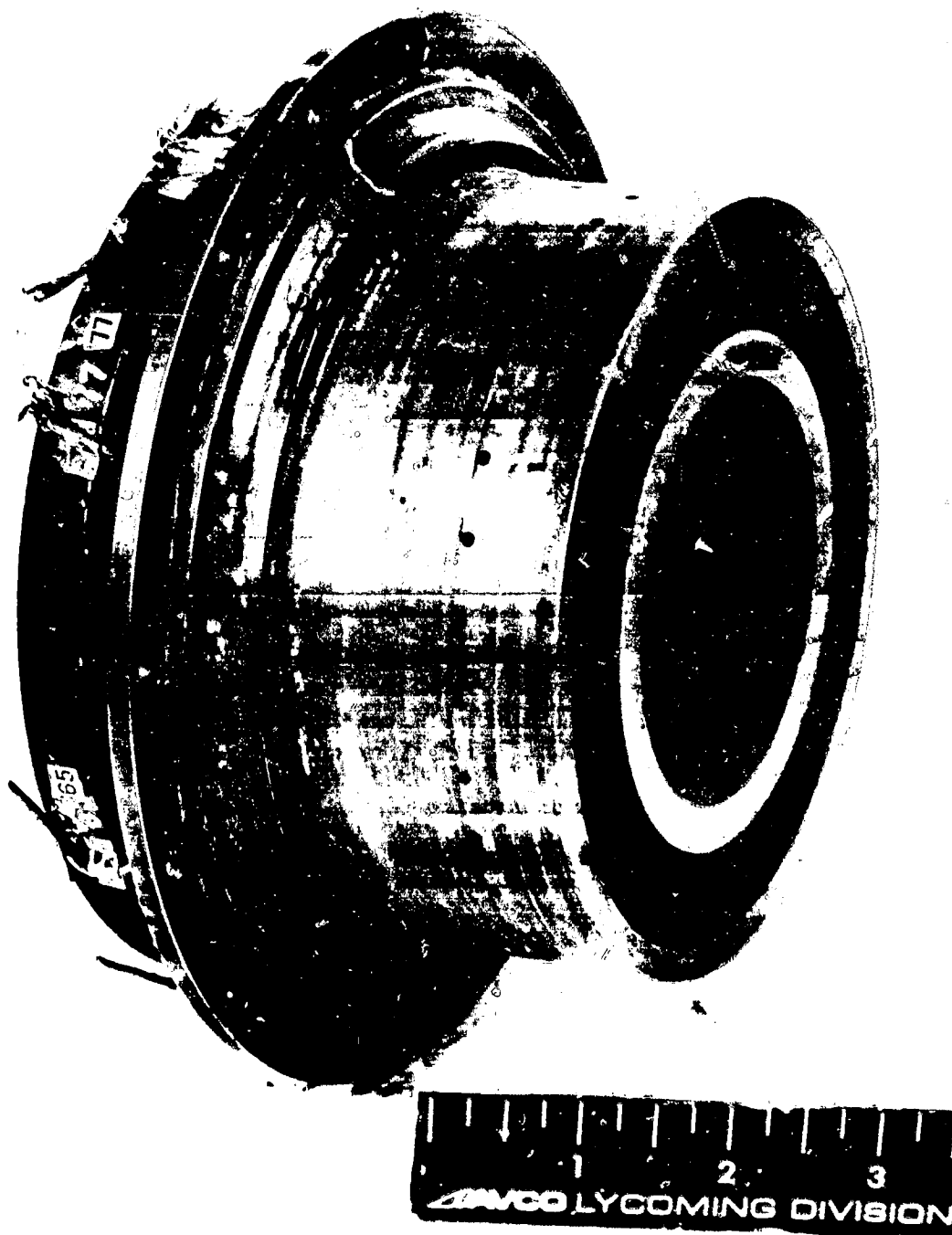


Figure 10. Exhaust Casing Assembly with Seal Buffer Air and Bypass Air Holes

ORIGINAL PAGE  
BLACK AND WHITE PHOTOGRAPH

The exit duct mounts directly onto existing test facility exhaust piping. It contains a slider joint sealed with O-rings. The joint allows the aft module to be moved for removal of the forward module.

### 3.2 TEST VARIABLES

#### 3.2.1 Boundary Layer

Two basic inlet duct configurations (Figure 11) were used. The short inlet duct produced a boundary layer thickness of 2 percent on each wall while the longer duct resulted in a 10 percent thickness, as measured with radial hot-film anemometer surveys. To achieve the 15 and 25 percent thicknesses, sheet metal rings were installed in the inlet duct. The ring size was experimentally determined during the calibration phase of the program and used throughout the testing.

The boundary layer thickness percentages quoted represent the full boundary layer thickness for each end-wall expressed as a percentage of the annulus height. The 2 percent boundary layer configuration was tested only at the minimum turbulence level due to the short inlet duct configuration.

#### 3.2.2 Free-Stream Turbulence

The base level of turbulence resulting from the test facility was found to be 2 percent for core flow in the inlet duct. Several turbulence-generating devices were evaluated resulting in selection of perforated and raised sheet metal plates (Figure 12). These plates were positioned in the inlet duct as shown in Figure 11. Combustor discharge turbulence levels of 15 to 18 percent are typically produced in engines; however, generation of high turbulence resulted in excessive local velocity distortion that was judged unacceptable. Therefore, a maximum turbulence of 12 percent was used.

#### 3.2.3 Surface Finish

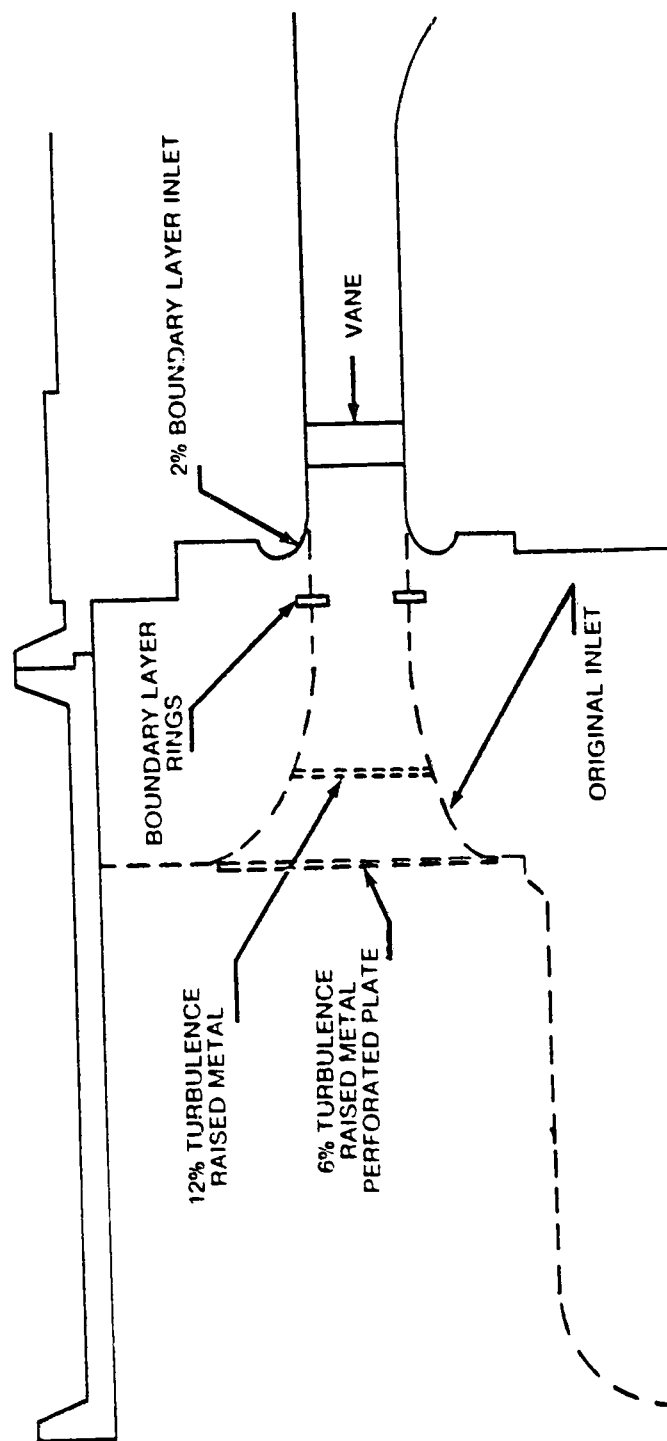
The vanes initially manufactured to a  $0.1 \mu\text{m}$  ( $4 \mu\text{inch}$ ) finish represent a polished surface finish. The test sequence was performed such that the surface finish was progressively roughened. This was accomplished by grit blasting both the vane and shroud surfaces of the cascade (Figure 13). Surface inspections were performed to establish the actual surface finish. The surface of the inlet duct was unaltered to maintain entry flow conditions.

The test matrix was completed with the same set of vanes. One configuration with a  $0.1 \mu\text{m}$  ( $4 \mu\text{inch}$ ) surface finish was tested with a second set of vanes, following testing of the initial matrix, to resolve an observed performance anomaly.

#### 3.2.4 Fillet Radius

The cascade was designed such that the vane extended through closely tolerated airfoil-shaped slots that were electro-discharge machined (EDM) in both the inner and outer shrouds. This produced a square corner (zero fillet radius) that was tested. An epoxy filler material (Figures 13 and 14) added by means of a hypodermic syringe, flowed to form a radiused corner. The size and shape of the fillets were measured using an optical comparator.

ORIGINAL PAGE IS  
OF POOR QUALITY



BF1127

Figure 11. Two Inlet Duct Configurations - Turbulence Generator, and Boundary Layer Ring Locations



ORIGINAL PAGE  
BLACK AND WHITE PHOTOGRAPH

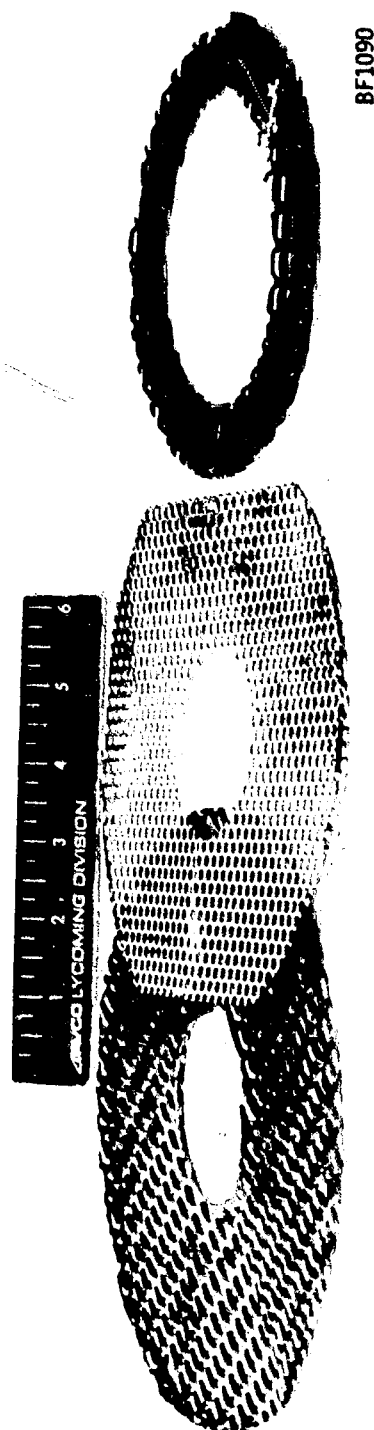


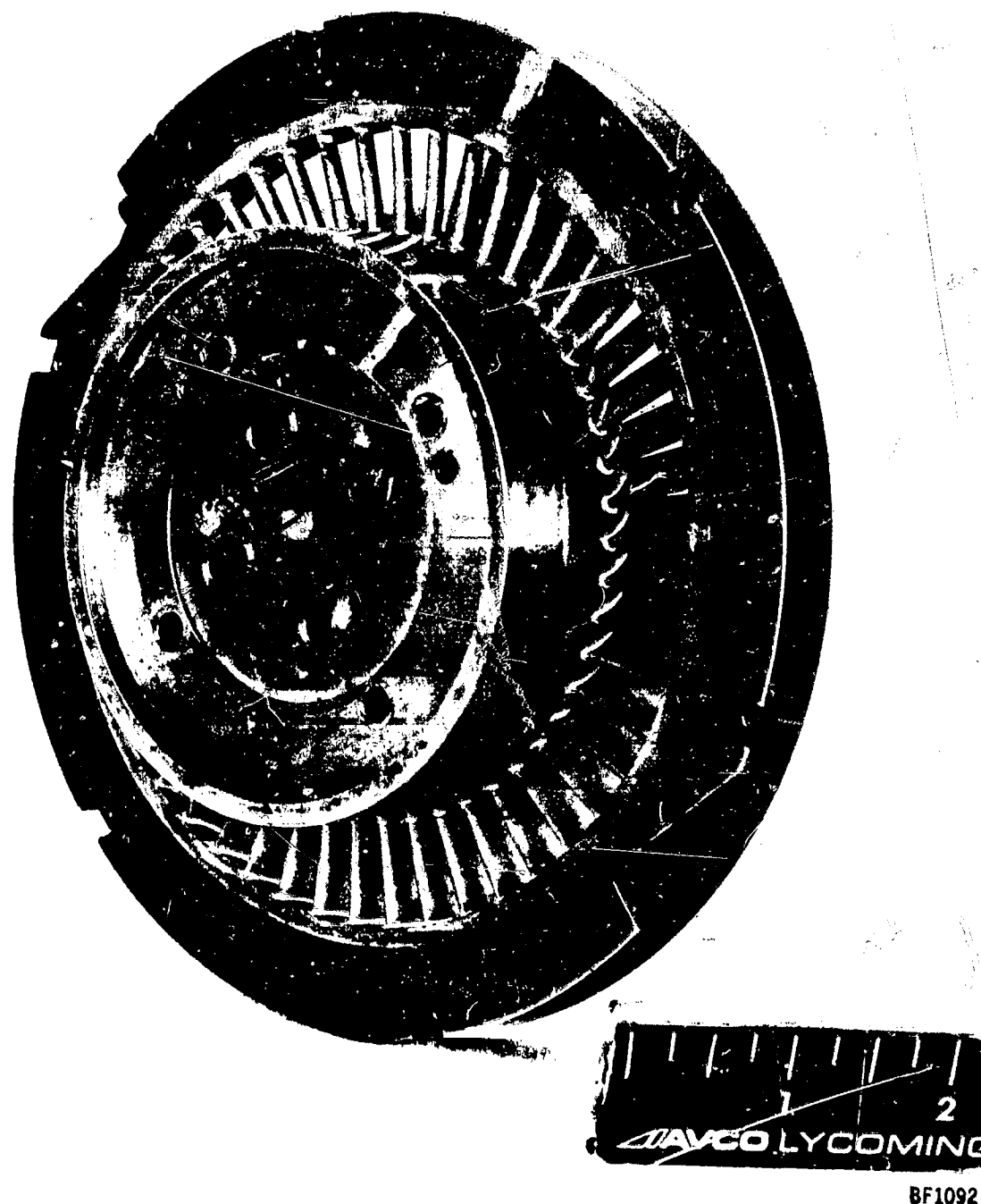
Figure 12. Turbulence Generators

ORIGINAL PAGE  
BLACK AND WHITE PHOTOGRAPH



Figure 13. Stator Details Showing Surface Finish and Fillet Radius

ORIGINAL C. 17000  
BLACK AND WHITE PHOTOGRAPH



BF1092

Figure 14. Stator Assembly with Fillet Radius Applied

### 3.3 INSTRUMENTATION

Instrumentation quantities and locations are shown in Figure 15 and outlined in Table II. These locations and quantities were specified in the program Statement of Work. Inlet total pressure was measured with six individual impact probes mounted on the outer wall and radially located at 10, 25, 50, 75, and 90 percent of the channel height. In addition, a total pressure probe was traversed across the channel for each data point to establish pressure distribution and the average total pressure. Six total temperature probes are located just ahead of the front module at three radial locations.

The total pressure probes used were 1.0 mm (.040 inch) diameter hypodermic tubing for minimum flow blockage. The probes were commercial boundary layer probes which have a flattened sensing head to minimize radial extent of the sensor, Figure 16. The same probe style was used for both stationary probes and for total pressure surveys. The hub wall was locally recessed to permit the probe head to travel below the nominal wall contour to define the distribution close to the wall without risk of probe damage. The recovery characteristics for these probes have been previously determined and were applied to correct measured values. The minimum recovery ratio used was 0.9998. A calibrated hot-film probe (Figure 16) was radially traversed across the flow channel to measure both the mean velocity and the velocity fluctuations as a function of channel height. The mean velocity distribution was used to establish the boundary layer thickness, and the RMS velocity was used to establish the turbulence level.

Inlet and exit static pressures were measured with four static pressures at each location and at each wall. On each wall, the four static pressures were equally spaced relative to the vane pitch. Additionally, the static pressure in the large chamber about the labyrinth seal cascade assembly was measured. Static pressures were measured in the chamber about the torque sensor, in the buffer air chamber, bypass air chamber, and in the chamber immediately behind the outer shroud. Four exit statics were measured in line axially on the inner wall of the duct directly behind the nozzle. A single static pressure was measured in the large exit duct downstream of the slider joint. This was only used to set the rig exit pressure.

Primary mass flow was measured with an ASME sharp edge orifice in the inlet piping system. The reaction torque level was measured using a commercial reaction torque sensor (Lebow Model 2102). The sensor was calibrated out of the rig at temperatures from 18°C to 104°C (65°F to 220°F). In the rig the sensor was calibrated at 18°C (65°F). A differential pressure gauge, along with an external air supply was used to equalize the pressure between the large chamber about the labyrinth seal and the buffer air chamber. An ohmmeter was used to verify clearance between the labyrinth seal cascade assembly and stationary rig components.

ORIGINAL PAGE IS  
OF POOR QUALITY

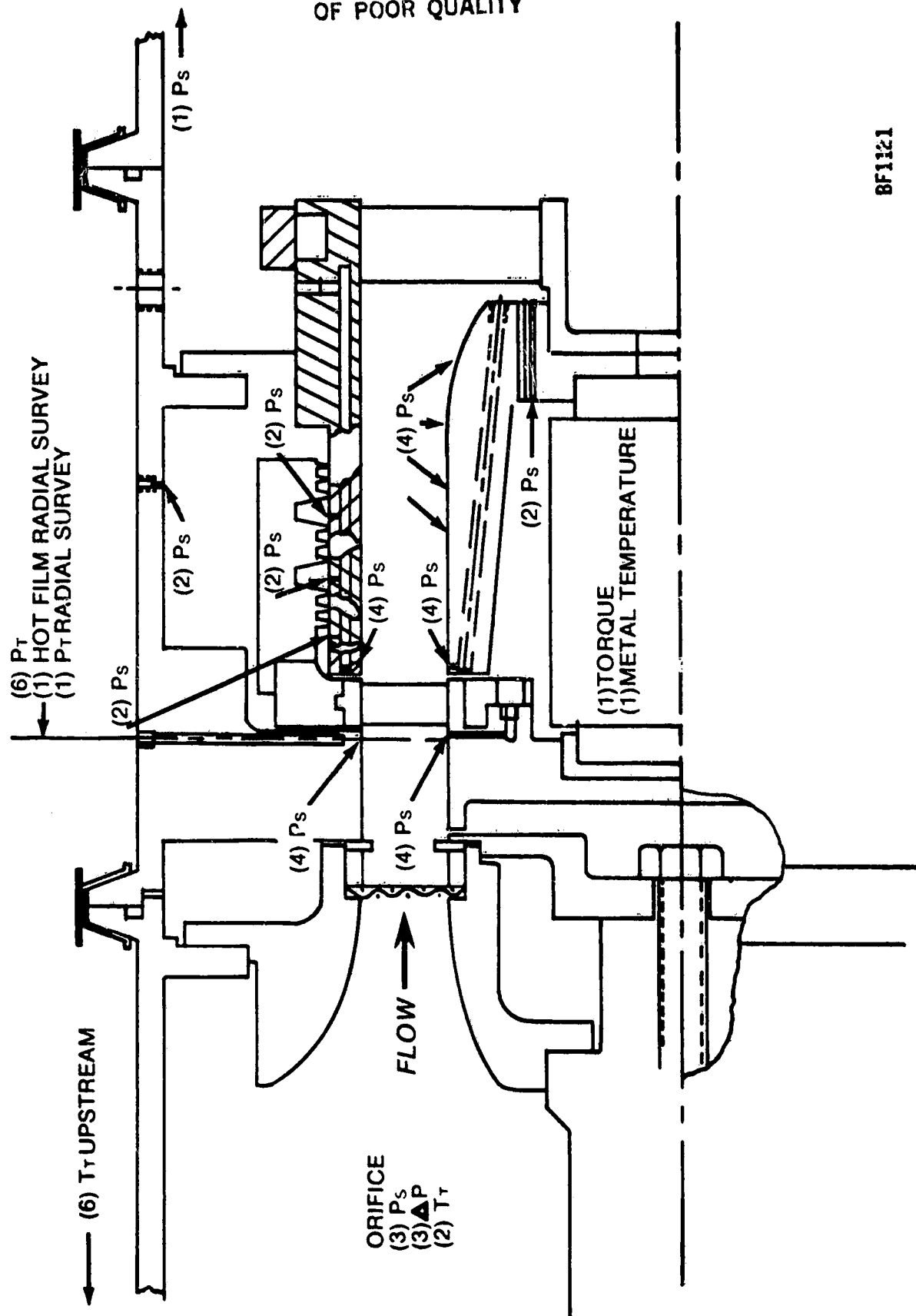


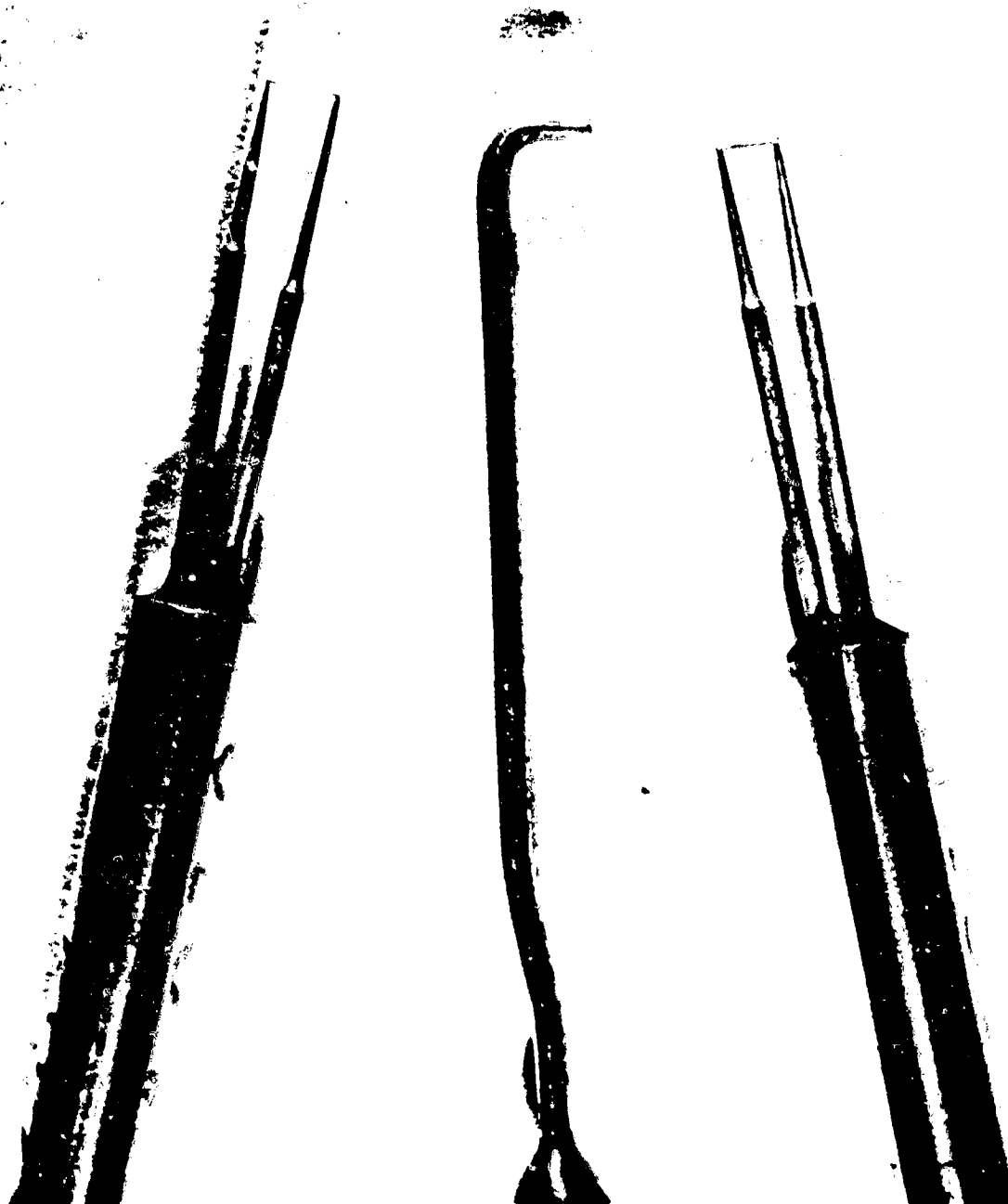
Figure 15. Test Rig Instrumentation Locations

BF1121

TABLE II. TEST RIG INSTRUMENTATION SUMMARY

	<u>Location</u>	<u>Type</u>	<u>Quantity</u>
Orifice		P <sub>S</sub>	3
		T <sub>T</sub>	2
		ΔP	3
Inlet Plenum	2 Each at 3 Radii 6 Circumferential Positions	T <sub>T</sub>	6
Before Nozzle	Outer Wall	P <sub>S</sub>	4
	Inner Wall	P <sub>S</sub>	4
	5 Radial Locations (2 at 50 Percent Point)	P <sub>T</sub>	6
	6 Circumferential Positions		
	Radial Survey	Hot Film	1
	Radial Survey	P <sub>T</sub>	1
	Outer Shroud Cavity	P <sub>S</sub>	2
Behind Nozzle	Outer Wall	P <sub>S</sub>	4
	Inner Wall	P <sub>S</sub>	4
	Inner Shroud Cavity	P <sub>S</sub>	2
Cascade	Torque Reaction Sensor	Torque	1
	Torque Sensor Temperature	T <sub>T</sub>	1
Labyrinth Seal	Buffer Air Chamber	P <sub>S</sub>	2
	Bypass Air Chamber	P <sub>S</sub>	2
	Outer Shroud Chamber	P <sub>S</sub>	2
Duct	Inner Wall, Axially Spaced	P <sub>S</sub>	4
Exit Duct	Downstream, Outer Wall	P <sub>S</sub>	1

ORIGINAL PAGE  
BLACK AND WHITE PHOTOGRAPH



BF1093

Figure 16. Hot-Film and Boundary Layer Pressure Probes

### 3.4 DATA ACQUISITION

Data were acquired using a computer controlled digital data system designed to scan, digitally convert, and record measured test data through the use of multiple port pressure scanning for absolute pressure, dedicated transducers for differential pressures, and thermocouple ice-point referencing. All analog data were converted to electrical signals for multiplexing and digital conversion. Digital data were recorded on a magnetic disc for subsequent computer analysis. A four-point calibration was performed on each absolute pressure transducer for each data point taken by reading accurately maintained reference pressures. Differential pressure transducers were separately calibrated before each test and at intervals of four hours maximum to correct for transducer drift of zero and span. A time-averaged value of the measured torque was digitally recorded.

Thermocouple voltages were converted to engineering units on the basis of parabolic interpolation of tables appropriate to Chromel-Alumel. The tables, which are smooth and of extended significance, are based on National Bureau of Standards Circular 561 (RP767 and RP1080). Absolute pressure readings were converted to engineering units by means of parabolic interpolation of the four reference pressures recorded for each data scan. Total pressure readings were adjusted based on the pressure recovery characteristics. The differential pressures were converted by interpolating between two calibration pressures measured for each transducer. Torque output was converted using an accurately established multipoint calibration curve for the torque reaction sensor with a correction for the operating temperature of the sensor.

Hot-film probes were radially traversed to establish the velocity distribution (boundary layer thickness measurement) and the turbulence level. A total pressure boundary-layer probe was simultaneously traversed to confirm the boundary-layer thickness measurement. The hot-film probe was velocity-calibrated in the test rig by using free-stream conditions as determined by corresponding pressure measurements in the rig. The velocity distribution was established by plotting the linearized anemometer analog output and applying the probe calibration. The root mean square of the linearized anemometer output was also plotted versus radius to establish the local turbulence level.

During performance testing, a total pressure probe was traversed across the channel. Total pressure sampled at 24 radial locations was used to calculate an average inlet total pressure.

On-line performance computations were made as the data were taken to provide a performance assessment and data check as the test progressed; this insured that the recorded data readings were correct and that the cascade performance results appeared reasonable prior to an overall performance assessment.



### 3.5 TEST PROCEDURE

The overall test sequence changed the surface finish twice by progressively roughening the vane surface. Either two or three fillet radius levels were run for each surface finish. Changing the surface finish or fillet radius required removal of the cascade from the test rig. An instrumentation leak check and rig flow check were made after each cascade removal to assure valid test results.

Turbulence generators and boundary layer rings were sized and calibrated in the rig prior to performance testing. Turbulence level and boundary layer thickness were measured at design flow using a hot-film probe traverse across the channel. The actual inlet pressure distribution measured just upstream of the cascade is shown in Figure 17 for the four boundary layer configurations tested. The radial distribution of the root mean square velocity and the velocity level were used to calculate the turbulence level. Measurements were made with the cascade installed to insure that the static pressure field produced by the cascade did not significantly affect the results.

The test facility was equipped with a positive-sealing exhaust valve that was closed after each rig disassembly. The test rig was pressurized to insure that all pressure lines read properly and to establish that no airflow leaks were present between the orifice and the test section. This effort assured accurate pressure and airflow measurements. All tests were conducted in Avco Lycoming test facilities. Air was supplied to the rig at 93°C (200°F) and 1.36 bars (20 psia) by facility compressors and preheaters. Exit pressure was set using exhausters and vacuum pumps. Each test configuration was run at four levels of pressure ratio ranging from 1.2 to 2.1. At each pressure ratio, a steady-state pressure and temperature condition was achieved. A performance data point was recorded at each pressure ratio before and after each radial survey. The results from the surveys were used to calculate entropy-averaged stator inlet total pressure.

ORIGINAL PAGE IS  
OF POOR QUALITY

BF1117

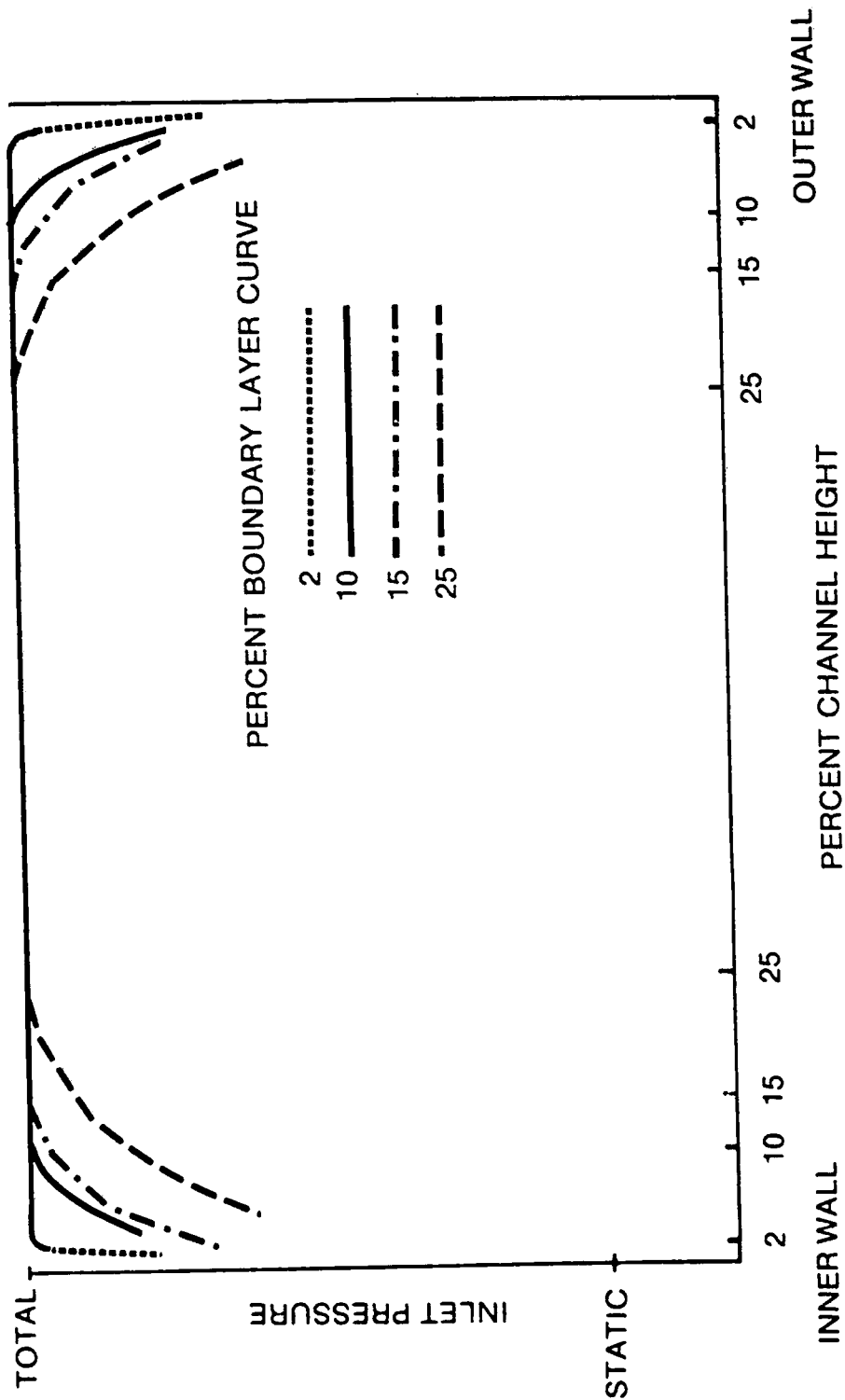


Figure 17. Boundary Layer Pressure Profiles (1.7 Pressure Ratio)

#### 4.0 DATA REDUCTION

Avco Lycoming data reduction program T181 was developed to reduce the NASA Small Axial Turbine Stator Technology Program data.

The digital data acquired were initially reduced during testing to provide an immediate assessment of the data's validity and overall cascade performance. Raw data were retained for further analysis following testing, and overall cascade results were analyzed to establish the effects produced by each test variable.

The conditions leaving the cascade were computed as follows: tangential velocity was obtained directly from

$$\tau = \dot{m} V_u r$$

where torque and flow rate are measured. The radius of reaction used was calculated based on full scale results (Reference 1).

Average velocity and flow angle are computed by simultaneously solving the continuity and moment of momentum (torque) equations. Thus,

Continuity

$$\dot{m} = \rho A V \cos \alpha$$

Moment of Momentum (Torque)

$$\tau = \dot{m} V \sin \alpha r$$

Average stator exit total pressure was obtained from isentropic relations, where  $P_T = f(P_S, V, T_T)$ . Stator total pressure loss is then directly calculated, thus

$$\%P_T \text{ Loss} = \frac{P_{T \text{ in}} - P_{T \text{ exit}}}{P_{T \text{ in}}} (100)$$

The ideal stator exit velocity is calculated from the isentropic relations, where  $V_{id} = f(P_{T \text{ in}}, P_{S \text{ exit}}, T_T)$ . The stator efficiency is then calculated from

$$\eta = \left[ \frac{V}{V_{id}} \right]^2$$

The average stator inlet total pressure was calculated by satisfying continuity using the measured wall inlet static pressures and measured orifice weight flow. This method was used since local total pressure gradients produced by turbulence generation precluded accurate determination of the average total pressure with a survey at a single circumferential position. The mean conditions for temperature were determined from measured total temperatures obtained from the six inlet thermocouples. All total temperatures and pressures were adjusted for probe recovery characteristics.

Blockage factors at the stator inlet plane were calculated using the average total pressure survey results to find a blockage factor for each of the four boundary layer conditions. The averages were taken at the 2 percent turbulence condition where no circumferential pressure gradients existed.

A more detailed analysis of Reference 2 data was made to examine errors produced with the simplified analysis described above. The effects of the stator exit angle radial variation of six degrees were analyzed to determine the effective radius of torque reaction. The actual torque produced by any stator may be expressed as

$$\tau = 2\pi \int_{r_1}^{r_2} \rho V_u V_x r^2 dr$$

An approximate solution of this expression indicated the effective radius to be extremely close to the geometric center of the annulus. This calculated effective radius, used in all data reduction, was 0.4 percent smaller than the center of area.

The overall test matrix was carefully selected to fully define the performance effects of each variable. The matrix approach results in a much higher degree of confidence in the trends observed, since multiple test results are averaged; this tends to eliminate random testing scatter that might otherwise be interpreted as a real effect. The above approach identifies the presence and relative importance of all main effects and interactions.

The influence coefficients shown in Table III indicate the effect on efficiency of a 1 percent error in either a constant or a measured parameter. The constant inputs into the data reduction program are inlet area, exit area, and reaction torque radius. The measured parameters are inlet and exit static pressures, temperature, mass flow, and torque. The analysis was done at nominal parameter conditions.

TABLE III. INFLUENCE COEFFICIENTS

	% ERROR	$\Delta \eta$
INLET AREA	-1%	-0.2
EXIT AREA	-1%	+0.4
P <sub>S</sub> INLET	+1%	+0.4
P <sub>S</sub> EXIT	+1%	+1.1
TORQUE	+1%	+1.4
MASS FLOW	+1%	-1.1
REACTION TORQUE RADIUS	+1%	-1.4

## 5.0 RESULTS AND DISCUSSIONS

The results presented below include:

Tabulated data results for all points

Tabulated data interpolated to stator pressure ratios of 1.2, 1.4, 1.7 and 2.1

Plots of stator efficiency versus pressure ratio, turbulence, fillet radius, surface finish, and boundary layer thickness

Corrected mass flow as a function of pressure ratio.

The direct effects of each test variable over the range tested are discussed and compared with published data. Interaction (nonadditive) effects of combinations of variables are also discussed.

A comparison of data obtained for the one-sixth scale testing performed under this program is compared with the full-scale test results obtained with conventional survey instrumentation. Reynold's number effects discussed are based on published empirical data.

A statistical analysis of the test results is described along with the conclusions for the 1.4 pressure ratio data.

### 5.1 TABULATED TEST DATA

The test results for all data points presented in Tables IV through XI represent the output of the data reduction method previously described.

Computed stator efficiencies were interpolated to pressure ratios of 1.2, 1.4, 1.7, and 2.1 (Tables XII through XV, respectively). These data were used to produce the performance plots and for statistical analysis discussed below.

### 5.2 DIRECT EFFECTS

The test matrix selected for this program lends itself to establishing the direct effects of each test variable with a high degree of confidence. These results were derived from multiple testing of each variable at many levels of the other variables. Consequently, averaged results of these effects that are established mask errors resulting from random testing error and interaction effects (addressed separately).

The direct effect of pressure ratio on stator efficiency is shown in Figure 18, where each point on the curve represents an average of about eighty points. The direct effects of turbulence, fillet radius, boundary layer thickness, and surface finish are indicated in Figure 19 where each point typically represents an average of thirty points. Ninety-five percent of the averaged data points will reside within the band in Figure 19.

ORIGINAL PAGE IS  
OF POOR QUALITY

TABLE IV. TEST RESULTS 0.1  $\mu$  m SURFACE FINISH 0.0 mm FILLET RADIUS

IDENT#	PRESS. RATIO	EQUIV. FLOW KG/SEC	EQUIV. TORQUE N-M	V <sub>U</sub> EXIT M SEC	V EXIT M SEC	PT EXIT P PA	% PT LOSS	% STATOR EFFICIENCY
121613	1.194	0.400	0.853	165.4	100.3	135.57	1.81	89.34
121614	1.398	0.483	1.421	228.5	248.4	134.05	2.71	91.35
121615	1.726	0.524	1.958	290.3	315.4	132.97	3.41	93.07
121616	2.033	0.530	2.298	335.4	364.5	133.18	3.32	94.05
121609	1.196	0.398	0.841	164.1	179.1	135.28	2.20	87.15
121610	1.407	0.483	1.424	229.1	249.2	134.23	3.11	90.25
121611	1.743	0.521	1.959	292.1	317.2	132.71	3.77	92.40
121612	2.102	0.529	2.283	335.7	365.1	132.68	3.28	94.04
121604	2.116	0.528	2.282	335.8	365.4	132.52	4.25	93.52
121605	1.196	0.395	0.837	164.3	179.1	135.94	2.25	86.94
121606	1.407	0.482	1.419	228.9	248.9	134.01	3.21	89.94
121607	1.745	0.521	1.955	291.7	316.9	133.36	3.95	92.13
121608	2.113	0.527	2.281	336.7	366.1	132.93	3.98	93.92
121601	1.204	0.400	0.859	166.4	181.4	135.74	2.40	88.53
121602	1.411	0.483	1.420	227.9	248.3	133.65	3.54	88.97
121603	1.732	0.520	1.938	289.4	314.4	132.38	4.00	91.92
121604	2.117	0.528	2.281	335.8	365.4	132.54	4.31	93.44
121509	1.194	0.396	0.842	164.8	179.6	135.40	2.02	88.16
121510	1.406	0.483	1.429	229.6	249.7	134.10	2.96	90.71
121511	1.735	0.521	1.952	291.3	316.3	132.81	3.67	92.62
121512	2.107	0.528	2.294	337.9	367.1	133.11	3.42	94.75
121505	1.196	0.395	0.841	165.2	179.8	135.59	2.07	88.81
121506	1.406	0.481	1.409	227.5	247.6	133.56	3.42	89.24
121507	1.738	0.521	1.937	288.5	313.9	131.86	4.41	91.14
121508	2.069	0.527	2.263	333.6	362.3	133.28	3.55	94.44
121501	1.192	0.392	0.829	164.1	178.5	135.23	1.94	88.49
121502	1.405	0.480	1.418	229.1	248.9	133.72	3.01	90.51
121503	1.745	0.522	1.957	291.3	316.6	132.32	3.99	92.05
121504	2.114	0.526	2.298	337.9	367.1	132.76	3.59	94.52
121513	1.199	0.394	0.810	159.4	174.5	134.39	2.52	84.91
121514	1.399	0.454	1.340	223.3	243.9	132.20	3.85	87.74
121515	1.721	0.524	1.918	284.2	310.8	138.68	4.82	90.17
121516	2.093	0.532	2.259	328.6	359.1	129.82	5.46	91.54
121517	1.188	0.391	0.799	158.2	173.0	133.87	2.52	84.82
121518	1.395	0.482	1.365	219.9	240.6	131.24	4.30	86.17
121519	1.722	0.522	1.908	283.8	308.7	129.80	5.19	89.41
121520	2.097	0.531	2.237	327.5	358.1	128.48	6.03	90.69
121521	1.184	0.391	0.788	155.1	170.2	133.87	2.77	82.94
121522	1.391	0.478	1.363	220.8	241.1	131.83	3.93	87.25
121523	1.715	0.525	1.894	280.4	306.7	128.89	5.45	88.80
121524	2.087	0.531	2.233	327.8	357.4	128.02	5.89	90.85

ORIGINAL PAGE IS  
OF POOR QUALITY

TABLE V. TEST RESULTS 0.1  $\mu$  m SURFACE FINISH 0.5 mm FILLET RADIUS

IDENT#	PRESS.RATIO	EQUIV.FLOW KG/SEC	EQUIV.TORQUE N-M	VU EXIT M/SEC	V EXIT M/SEC	PT EXIT K PA	% PT LOSS	% STATOR EFFICIENCY
72405	1.187	0.388	0.829	165.6	179.6	135.42	1.42	91.39
72406	1.396	0.476	1.413	230.4	249.5	134.40	2.28	92.67
72407	1.721	0.515	1.939	292.1	316.1	133.35	2.94	93.99
72408	2.099	0.521	2.275	339.1	367.2	133.45	2.98	95.41
72401	1.193	0.390	0.832	165.2	179.4	135.83	1.91	89.76
72402	1.405	0.475	1.414	230.7	250.0	134.36	2.71	91.44
72403	1.742	0.514	1.944	293.7	317.9	133.97	3.43	93.15
72404	2.104	0.520	2.265	338.0	366.3	133.45	3.46	94.70
72101	1.196	0.392	0.838	165.6	180.0	135.27	2.05	88.11
72102	1.406	0.474	1.410	230.6	249.8	134.57	2.81	91.14
72103	1.737	0.513	1.939	293.4	317.4	133.75	3.28	93.42
72104	2.085	0.518	2.253	337.3	365.0	134.12	3.09	95.20
72106	1.402	0.475	1.405	229.7	248.9	133.90	2.80	91.11
72107	1.731	0.513	1.928	291.5	315.6	132.88	3.55	92.84
72108	2.073	0.518	2.247	336.6	364.1	133.35	2.98	95.35
72109	1.188	0.385	0.816	164.1	178.0	135.27	1.79	89.24
72117	1.187	0.388	0.807	161.5	175.8	134.82	2.03	87.62
72118	1.395	0.475	1.396	228.2	247.5	133.98	2.71	91.29
72119	1.731	0.514	1.942	293.3	317.3	133.47	3.05	93.83
72120	2.075	0.519	2.256	337.3	364.9	134.20	2.81	95.60
72113	1.192	0.388	0.824	164.5	178.6	135.41	1.98	88.33
72114	1.399	0.473	1.397	229.2	248.4	133.98	2.82	91.03
72115	1.725	0.512	1.928	293.1	316.9	133.62	3.08	93.73
72116	2.092	0.518	2.257	339.9	367.7	133.74	3.04	95.30
72110	1.399	0.474	1.404	229.7	248.9	134.29	2.84	91.60
72111	1.716	0.513	1.927	291.7	315.4	133.61	2.89	94.07
72112	2.073	0.519	2.256	337.8	365.2	133.68	2.64	95.87
72113	1.193	0.388	0.823	164.5	178.6	135.42	2.01	88.15
72121	1.195	0.397	0.831	162.4	177.4	135.41	2.37	86.15
72122	1.404	0.483	1.410	226.5	246.7	133.97	3.43	89.18
72123	1.724	0.520	1.937	289.4	314.1	133.27	3.65	92.58
72124	2.049	0.527	2.253	331.8	360.2	133.72	3.36	94.67
72301	1.196	0.394	0.835	164.0	178.7	135.74	2.22	87.14
72302	1.408	0.475	1.417	231.7	250.9	135.41	2.74	91.42
72303	1.741	0.514	1.942	293.7	317.9	134.58	3.44	93.13
72304	2.099	0.518	2.258	338.3	366.3	134.45	3.35	94.84
72305	1.187	0.384	0.814	164.5	178.3	136.15	1.79	89.21
72306	1.404	0.474	1.408	230.6	249.8	134.72	2.78	91.24
72307	1.734	0.505	1.941	294.0	316.4	136.13	2.89	95.84
72308	2.10	0.519	2.265	339.2	367.3	134.84	3.34	94.89



ORIGINAL PAGE IS  
OF POOR QUALITY

TABLE VI. TEST RESULTS 0.1  $\mu$  m SURFACE FINISH 1.0 mm FILLET RADIUS

IDENT#	PRESS. RATIO	EQUIV. FLOW KG/SEC	EQUIV. TORQUE N-M	VU EXIT M/SEC	V EXIT M/SEC	PT EXIT K PA	% PT LOSS	% STATOR EFFICIENCY
63001	1.191	0.391	0.637	166.0	180.3	135.51	1.66	89.98
63002	1.393	0.472	1.389	220.6	247.6	134.08	2.60	91.63
63003	1.720	0.511	1.905	289.8	313.7	132.29	3.63	92.49
63004	2.040	0.516	2.233	336.2	363.7	132.80	3.45	94.63
63005	1.193	0.383	0.622	164.6	178.7	135.42	2.02	89.04
63006	1.404	0.471	1.390	228.9	248.1	134.25	3.15	90.06
63007	1.742	0.509	1.910	291.4	315.5	132.78	4.16	91.60
63008	2.105	0.512	2.234	339.0	366.4	133.26	3.53	94.58
63010	1.197	0.389	0.632	166.1	180.3	135.55	2.14	87.66
63011	1.407	0.470	1.391	230.0	249.0	134.29	3.15	90.10
63012	1.735	0.507	1.891	289.7	313.6	132.54	4.30	91.18
63013	2.106	0.510	2.227	339.6	366.7	133.78	3.43	94.66
63014	1.194	0.386	0.625	165.8	179.8	135.83	1.97	88.42
63015	1.406	0.472	1.394	229.1	248.3	134.22	3.24	89.82
63016	1.736	0.508	1.900	290.7	314.6	132.36	4.12	91.71
63017	2.094	0.515	2.224	335.7	363.5	132.49	4.09	93.69
70105	1.189	0.382	0.614	165.3	178.9	135.51	1.73	89.63
70106	1.402	0.469	1.394	230.8	249.5	134.66	2.70	91.43
70107	1.745	0.508	1.914	292.9	316.8	133.27	3.91	92.20
70108	2.081	0.513	2.221	336.1	363.4	132.99	3.60	94.40
70101	1.194	0.384	0.622	165.8	179.6	135.80	1.92	88.75
70102	1.401	0.466	1.379	229.7	248.3	134.20	2.87	90.87
70103	1.742	0.505	1.906	293.2	316.6	133.28	3.76	92.40
70104	2.119	0.513	2.235	338.5	366.3	132.95	3.98	93.94
63018	1.195	0.386	0.627	166.0	180.0	135.92	1.96	89.58
63019	1.403	0.469	1.397	229.6	248.5	134.28	3.02	90.46
63020	1.740	0.504	1.909	294.4	317.8	133.48	3.49	93.01
63021	2.101	0.515	2.230	336.9	364.8	132.71	4.04	93.79
70109	1.201	0.448	0.813	140.7	162.6	132.02	5.16	70.48
70110	1.396	0.469	1.377	227.7	246.7	133.89	2.95	90.55
70111	1.729	0.506	1.911	293.3	316.6	134.11	3.22	93.47
70112	2.084	0.513	2.229	337.4	364.6	133.40	3.30	94.87
70113	1.192	0.384	0.611	163.8	177.8	135.20	2.11	87.47
70114	1.398	0.465	1.353	225.9	244.4	133.34	2.93	90.46
70115	1.731	0.507	1.897	290.7	314.4	132.28	3.92	92.09
70116	2.114	0.514	2.234	337.7	365.6	133.91	4.06	93.81
70117	1.188	0.382	0.605	163.5	177.3	135.53	1.92	88.37
70118	1.401	0.469	1.371	230.3	249.0	134.84	2.73	91.32
70119	1.740	0.506	1.913	294.0	317.5	134.45	3.45	93.10
70120	2.096	0.513	2.235	338.2	365.6	134.94	3.40	94.75

ORIGINAL PAGE IS  
OF POOR QUALITY

TABLE VII. TEST RESULTS 0.6  $\mu$  m SURFACE FINISH 0.0 mm FILLET RADIUS

IDENT#	PRESS. RATIO	EQUIV. FLOW KG/SEC	EQUIV. TORQUE N-M	VU EXIT M/SEC	V EXIT M/SEC	PT EXIT K PA	% PT LOSS	% STATOR EFFICIENCY
83125	1.193	0.394	0.831	163.2	177.9	135.06	2.13	87.52
83126	1.410	0.484	1.426	228.7	249.0	133.81	3.31	89.66
83127	1.732	0.521	1.738	289.2	314.3	132.60	4.04	91.84
83128	2.110	0.526	2.265	334.5	364.0	131.86	4.51	93.11
83113	1.192	0.394	0.838	164.8	179.4	135.40	1.87	88.97
83114	1.398	0.482	1.412	227.7	247.6	133.93	2.87	90.83
83115	1.726	0.522	1.944	289.1	314.2	132.95	3.73	92.43
83116	2.105	0.529	2.276	334.2	363.9	131.71	4.32	93.38
83117	1.193	0.395	0.833	163.6	178.4	135.04	2.13	87.42
83118	1.402	0.482	1.416	228.2	248.2	133.56	3.02	90.42
83119	1.729	0.521	1.941	289.6	314.6	132.42	3.84	92.23
83120	2.122	0.526	2.266	334.6	364.3	131.54	4.80	92.71
83121	1.195	0.395	0.841	164.7	179.5	135.39	2.08	87.83
83122	1.401	0.481	1.416	228.5	248.4	133.56	2.89	90.82
83123	1.724	0.524	1.940	287.7	313.1	131.95	3.99	91.88
83124	2.119	0.528	2.268	333.6	363.6	131.11	4.94	92.49
90105	1.183	0.392	0.785	155.2	170.4	133.25	2.64	83.66
90106	1.381	0.479	1.353	219.5	239.6	130.96	3.60	88.10
90107	1.708	0.522	1.897	282.3	307.7	129.29	4.76	90.15
90108	2.084	0.530	2.235	327.6	357.7	128.03	5.61	91.28
90201	1.191	0.397	0.842	164.4	179.2	135.22	1.79	89.37
90202	1.396	0.484	1.426	228.2	248.1	133.79	2.65	91.51
90203	1.723	0.521	1.948	289.6	314.3	133.23	3.43	93.04
90204	2.101	0.526	2.281	336.0	364.8	132.99	3.52	94.60
90101	1.174	0.394	0.838	164.9	179.6	135.07	2.01	88.22
90102	1.403	0.481	1.416	228.4	248.4	133.70	3.04	90.48
90103	1.733	0.521	1.944	290.1	315.1	132.71	3.88	92.19
90104	2.113	0.527	2.271	334.5	364.2	131.65	4.55	93.06
83129	1.194	0.397	0.837	163.7	178.7	135.17	2.20	87.86
83130	1.406	0.484	1.423	228.4	248.7	133.88	3.17	90.83
83131	1.733	0.521	1.941	289.3	314.5	132.75	4.08	91.78
83132	2.113	0.527	2.247	334.0	363.7	132.05	4.48	92.85
83105	1.189	0.390	0.800	159.4	174.8	134.37	2.49	85.81
83106	1.396	0.478	1.382	224.3	244.4	133.83	3.49	88.80
83107	1.737	0.528	1.929	287.9	313.2	132.28	4.51	90.94
83108	2.111	0.528	2.254	331.5	361.4	130.88	5.25	91.97
83101	1.192	0.393	0.804	158.7	173.8	134.13	2.76	83.58
83102	1.402	0.479	1.384	224.7	244.8	132.88	3.79	87.98
83103	1.723	0.520	1.914	286.0	311.2	131.21	4.48	90.87
83104	2.111	0.528	2.254	332.1	362.0	130.62	5.13	92.15

ORIGINAL PAGE IS  
OF POOR QUALITY

TABLE VIII. TEST RESULTS 0.6  $\mu$  m SURFACE FINISH 1.0 mm FILLET RADIUS

IDENT#	PRESS. RATIO	EQUIV. FLOW KG/SEC	EQUIV. TORQUE N-M	U EXIT M/SEC	V EXIT M/SEC	PT EXIT K PA	% PT LOSS	% STATOR EFFICIENCY
100626	1.192	0.391	0.833	164.9	179.2	135.49	1.82	89.23
100627	1.409	0.476	1.425	232.1	251.2	134.91	2.36	92.55
100628	1.732	0.513	1.950	294.8	318.5	134.01	2.69	94.57
100629	2.130	0.518	2.279	341.6	369.7	133.35	3.14	95.25
100610	1.196	0.390	0.843	167.6	181.7	135.75	1.78	89.67
100611	1.408	0.474	1.423	233.2	252.2	135.16	2.48	92.23
100612	1.735	0.510	1.949	296.7	320.1	134.27	2.46	95.05
100613	2.082	0.517	2.252	338.1	365.6	134.11	2.86	95.55
100606	1.190	0.386	0.817	164.3	178.3	135.65	1.87	88.80
100607	1.411	0.474	1.424	233.2	252.3	135.09	2.59	91.40
100608	1.742	0.510	1.940	295.1	318.8	134.05	3.14	93.73
100609	2.074	0.515	2.231	336.4	363.6	134.09	3.21	94.99
100601	1.213	0.399	0.906	175.6	190.0	135.60	1.62	91.35
100602	1.434	0.480	1.483	239.3	258.8	137.79	2.44	92.68
100604	1.740	0.508	1.949	297.5	320.8	135.14	2.38	95.23
100605	2.081	0.515	2.244	337.9	365.1	133.84	2.91	95.47
100514	1.199	0.391	0.841	166.7	181.0	136.13	2.13	87.84
100515	1.415	0.477	1.426	231.9	251.4	135.07	3.04	90.61
100516	1.730	0.510	1.934	294.1	317.9	134.39	3.21	93.50
100517	2.142	0.517	2.258	338.8	367.5	133.06	4.35	93.46
100518	1.207	0.392	0.846	167.2	181.6	136.10	2.27	87.20
100519	1.417	0.475	1.422	232.5	251.9	135.03	3.09	90.49
100520	1.745	0.510	1.932	294.0	317.9	134.45	3.53	92.97
100521	2.140	0.514	2.254	340.1	368.5	133.50	4.28	93.59
100522	1.199	0.391	0.837	166.2	180.5	136.09	2.22	87.32
100523	1.415	0.475	1.424	232.7	252.0	134.92	2.90	91.02
100524	1.741	0.509	1.934	294.6	318.3	134.47	3.22	93.56
100525	2.152	0.515	2.260	340.6	369.0	133.16	4.21	93.70
100510	1.177	0.382	0.780	154.2	168.6	133.14	2.42	84.53
100511	1.332	0.472	1.351	222.1	241.4	131.83	3.26	89.25
100512	1.725	0.513	1.914	299.5	313.7	131.46	3.78	92.33
100513	2.025	0.520	2.232	333.2	361.5	130.96	4.20	93.37
100506	1.175	0.377	0.748	153.8	167.0	132.84	2.41	84.47
100507	1.379	0.469	1.339	221.8	240.9	131.21	3.22	89.32
100508	1.784	0.512	1.892	295.0	309.1	130.84	4.16	91.37
100509	2.089	0.517	2.224	334.3	362.4	130.81	4.29	93.36
100501	1.173	0.374	0.747	154.1	167.8	133.29	2.24	85.51
100502	1.374	0.468	1.326	220.2	239.2	132.82	3.24	89.81
100504	1.782	0.510	1.879	295.1	309.9	130.44	3.77	91.04
100505	2.074	0.521	2.215	333.3	363.3	133.27	4.61	92.43

ORIGINAL PAGE IS  
OF POOR QUALITY

TABLE IX. TEST RESULTS 2.4  $\mu$  m SURFACE FINISH 0.0 mm FILLET RADIUS

IDENT	GROSS RATIO	EQUIV. FLOW KG SEC	EQUIV. TORQUE N M	V <sub>0</sub> INLET M SEC	V <sub>1</sub> INLET M SEC	P <sub>0</sub> INLET K PA	P <sub>1</sub> LOSS	% STATOR EFFICIENCY
110202	1.193	0.397	0.051	166.5	161.2	135.67	1.67	90.10
110203	1.401	0.402	1.433	231.1	230.9	136.59	2.43	92.30
110204	1.725	0.522	1.962	292.2	316.9	136.36	3.01	93.69
110205	2.038	0.528	2.259	332.7	360.9	133.83	2.85	95.44
110206	1.195	0.395	0.045	165.9	160.5	135.73	1.90	88.90
110207	1.405	0.403	1.429	229.9	249.9	136.71	2.86	91.05
110208	1.724	0.521	1.946	290.2	315.0	132.30	3.49	92.90
110209	2.035	0.527	2.240	331.6	359.8	133.83	3.22	94.86
110210	1.194	0.394	0.033	164.1	170.6	135.51	2.16	87.33
110211	1.409	0.402	1.430	230.6	250.6	136.75	2.90	90.68
110212	1.730	0.519	1.945	291.2	315.9	133.42	3.55	92.83
110213	2.025	0.524	2.234	331.6	359.2	136.29	2.92	95.10
110214	1.195	0.395	0.039	165.1	179.7	135.59	2.02	88.14
110215	1.404	0.400	1.424	230.6	250.3	136.30	2.73	91.39
110216	1.729	0.519	1.950	292.2	316.7	133.77	3.27	93.39
110217	2.021	0.525	2.238	331.6	359.3	136.14	2.75	95.56
110220	1.193	0.395	0.040	164.8	179.5	135.49	1.95	88.46
110229	1.403	0.400	1.425	230.5	250.1	136.46	2.66	91.59
110230	1.725	0.519	1.953	291.9	316.4	133.91	3.03	93.85
110231	2.041	0.526	2.254	332.9	360.8	136.22	2.84	95.47
110222	1.193	0.393	0.032	164.3	170.9	135.29	2.03	88.00
110223	1.404	0.409	1.419	229.8	249.5	136.32	2.82	91.09
110224	1.725	0.519	1.942	290.9	315.5	133.32	3.37	93.14
110227	2.001	0.526	2.267	334.9	363.6	133.27	3.54	96.49
110218	1.195	0.394	0.042	165.6	160.1	135.63	1.93	88.67
110219	1.400	0.409	1.415	229.3	249.0	133.90	2.75	91.26
110220	1.737	0.520	1.963	293.4	318.2	136.23	3.23	93.50
110221	2.004	0.525	2.227	329.8	357.2	136.02	2.71	95.47
110313	1.163	0.358	0.103	156.5	171.2	133.47	2.46	84.70
110314	1.391	0.427	1.351	219.6	239.6	131.21	3.55	85.17
110315	1.703	0.520	1.905	274.7	309.6	129.53	4.20	91.31
110316	2.001	0.529	2.230	327.6	357.0	128.49	4.92	92.29
110305	1.157	0.356	0.104	157.4	172.3	133.77	2.30	85.69
110306	1.362	0.476	1.348	220.8	239.9	131.15	3.83	85.04
110307	1.709	0.519	1.893	264.8	304.0	129.63	4.43	90.85
110308	2.105	0.527	2.249	330.9	360.9	129.73	5.33	91.82
110309	1.177	0.363	0.107	153.3	167.7	133.14	2.51	83.44
110310	1.377	0.474	1.333	215.8	237.8	132.53	3.65	87.73
110311	1.699	0.518	1.853	262.0	306.8	128.88	4.40	90.62
110312	2.056	0.527	2.236	324.6	359.2	127.96	5.15	92.01

ORIGINAL PAGE IS  
OF PCOR QUALITY

TABLE X. TEST RESULTS  $2.4 \mu$  m SURFACE FINISH 0.5 mm FILLET RADIUS

IDENT#	PRESS. RATIO	EQUIV. FLOW G/G SEC	EQUIV. TORQUE N.M	VU EXIT U/SEC	V EXIT U/SEC	PT EXIT K. PA	Δ PT LOSS	% STATOR EFFICIENCY
111305	1.193	0.395	0.642	165.1	179.6	135.69	1.81	89.34
111306	1.410	0.482	1.442	231.7	251.5	134.05	2.66	91.63
111307	1.746	0.521	1.980	294.5	318.5	133.44	3.51	93.09
111308	2.152	0.528	2.305	350.4	364.5	132.04	4.33	93.83
111223	1.199	0.397	0.657	167.5	187.1	135.61	1.90	89.11
111224	1.405	0.450	1.430	231.2	250.8	134.22	2.69	91.56
111225	1.762	0.519	1.978	298.9	320.7	133.27	3.47	93.20
111226	2.141	0.525	2.294	338.8	363.3	132.68	4.02	93.96
111219	1.406	0.451	1.426	229.7	249.6	134.19	2.91	90.63
111220	1.760	0.518	1.976	295.9	320.7	133.55	3.37	93.37
111221	2.137	0.525	2.291	338.6	363.0	132.43	3.98	94.00
111222	1.198	0.396	0.653	167.0	181.6	135.40	1.92	89.54
111213	1.196	0.397	0.648	166.0	180.8	135.49	2.00	88.39
111214	1.402	0.478	1.415	230.2	249.7	134.12	2.70	91.45
111215	1.753	0.518	1.969	295.4	320.1	133.02	3.43	93.21
111216	2.134	0.521	2.292	342.3	370.8	133.55	3.21	95.16
111201	1.194	0.393	0.643	166.3	180.6	135.25	1.77	89.61
111202	1.410	0.420	1.433	232.7	242.3	134.04	2.57	91.93
111203	1.751	0.518	1.970	295.4	320.0	133.87	3.20	93.51
111204	2.164	0.524	2.305	341.7	371.3	132.04	4.05	93.93
111205	1.195	0.392	0.641	166.4	180.0	136.01	1.89	89.97
111206	1.408	0.479	1.425	231.2	250.8	134.45	2.79	91.26
111207	1.760	0.517	1.970	295.8	320.6	133.36	3.55	93.03
111208	2.155	0.524	2.296	340.6	370.1	132.74	4.13	93.04
111209	1.191	0.389	0.634	166.1	180.2	135.42	1.68	90.07
111210	1.404	0.477	1.423	231.6	251.1	134.27	2.45	92.17
111211	1.759	0.518	1.978	296.8	321.5	133.47	3.26	93.75
111212	2.159	0.525	2.303	341.3	371.0	132.07	4.03	94.03
111227	1.174	0.393	0.720	157.7	171.9	133.99	2.00	87.31
111228	1.333	0.473	1.347	229.4	243.6	131.06	2.84	90.67
111229	1.747	0.510	1.933	293.5	314.1	133.17	4.04	91.84
111230	2.108	0.514	2.254	334.7	363.4	129.21	4.64	92.43
111231	1.182	0.392	0.722	157.6	171.6	133.47	2.12	86.64
111232	1.333	0.473	1.363	227.8	242.1	131.42	3.11	89.76
111233	1.726	0.517	1.913	287.1	311.6	129.84	4.28	91.37
111234	2.124	0.523	2.249	333.1	362.3	129.24	4.38	92.33
111331	1.174	0.391	0.765	156.2	170.3	133.12	2.24	87.27
111332	1.333	0.473	1.365	227.0	241.4	131.64	3.24	89.23
111333	1.732	0.517	1.923	287.7	313.4	130.17	4.00	91.74
111334	2.171	0.518	2.263	333.2	363.6	128.76	4.91	92.44

ORIGINAL PAGE IS  
OF POOR QUALITY

TABLE XI. TEST RESULTS 2.4  $\mu$  m SURFACE FINISH 1.0 mm FILLET RADIUS

IDENT	PRSS. RATIO	EQUIV. FLOW G/G SEC	EQUIV. TORQUE N-M	VU EXIT M SEC	V EXIT M SEC	PT EXIT N PA	% PT LOSS	% STATOR EFFICIENCY
101901	1.192	0.393	0.015	160.9	175.0	134.17	2.52	85.09
101902	1.401	0.479	1.397	226.0	246.6	132.04	3.33	89.43
101903	1.724	0.513	1.922	291.1	315.1	132.07	3.55	92.00
101904	2.121	0.520	2.245	334.9	363.9	131.47	4.79	92.72
102021	1.194	0.393	0.038	165.4	179.9	135.03	1.90	85.41
102022	1.406	0.477	1.421	231.4	250.0	134.40	2.64	91.70
102023	1.733	0.512	1.937	293.0	317.0	133.95	3.08	93.00
102024	2.105	0.520	2.255	330.9	365.3	132.01	3.81	94.16
102017	1.194	0.397	0.026	165.1	179.2	135.23	1.93	88.43
102018	1.405	0.474	1.414	231.0	250.7	134.02	2.76	91.33
102019	1.734	0.511	1.929	293.1	316.0	133.04	3.32	93.33
102020	2.136	0.517	2.263	340.0	368.3	132.94	3.85	94.19
102013	1.195	0.390	0.040	167.3	181.4	135.06	1.60	89.50
102014	1.404	0.474	1.419	232.3	251.3	134.95	2.37	92.50
102015	1.735	0.512	1.945	294.9	318.7	133.06	2.85	94.27
102016	2.097	0.516	2.250	310.1	365.9	133.27	3.32	94.64
102001	1.197	0.393	0.035	164.9	179.4	135.40	2.10	87.90
102002	1.409	0.475	1.422	232.5	251.7	134.97	2.04	91.73
102003	1.742	0.512	1.950	295.7	319.5	134.71	2.96	94.09
102004	2.115	0.510	2.263	339.1	367.1	133.60	3.39	94.83
102005	1.192	0.388	0.026	165.1	179.2	135.25	1.85	89.02
102006	1.404	0.473	1.413	232.1	251.0	134.00	2.48	92.10
102007	1.733	0.512	1.938	293.4	317.4	133.03	3.32	93.35
102008	2.139	0.510	2.260	339.7	368.2	132.43	3.98	94.02
102009	1.193	0.389	0.034	166.4	180.5	135.63	1.75	87.63
102010	1.403	0.473	1.409	231.3	250.3	134.23	2.31	92.61
102011	1.732	0.513	1.946	294.5	318.2	133.89	2.68	94.02
102012	2.133	0.517	2.277	341.2	369.2	132.42	3.20	95.10
101913	1.204	0.400	0.056	166.0	181.2	135.98	2.48	86.97
101914	1.415	0.490	1.435	232.2	251.9	135.78	2.97	90.62
101915	1.745	0.514	1.943	294.2	318.6	134.37	3.36	93.32
101916	2.164	0.523	2.279	333.7	369.0	133.33	4.43	92.72
101909	1.208	0.396	0.153	168.0	182.7	136.20	2.35	86.93
101910	1.420	0.491	1.432	232.7	252.0	135.45	3.51	89.24
101911	1.751	0.514	1.950	294.3	318.6	134.43	3.55	92.43
101912	2.184	0.520	2.264	333.5	368.0	133.73	4.94	92.67
101925	1.209	0.397	0.055	167.1	182.0	136.20	2.48	86.15
101926	1.430	0.493	1.433	233.6	253.2	135.93	3.02	90.76
101927	1.747	0.513	1.946	294.8	319.0	135.59	3.43	93.19
101928	2.187	0.521	2.273	333.8	368.3	133.50	4.94	92.65

ORIGINAL PAPER  
OF POOR QUALITY

TABLE XII. TEST MATRIX 1.2 PRESSURE RATIO

		SURFACE FINISH		
		0.1 $\mu$ M TURBULENCE	0.6 $\mu$ M	2.4 $\mu$ M
RADIUS	BOUNDARY LAYER	2% 2% 89.47 6% 12% 10 87.57 88.37 85.07 15 87.28 88.18 83.98 25 86.59 88.59 83.59	89.57 89.37 89.17 84.17 88.58 82.28 85.28 88.69 88.19 83.89	90.47 88.97 88.87 85.17 87.98 88.48 85.98 88.69 88.99 84.59
	0.5MM	91.47 89.17 88.67 86.37 88.48 88.58 86.38 88.99 89.59 89.39		89.57 89.17 89.67 88.47 88.98 88.98 87.68 88.49 89.59 86.59
	1.0MM	90.17 88.17 89.67 88.97 87.98 88.98 88.18 88.49 88.79 89.09	89.47 89.77 87.77 85.37 88.98 87.18 85.28 89.69 87.49 85.99	87.77 88.57 88.07 86.07 88.58 89.18 86.98 89.69 89.79 86.09
	FILLET			

ORIGINAL PAGE IS  
OF POOR QUALITY

TABLE XIII. TEST MATRIX 1.4 PRESSURE RATIO

		SURFACE FINISH		
		0.1 $\mu$ M TURBULENCE	0.6 $\mu$ M	2.4 $\mu$ M
0MM	BOUNDARY LAYER	2%		
		91.35	91.55	92.35
	10	90.32	90.92	91.02
	15	89.95	89.95	90.75
0.5MM	25	89.0	89.70	91.40
		90.72	88.22	91.62
		90.35	88.95	91.15
		86.75	89.10	88.35
1.0MM		86.3		88.20
F I L L E T				



ORIGINAL PAGE IS  
OF POOR QUALITY

TABLE XIV. TEST MATRIX 1.7 PRESSURE RATIO

SURFACE FINISH

RADIUS	FILLET	BOUNDARY LAYER	0.1 $\mu$ M			0.6 $\mu$ M			2.4 $\mu$ M		
			TURBULENCE								
			2%								
			2%	6%	12%						
0MM		2%	93.15			92.95			93.75		
		10	92.31	92.71	90.11	92.01	92.11	90.11	92.81	93.71	91.31
		15	92.0	92.6	89.3	91.7	92.1	90.8	92.7	93.2	90.9
		25	91.78	92.58	88.78	91.78	91.88	90.78	93.28	93.28	90.78
0.5MM			93.85						93.75		
			93.01	93.61	93.61				93.81	94.01	92.41
			93.2	93.6	93.6				92.9	93.5	91.9
			92.68	93.98	93.58				93.78	94.08	92.18
1.0MM			92.45			94.45			92.55		
			91.51	92.21	93.31	93.91	93.31	92.31	93.71	94.01	94.31
			91.1	92.3	92.0	93.6	92.8	91.4	93.2	93.6	93.9
			91.68	92.78	92.98	94.98	93.38	91.98	94.18	94.48	93.18

ORIGINAL PAGE IS  
OF POOR QUALITY

TABLE XV. TEST MATRIX 2.1 PRESSURE RATIO

SURFACE FINISH

0.1  $\mu$ M

0.6  $\mu$ M

2.4  $\mu$ M

TURBULENCE

2%

RADIUS	BOUNDARY LAYER	0.1 $\mu$ M		
		2%	6%	12%
	2%	94.9		
	10	94.02	94.72	91.62
0MM	15	93.92	94.72	90.82
	25	93.4	94.54	90.94

RADIUS	BOUNDARY LAYER	0.6 $\mu$ M		
	2%	94.6		
	10	93.02	93.32	91.22
	15	92.82	92.72	91.92
	25	93.14	92.44	92.14

RADIUS	BOUNDARY LAYER	2.4 $\mu$ M		
	2%	95.5		
	10	94.92	95.62	92.32
	15	95.52	94.52	91.82
	25	95.84	95.84	92.04

RADIUS	BOUNDARY LAYER	0.1 $\mu$ M		
		2%	6%	12%
	2%	95.4		
	10	94.72	95.72	89.82
0.5MM	15	95.32	95.32	89.82
	25	95.44	95.84	89.84

RADIUS	BOUNDARY LAYER	0.6 $\mu$ M		
	2%	94.9		
	10	95.42	94.92	93.72
	15	95.32	95.12	94.02
	25	96.54	95.24	93.74

RADIUS	BOUNDARY LAYER	2.4 $\mu$ M		
	2%	94.7		
	10	93.42	94.42	94.12
1.0MM	15	94.62	93.92	93.82
	25	93.74	93.84	94.74

RADIUS	BOUNDARY LAYER	0.1 $\mu$ M		
		2%	6%	12%
	2%	95.2		
	10	95.52	93.42	95.62
	15	95.02	93.52	93.32
	25	95.44	93.64	92.54

RADIUS	BOUNDARY LAYER	0.6 $\mu$ M		
	2%	92.8		
	10	94.62	94.82	93.02
	15	94.12	94.02	92.82
	25	94.84	95.14	92.84

ORIGINAL PAGE IS  
OF POOR QUALITY

BF1119

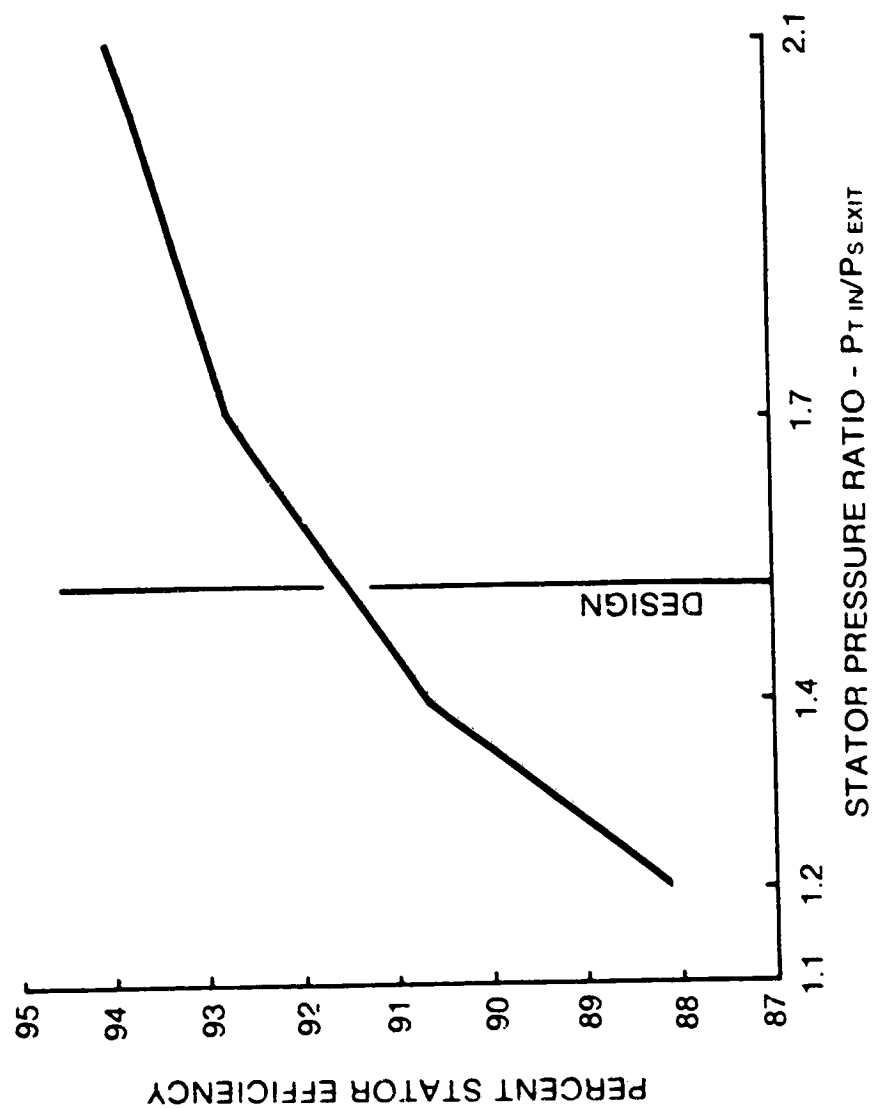
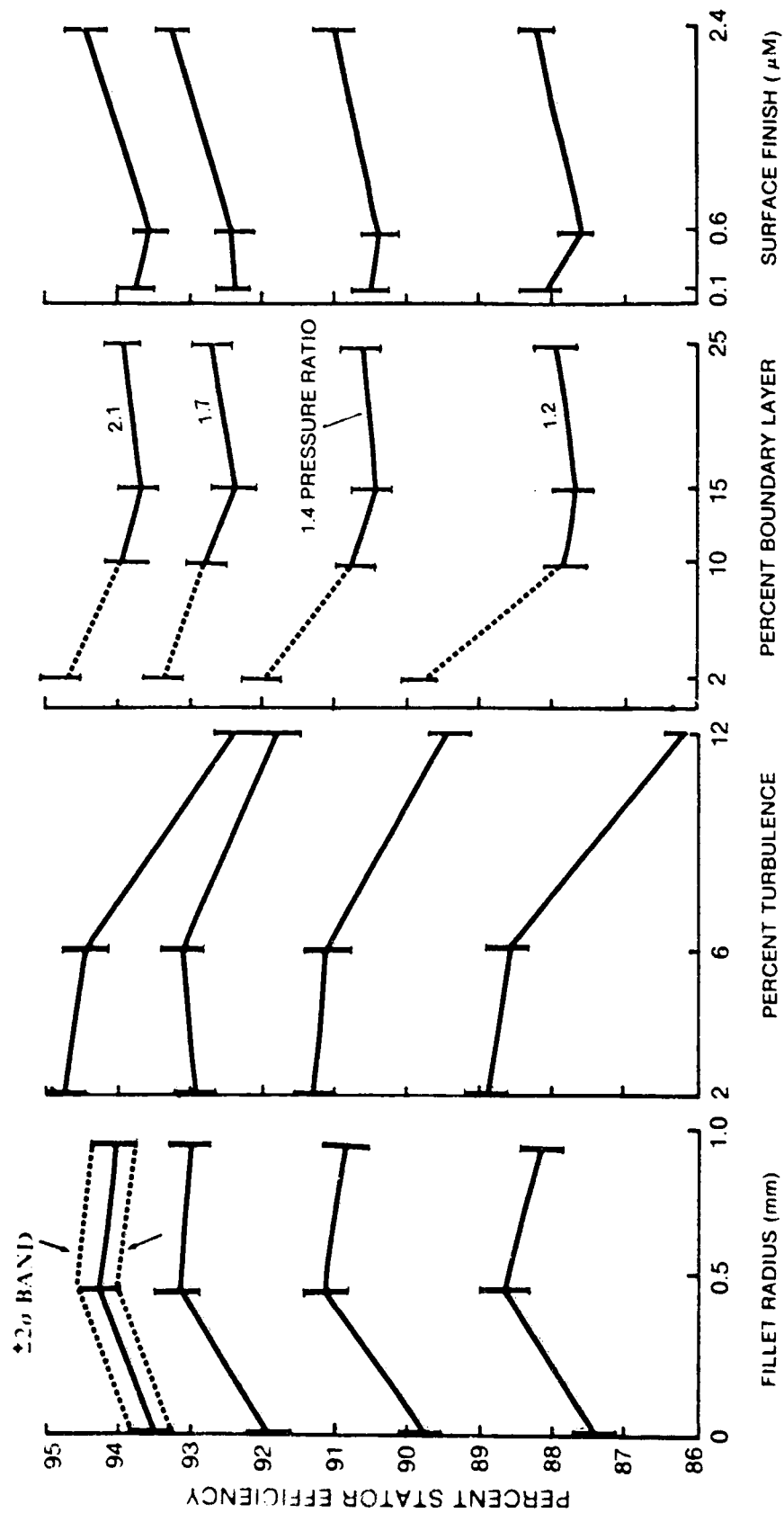


Figure 18. Average Stator Efficiency Versus Pressure Ratio



BF1120

Figure 19. Efficiency Versus Each Variable at Constant Pressure Ratio

### 5.2.1 Pressure Ratio

The average stator efficiency plotted as a function of pressure ratio in Figure 18 shows a 6 percent increase in efficiency over the tested range, with the highest efficiency at the largest pressure ratio tested. The design point pressure ratio of 1.52 shows an average efficiency of 91.5 percent.

The effects of each of the four test variables are presented in Figure 20. The individual points in this figure typically represent an average of thirty points. The effect of each variable over the tested pressure ratio range is roughly the same since the curve shapes within each plot are nearly the same. The 12 percent turbulence data, however, indicate a different sensitivity to pressure ratio level than the lower levels of turbulence tested.

The efficiency trend with pressure ratio is similar to that measured for the full-scale stator (Reference 2). Comparative results are presented below in Section 5.5.

### 5.2.2 Fillet Radius

The direct effect of fillet radius on stator efficiency is shown in Figure 19, for each of the pressure ratio levels tested. The 0.5mm (0.020 inch) fillet radius had the highest efficiency. Only slightly lower in efficiency was the 1.0mm (.040 inch) fillet. The zero fillet radius exhibited a 1.4 percent average drop in efficiency compared with the 0.5mm (.020 inch) fillet radius. This indicates that an optimum fillet size exists for this stator between the zero and maximum fillet size tested.

L.L. Dubruge (Reference 3) concludes that there is a drastic reduction of separation probability in the corners of a compressor stator when a fillet is provided. The separation, which is most common in corners, sets up a tertiary flow vortex that is independent of the secondary flows. The fillet retards separation and subsequent vortex formations.

The addition of too large a fillet radius merely adds to the profile drag of the airfoil. Dubruge also discusses varying the size of the fillet to optimize the compromise between profile drag of the fillet and probability of separation. The slight decrease in efficiency in going from the 0.5mm (.020 inch) fillet radius to the 1.0mm (.040 inch) fillet radius may be due to an increase in the profile drag.

ORIGINAL PAGE IS  
OF POOR QUALITY

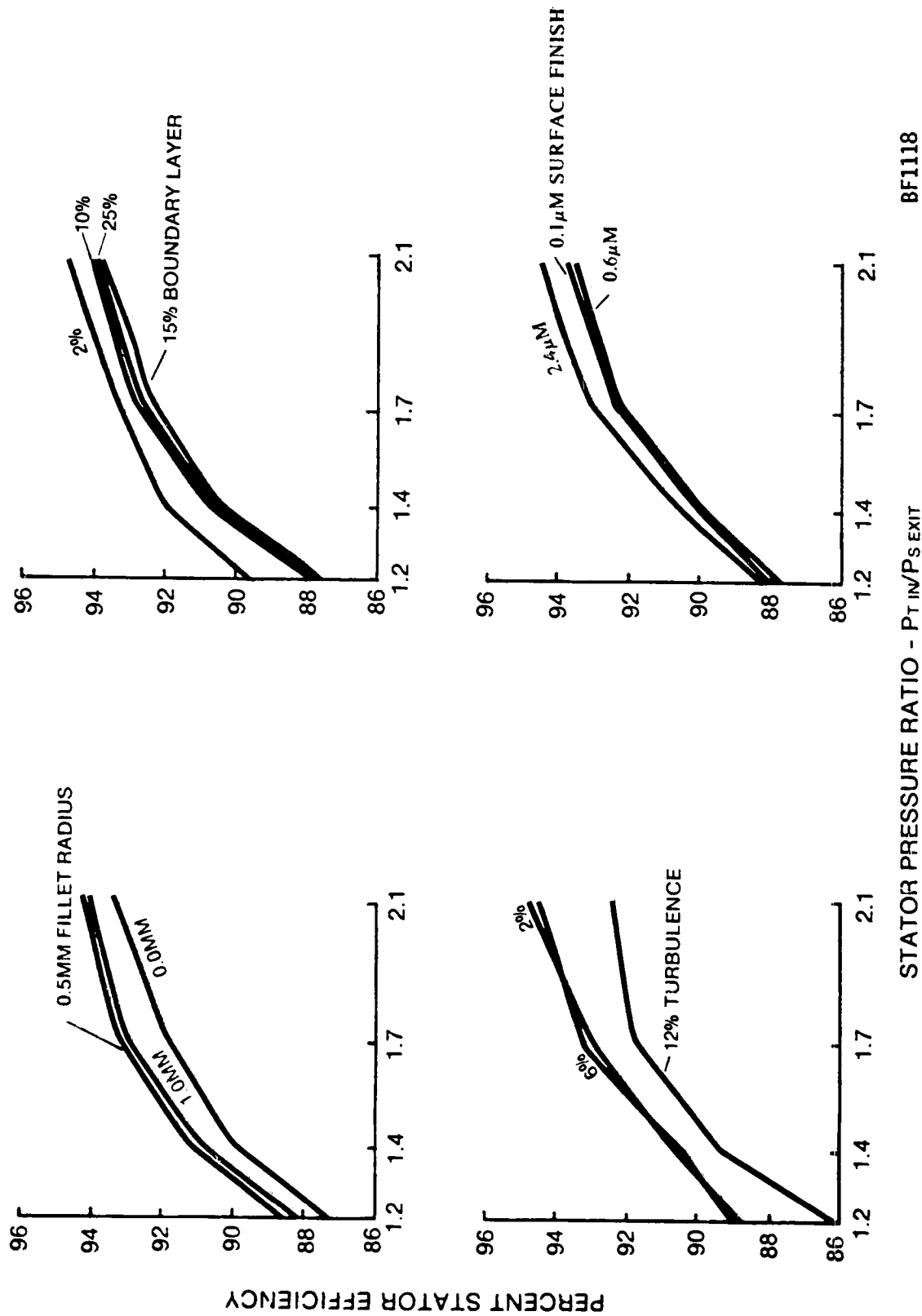


Figure 20. Efficiency Versus Pressure Ratio Showing Effects of Each Variable

### 5.2.3 Free-Stream Turbulence

The direct effect of free-stream turbulence on stator efficiency is shown in Figure 19 for each of the pressure ratio levels tested. The highest stator efficiency was produced at a turbulence level of 2 percent with a small drop at 6 percent and a significant loss at 12 percent turbulence. The efficiency level at 2 percent turbulence is slight' inflated relative to 6 and 12 percent since 32 data points were averaged for the 2 percent case including a 2 percent boundary layer data point. The 6 and 12 percent points represent averages of 24 data points, none at 2 percent boundary layer thickness. This will have only a minimal effect on the conclusions for turbulence effects.

Reference 4 was used to determine the boundary layer growth along the surfaces of the subject stator. The pressure side sees a laminar boundary layer which separates before the 7 percent chord point. The suction side has a laminar boundary layer over 11 percent of the chord which transitions to a turbulent boundary layer and this does not separate. An earlier transition point on the suction surface would result in a slightly larger boundary layer growth. An earlier transition on the pressure side triggered by free-stream turbulence could eliminate the laminar separation. This could possibly reduce losses.

The mechanism that produces higher stator losses with increasing turbulence is the earlier boundary layer transition from laminar to turbulent which increases the size of the boundary layer (Reference 5). The increased vane surface boundary layer increases losses in two ways, i.e., it contributes low momentum fluid to the secondary flow and it increases the profile loss. Horlock (Reference 6) attributes stator cascade losses to three causes: profile loss, annulus loss, and secondary loss. He also associated profile loss with boundary layer growth over the blade profile. Faster boundary layer growth on the vane surface would significantly increase the associated profile loss. Due, Easterling, and Rogo (Reference 7) investigated the effects of turbulence on stator performance and tested free-stream turbulence at intensities of 3.7 to 11 percent. At a nozzle exit Mach number of 1.18, the stator loss nearly doubled with the increase in turbulence. However, their loss levels are much greater than what was experienced in the scaled stator; therefore, results may not be directly comparable.

### 5.2.4 Wall Boundary Layer

The direct effect of boundary layer thickness on stator efficiency (Figure 19) shows a 1.5 percent reduction in efficiency at 1.4 pressure ratio when increasing the boundary layer thickness from 2 to 10 percent, and little effect for thicker boundary layers. The effect of pressure ratio level on the boundary layer effect is discussed in Section 5.3.

The boundary layer effects shown in Figure 19 from the 2 percent boundary layer to the 10 percent boundary layer are not as strong as the figure indicates. This is because the 2 percent boundary layer data were measured at only 2 percent turbulence, whereas the efficiency levels for the thicker boundary layers are lowered by the 6 and 12 percent turbulence data.

As mentioned previously, in reducing and analyzing the experimental data, the average calculated inlet pressure was used with corrections made for blockage. If the free-stream pressure had been used instead, there would have been significant differences in the efficiency levels between the 10, 15 and 25 percent boundary layers. By using the average calculated inlet pressure the impact of the losses associated with the inlet boundary layers themselves were removed from the stator efficiency value and only the effect of the inlet boundary layer on the losses developing within the stator itself remained.

Dunham (Reference 8) concluded that the magnitude of the secondary losses in a cascade is dependent on the upstream wall boundary layers. This agrees with the large increase in loss from the 2 to 10 percent boundary layer. Dunham also mentions the observation by Wolf, who concluded that thickening a thin upstream wall boundary layer has an important effect, while thickening an already thick one has little effect. This latter conclusion also agrees with the results of the subject investigation where there was no significant change in efficiency levels from the 10 through 25 percent inlet boundary layers.

Booth (Reference 9), who investigated the effects of inlet boundary layer, found that secondary flow loss increases in direct proportion to upstream momentum thickness. However, the range of momentum thicknesses investigated were below 0.5 percent of channel height, while the minimum momentum thickness for the scaled stator was approximately 1 percent.

#### 5.2.5 Surface Finish

The direct effect of surface finish on stator efficiency shown in Figure 19 indicates that the roughest surface produced the highest stator efficiency. At 1.4 pressure ratio the smooth  $0.1 \mu\text{m}$  ( $4 \mu\text{inch}$ ) finish was 0.5 percent lower in efficiency than the rough  $2.4 \mu\text{m}$  ( $95 \mu\text{inch}$ ) finish.

Schlichting (Reference 5) states that roughness affects the resistance offered by the wall by moving the point of transition in an upstream direction and, depending on the shape of the body, the drag may be either increased or decreased. The drag is increased by such a shift in the point of transition when the drag of the body is predominantly caused by skin friction (an airfoil). This drag may be decreased under certain circumstances if the drag of the body is due mainly to form drag (a cylinder).



A case can then be made for the stator airfoils to have drag caused by both skin friction and form drag. On the suction side of the vane, the boundary layer is initially laminar and then fairly quickly transitions to turbulent. In this particular case, skin friction is the primary cause of drag. On the pressure side of the vane, the boundary layer is initially laminar and then separates. In this case, the pressure side of the nozzle behaves more like a cylinder than an airfoil. With a rougher finish, the boundary layer may become turbulent earlier, this may forestall any separation. Therefore, the experimental effects of surface finish could be attributed to a combination of an increase in drag on the suction side and a decrease in drag on the pressure side. The result was a slight increase in the efficiency level with an increase in roughness.

### 5.3 INTERACTION EFFECTS

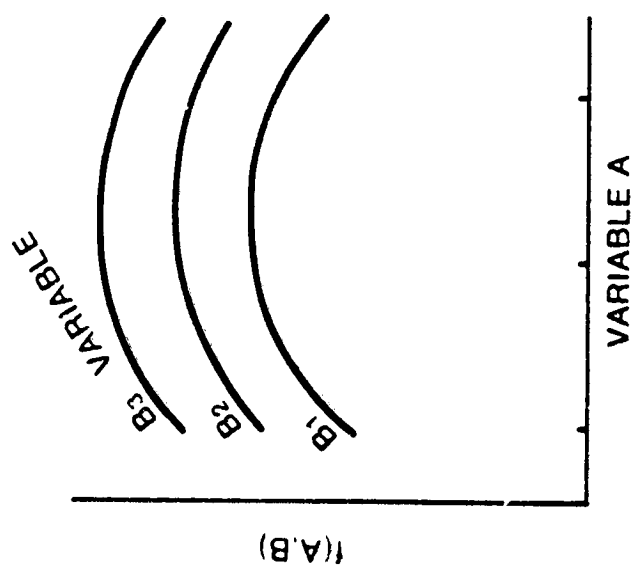
In general, when more than one variable is being investigated not only the direct effects of each variable but also the interaction between any two variables must be considered. The interactive effects of two or more variables produce results different from the sum of direct effects of individual variables. Interactive effects are illustrated schematically in Figure 21. This illustration shows that when the response curves produced by constant levels of one variable are the same shape the variables do not interact, while differences in shape (or slope) indicate that interactions exist. Direct effects are not totally separable from interaction effects.

The data presented in Figure 19 were expanded by plotting the same data as separate lines, each having another variable held constant. Figure 22 shows the 1.2 pressure ratio curve of stator efficiency versus fillet radius from Figure 19, plotted as a dashed line on three separate plots. The data used to construct this line are then plotted at constant levels of surface finish for the first plot, boundary layer thickness for the second, and turbulence level for the third. Figures 23, 24, and 25 are similar plots for 1.4, 1.7 and 2.1 pressure ratio, respectively.

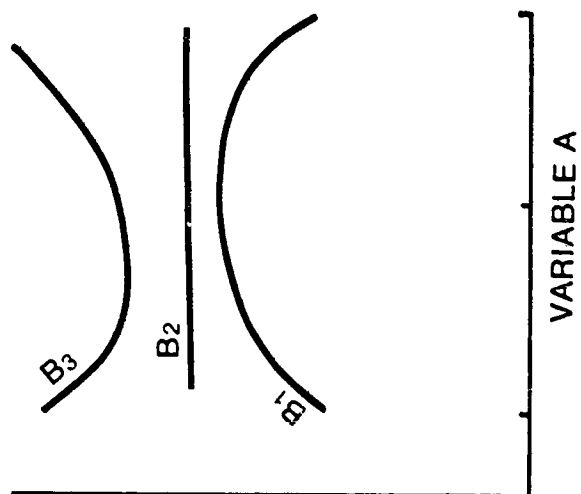
Figures 26 through 37 show similar plots to those listed above. Figures 26 through 29 show stator efficiency versus free-stream turbulence at the four pressure ratios. Figures 30 through 33 show stator efficiency versus inlet boundary layer thickness at the four pressure ratios and Figures 34 through 37 show efficiency versus surface finish at the four pressure ratios.

Examination of Figure 23 shows that fillet radius and turbulence interact at low levels of fillet radius. The 12 percent turbulence curve between zero and 0.5mm (.020 inch) has a much greater slope than the lower turbulence conditions tested. An alternative method illustrating this is seen in the contour plot (Figure 38) of the same data. These figures show that the high turbulence level combined with small fillet radius produces about 2 percent lower efficiency. The strength of the interaction is indicated by the magnitude of the change in efficiency level.

ORIGINAL PAGE IS  
OF POOR QUALITY



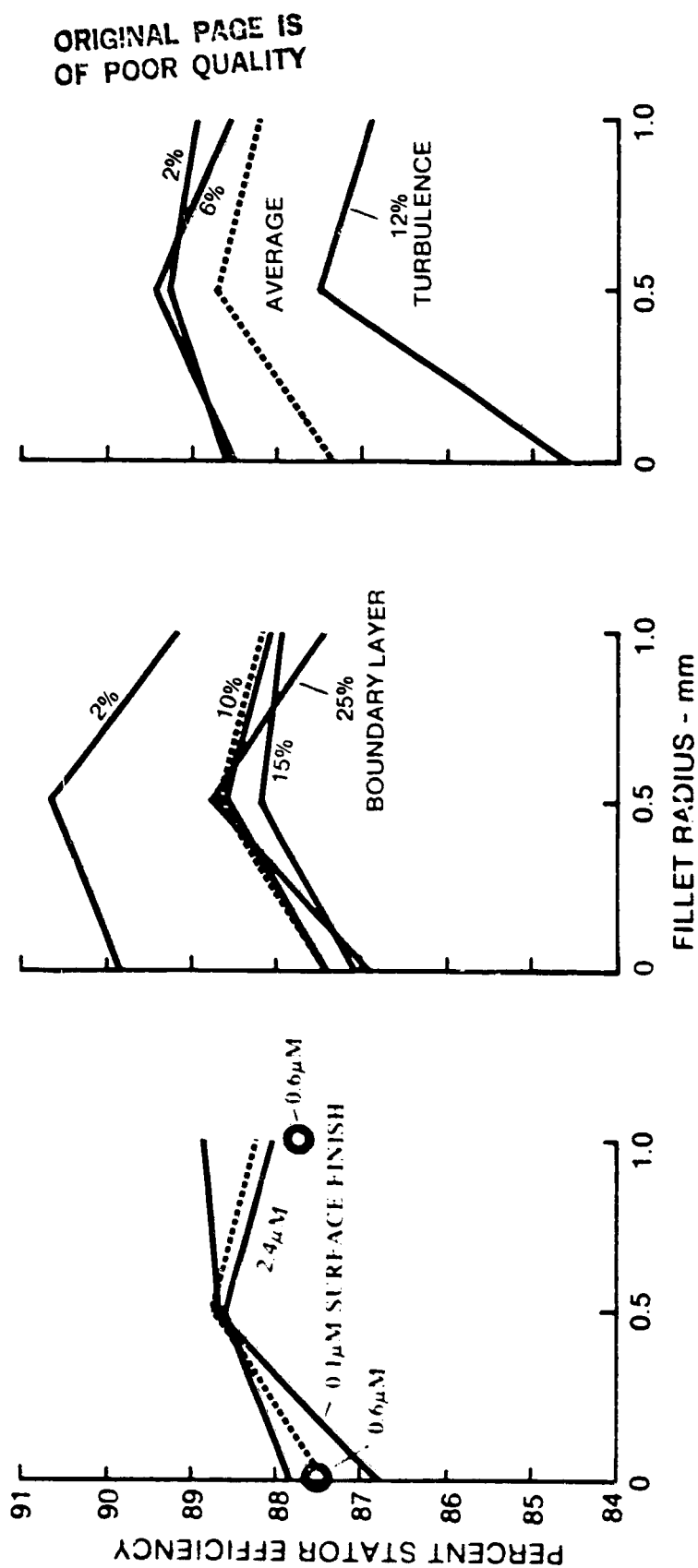
A and B DO NOT INTERACT



A and B INTERACT

BF1122

Figure 21. Example of Variable Interactions



BF1101

Figure 22. Efficiency Versus Fillet Radius at 1.2 Pressure Ratio

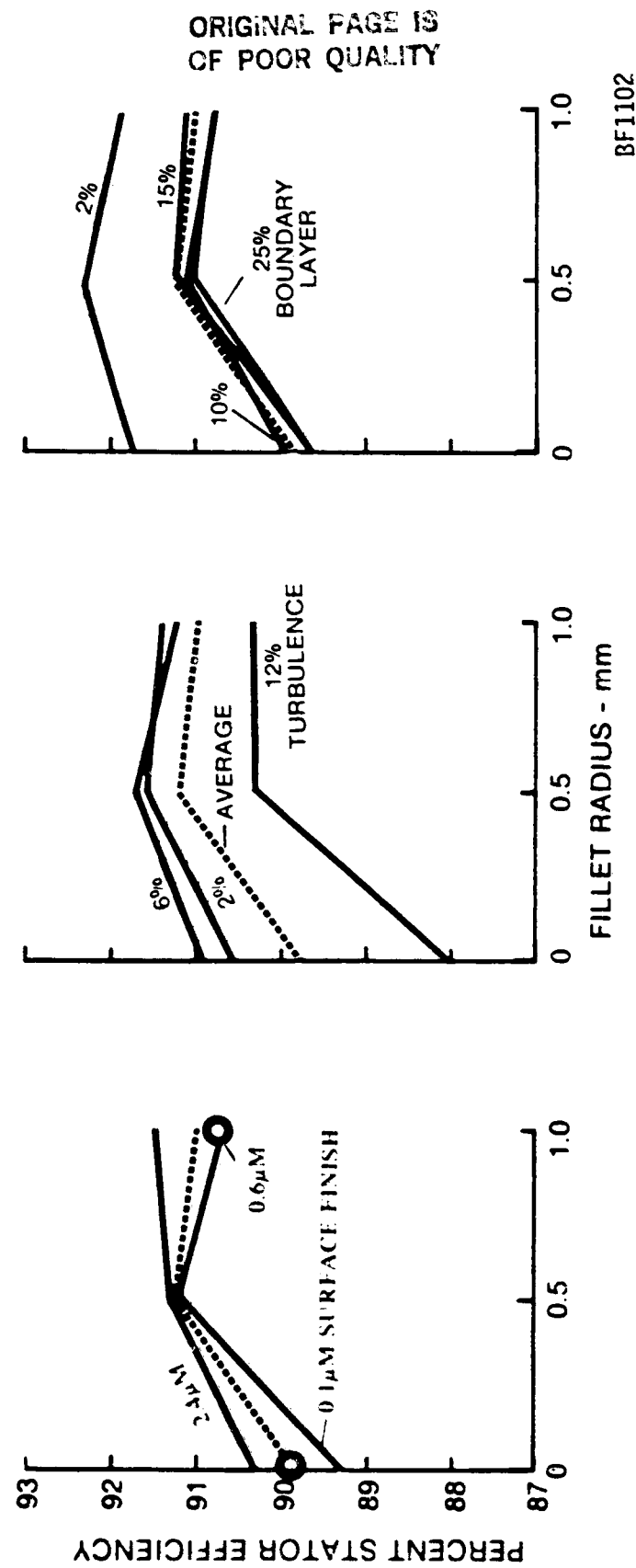


Figure 23. Efficiency Versus Fillet Radius at 1.4 Pressure Ratio

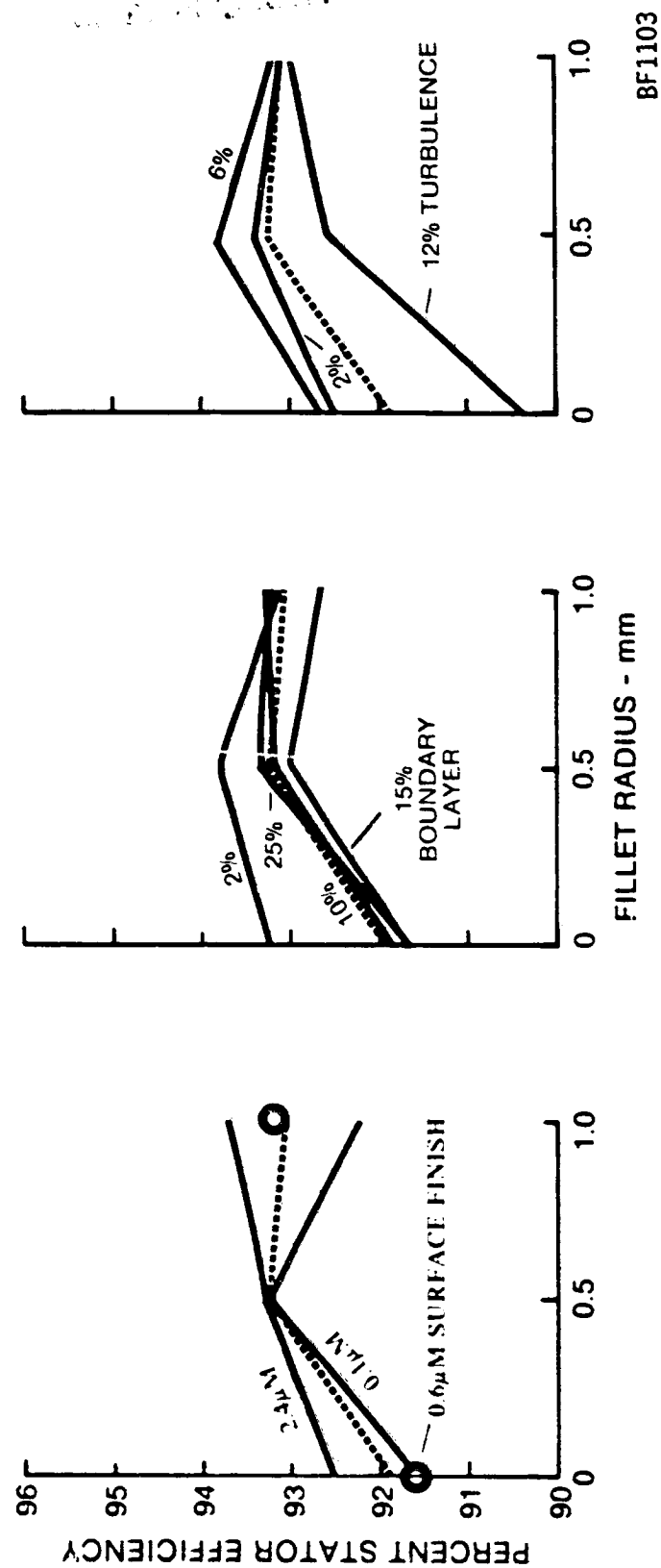


Figure 24. Efficiency Versus Fillet Radius at 1.7 Pressure Ratio

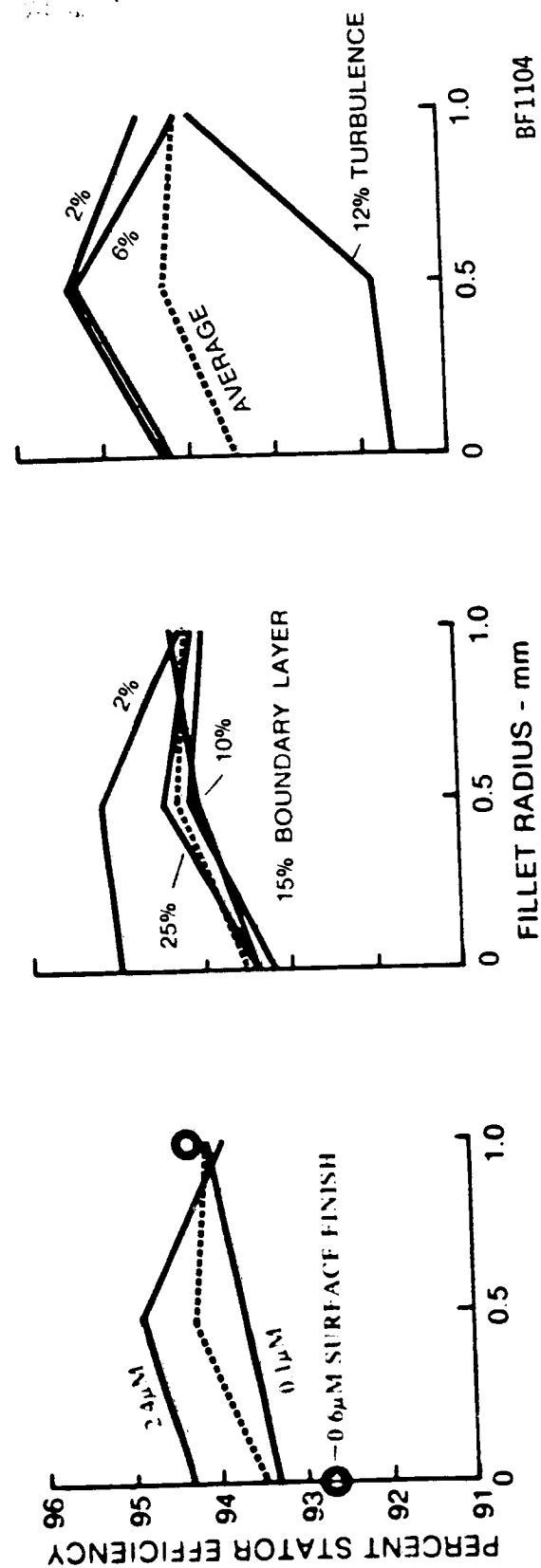


Figure 25. Efficiency Versus Fillet Radius at 2.1 Pressure Ratio

ORIGINAL PAGE IS  
OF POOR QUALITY

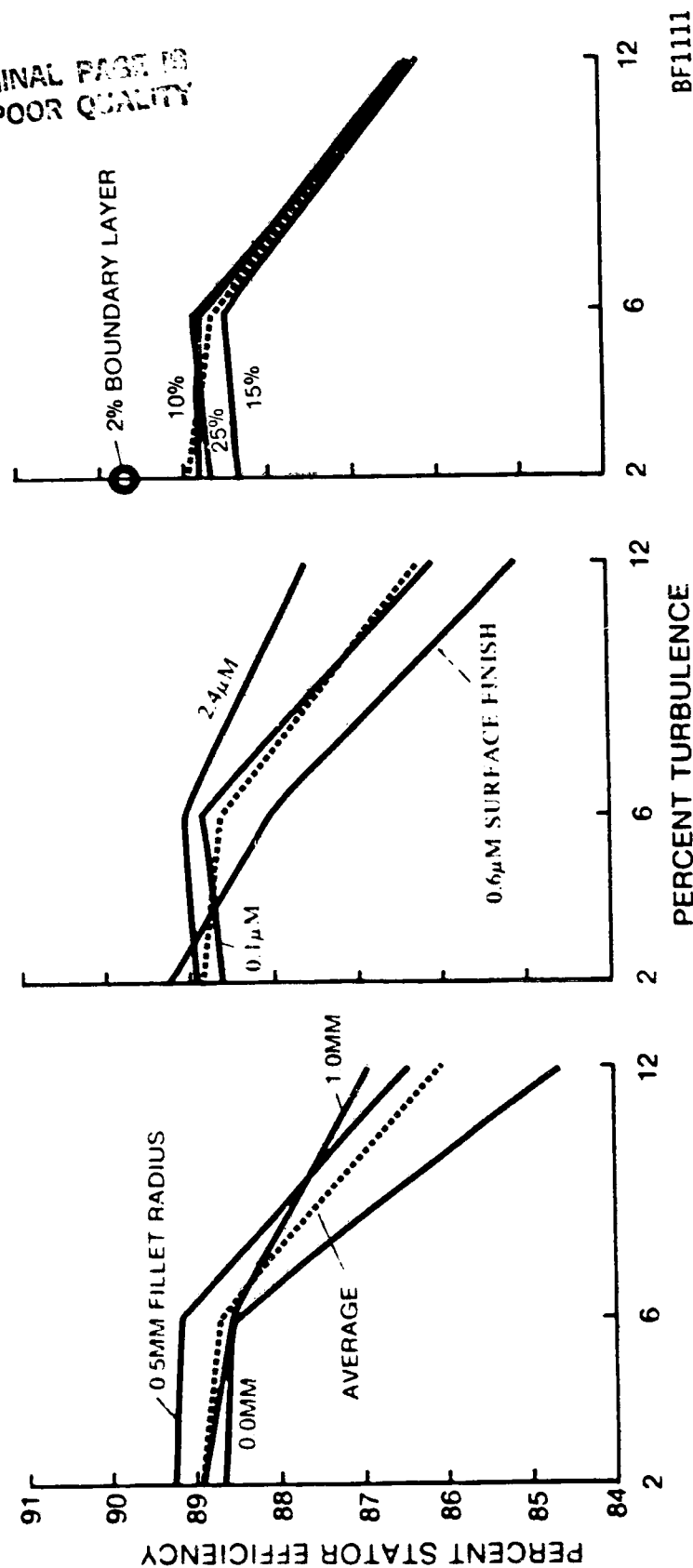


Figure 26. Efficiency Versus Turbulence at Pressure 1.2 Ratio

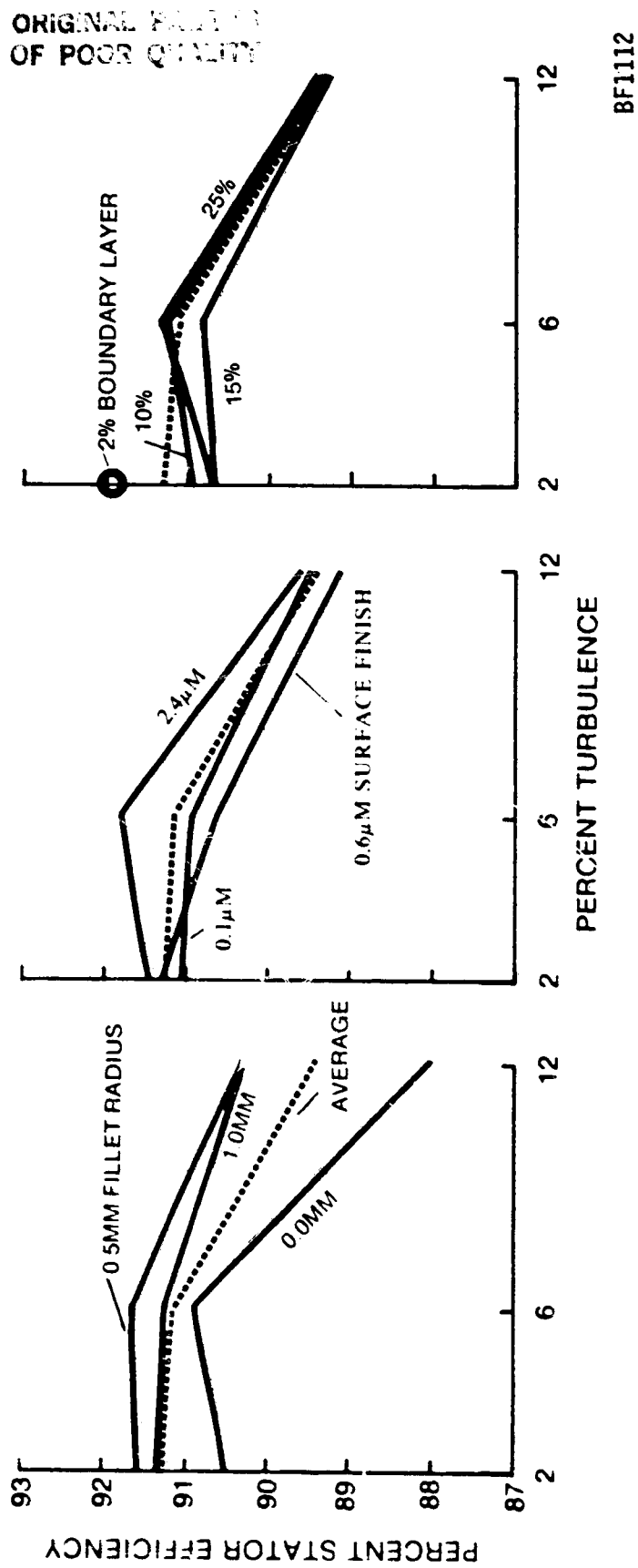


Figure 27. Efficiency Versus Turbulence at 1.4 Pressure Ratio



ORIGINAL PAGE IS  
OF POOR QUALITY

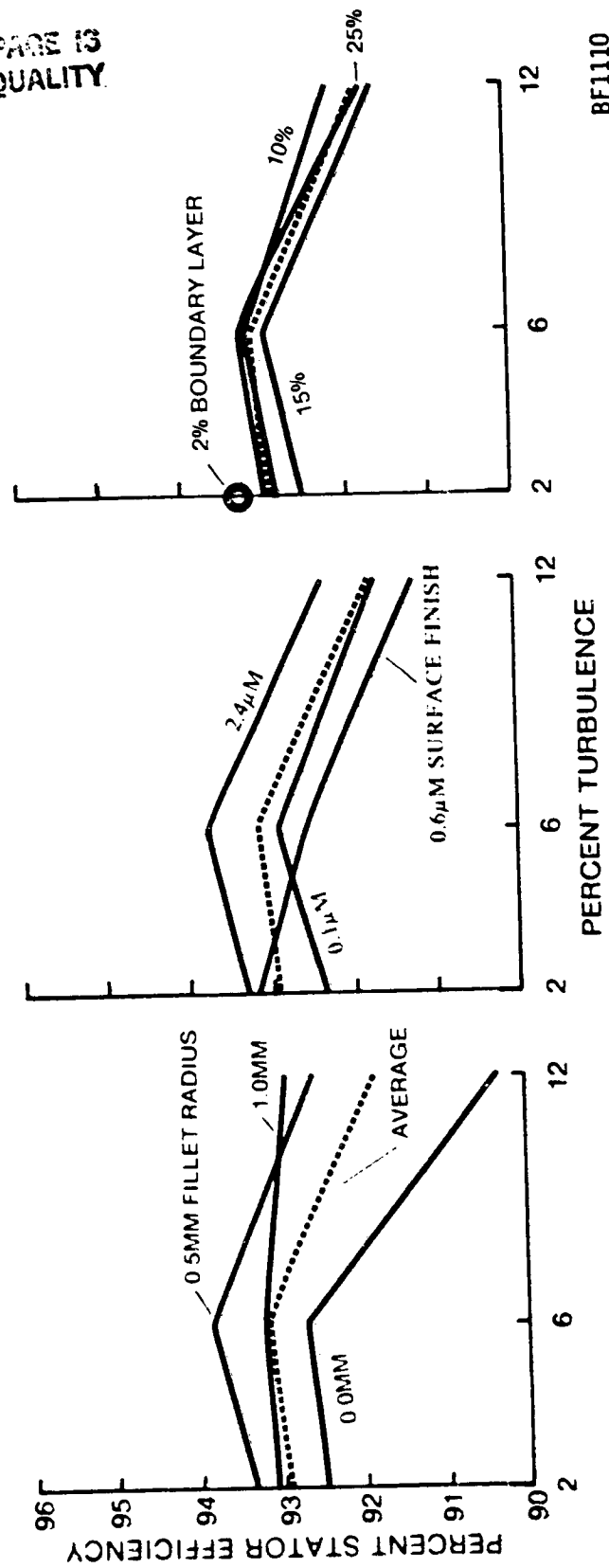
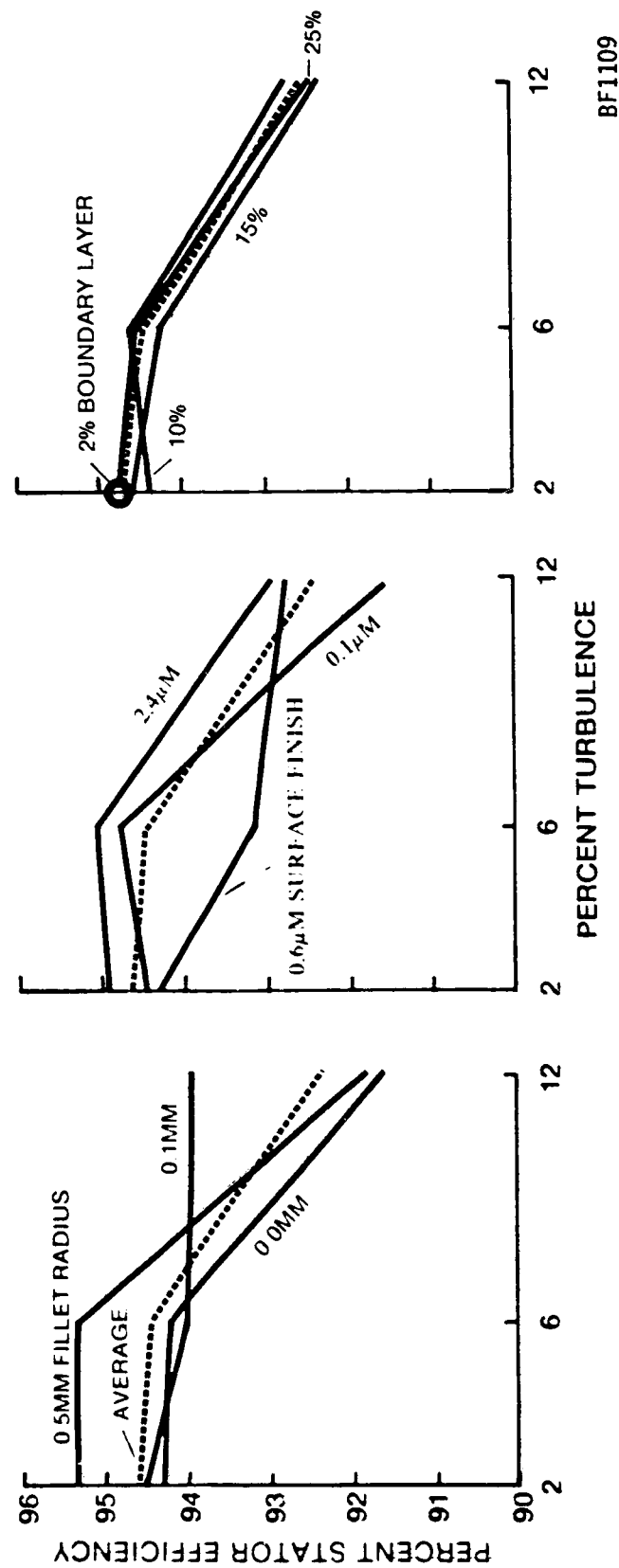


Figure 28. Efficiency Versus Turbulence at 1.7 Pressure Ratio

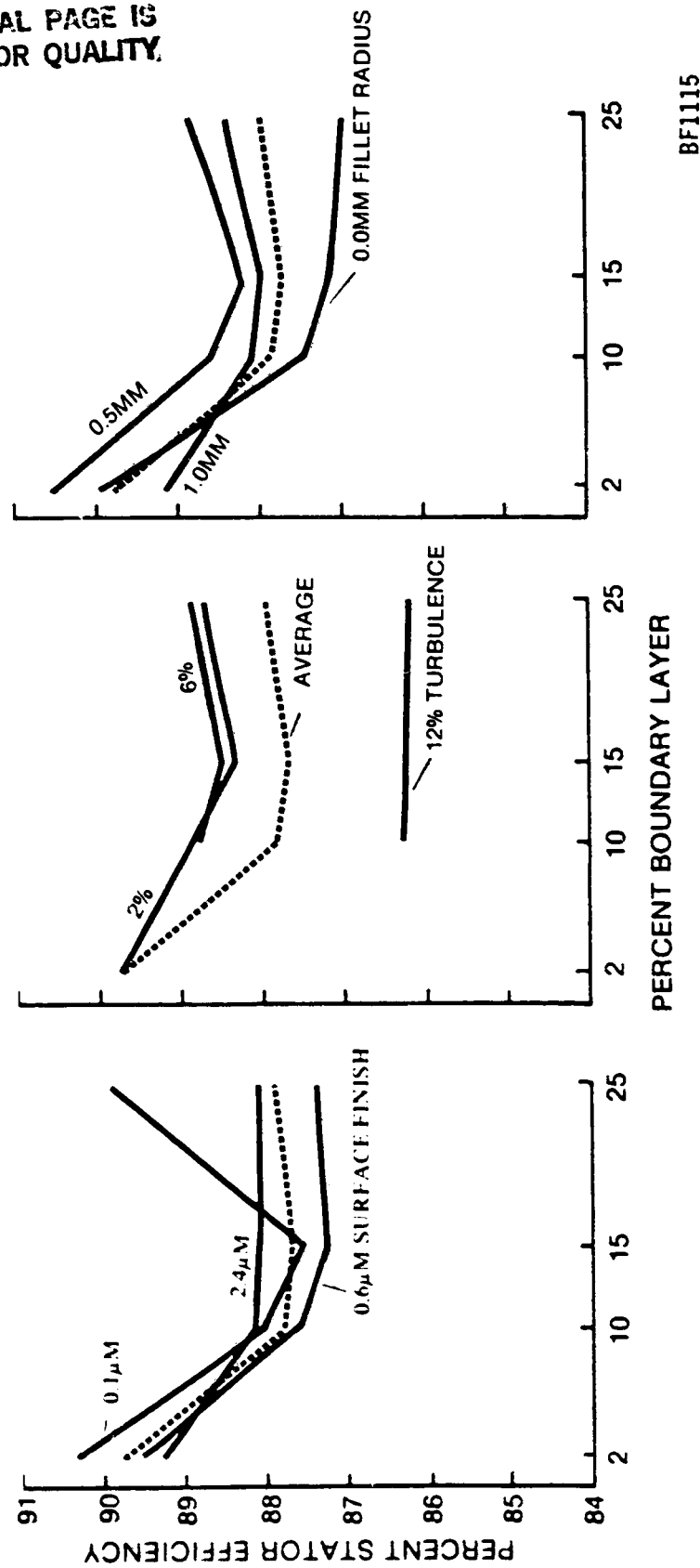
ORIGINAL PAGE IS  
OF POOR QUALITY



BF1109

Figure 29. Efficiency Versus Turbulence at 2.1 Pressure Ratio

ORIGINAL PAGE IS  
OF POOR QUALITY.



BF1115

Figure 30. Efficiency Versus Boundary Layer at 1.2 Pressure Ratio

ORIGINAL PAGE IS  
OF POOR QUALITY

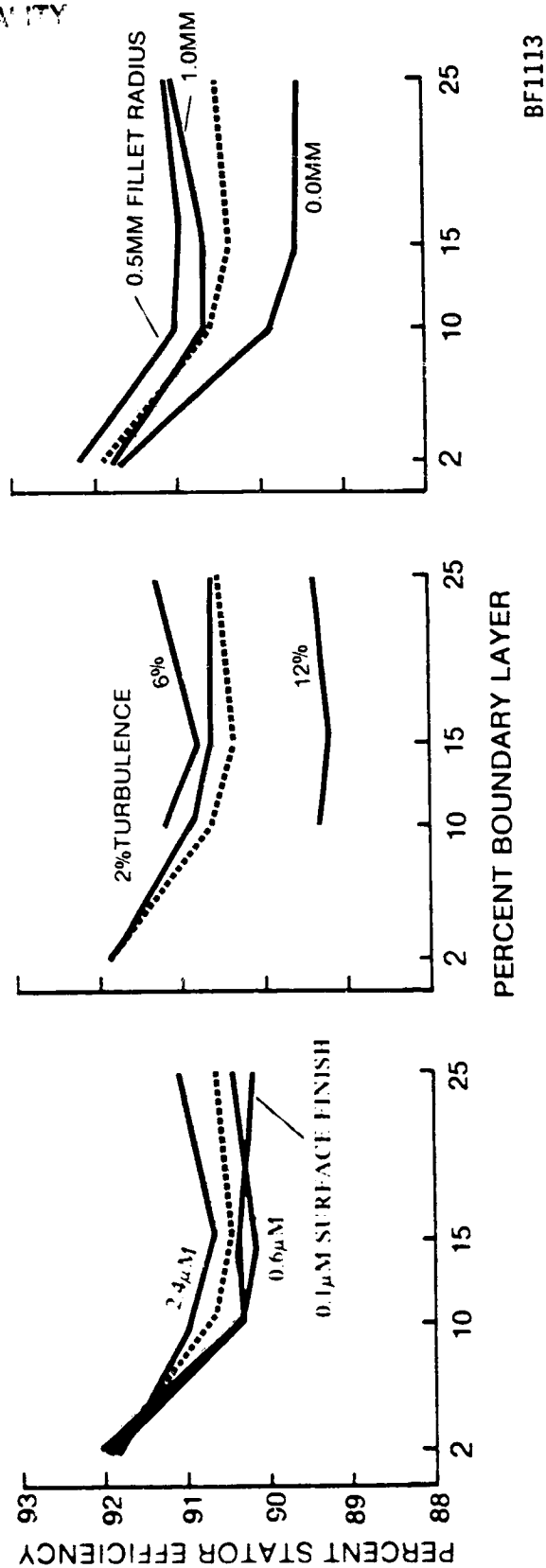


Figure 31. Efficiency Versus Boundary Layer at 1.4 Pressure Ratio

ORIGINAL PAGE IS  
OF POOR QUALITY

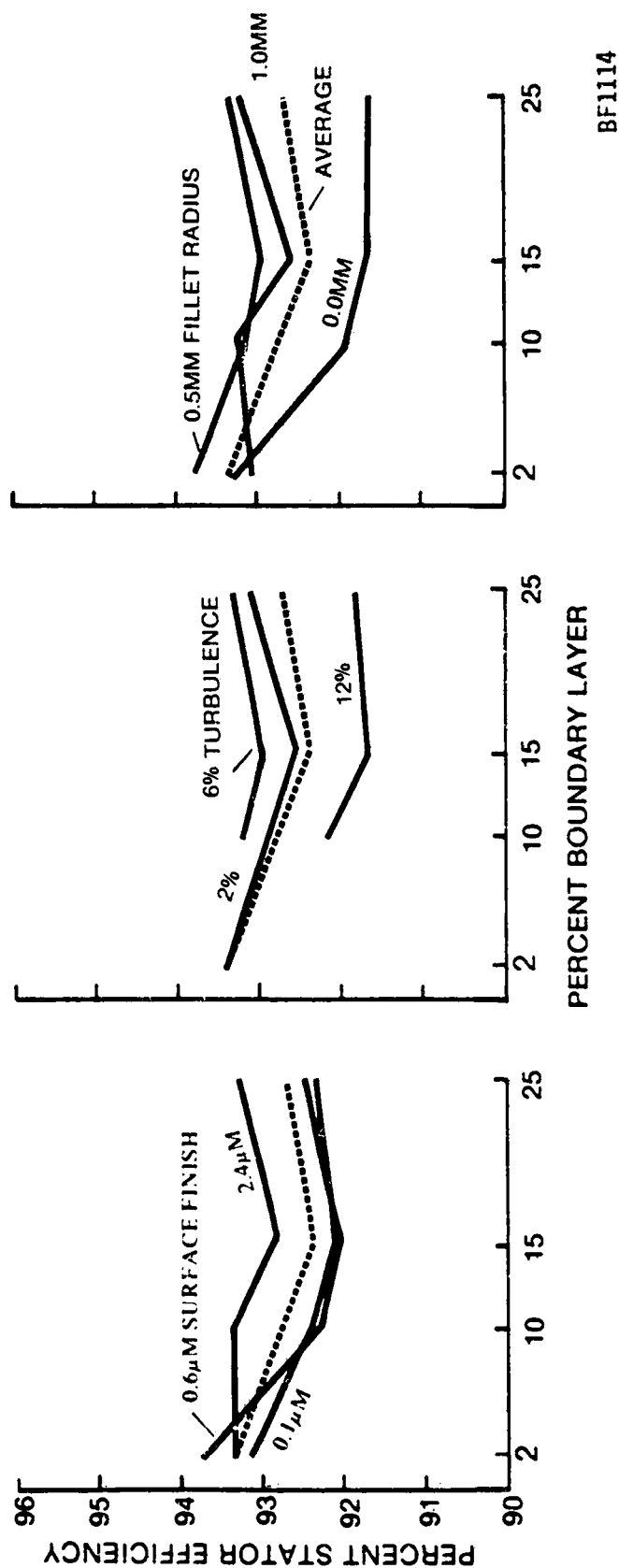
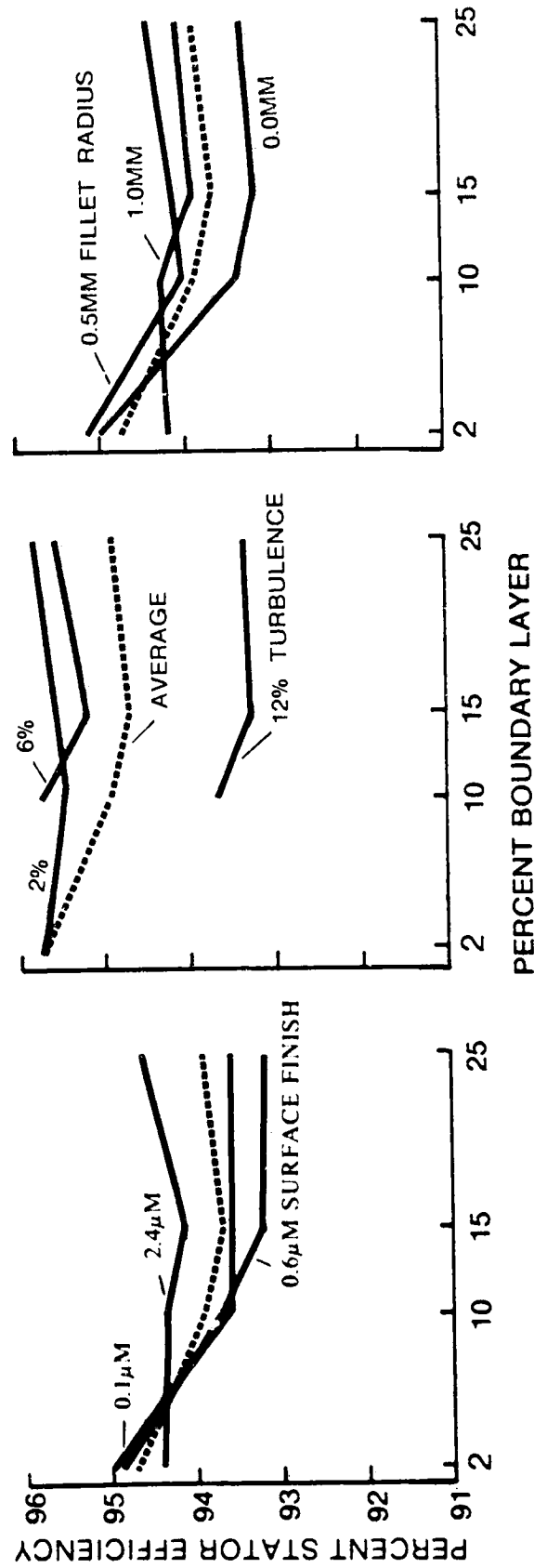


Figure 32. Efficiency Versus Boundary Layer at 1.7 Pressure Ratio

ORIGINAL PAGE IS  
OF POOR QUALITY



BF1116

Figure 33. Efficiency Versus Boundary Layer at 2.1 Pressure Ratio

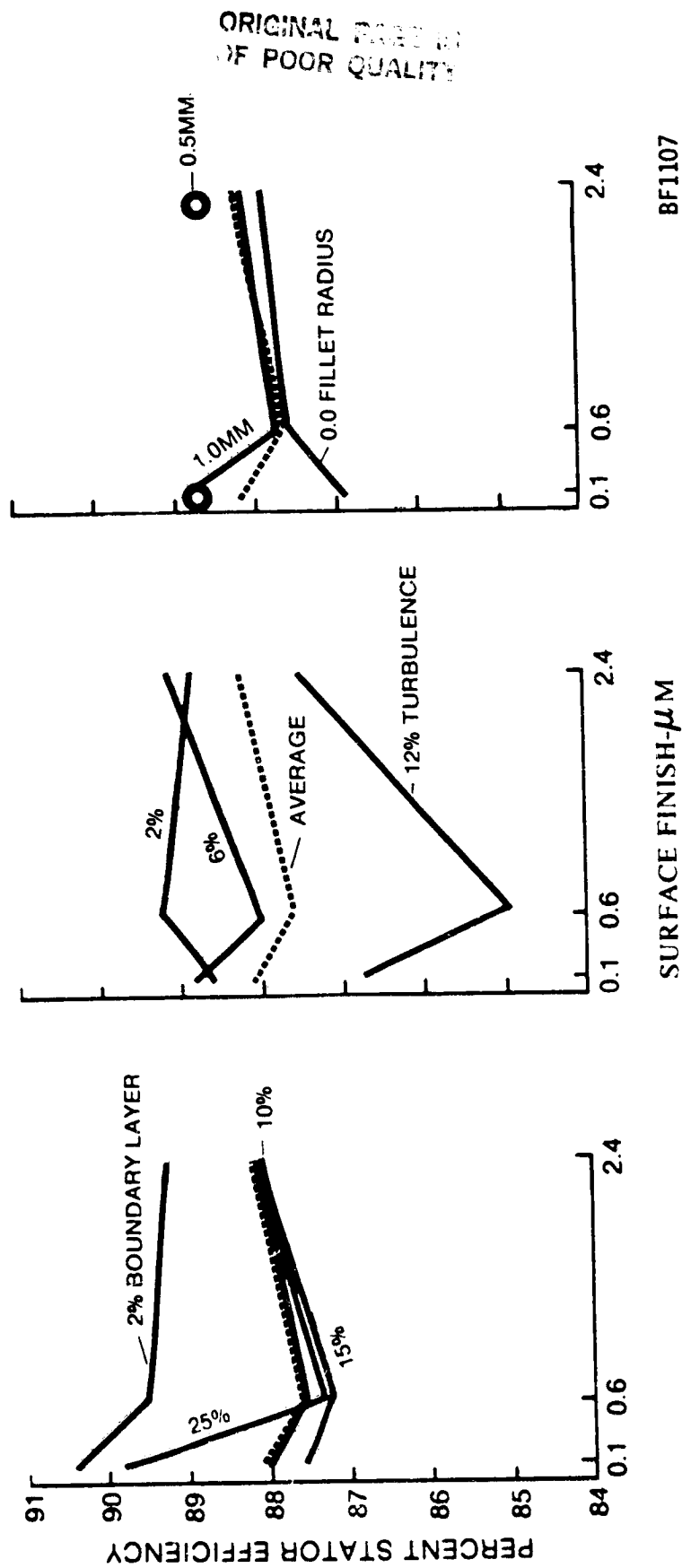


Figure 34. Efficiency Versus Surface Finish at 1.2 Pressure Ratio

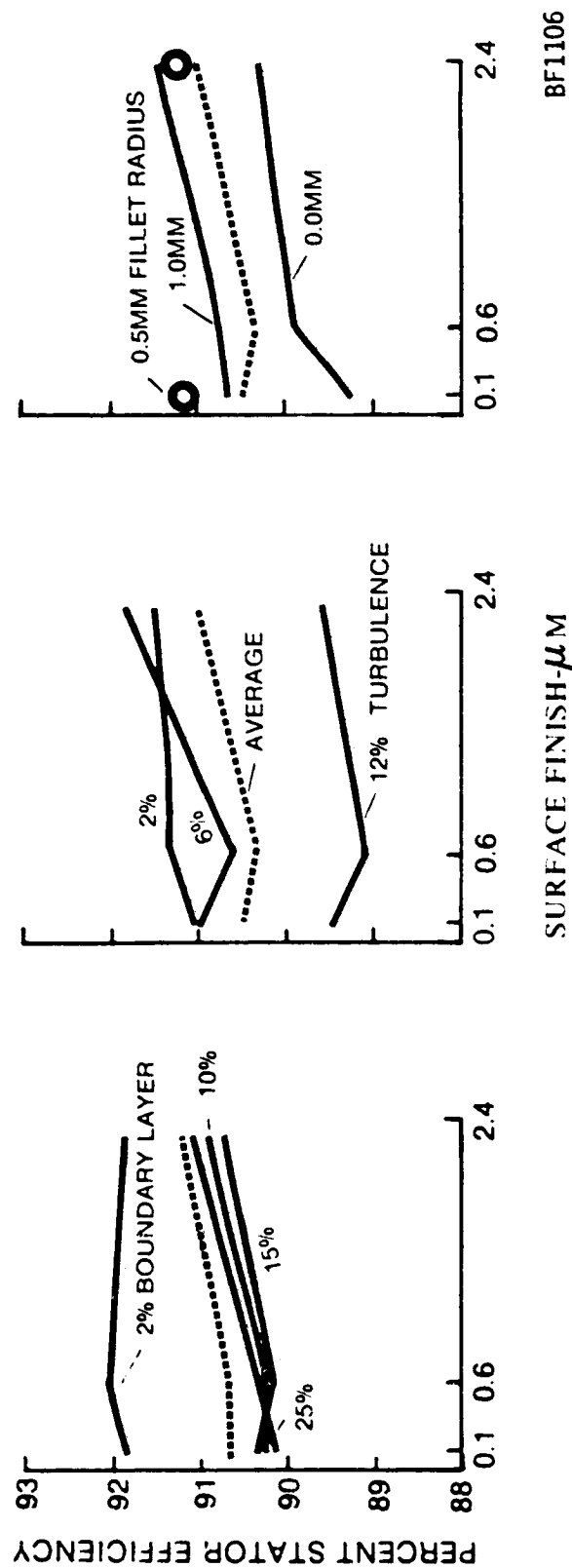
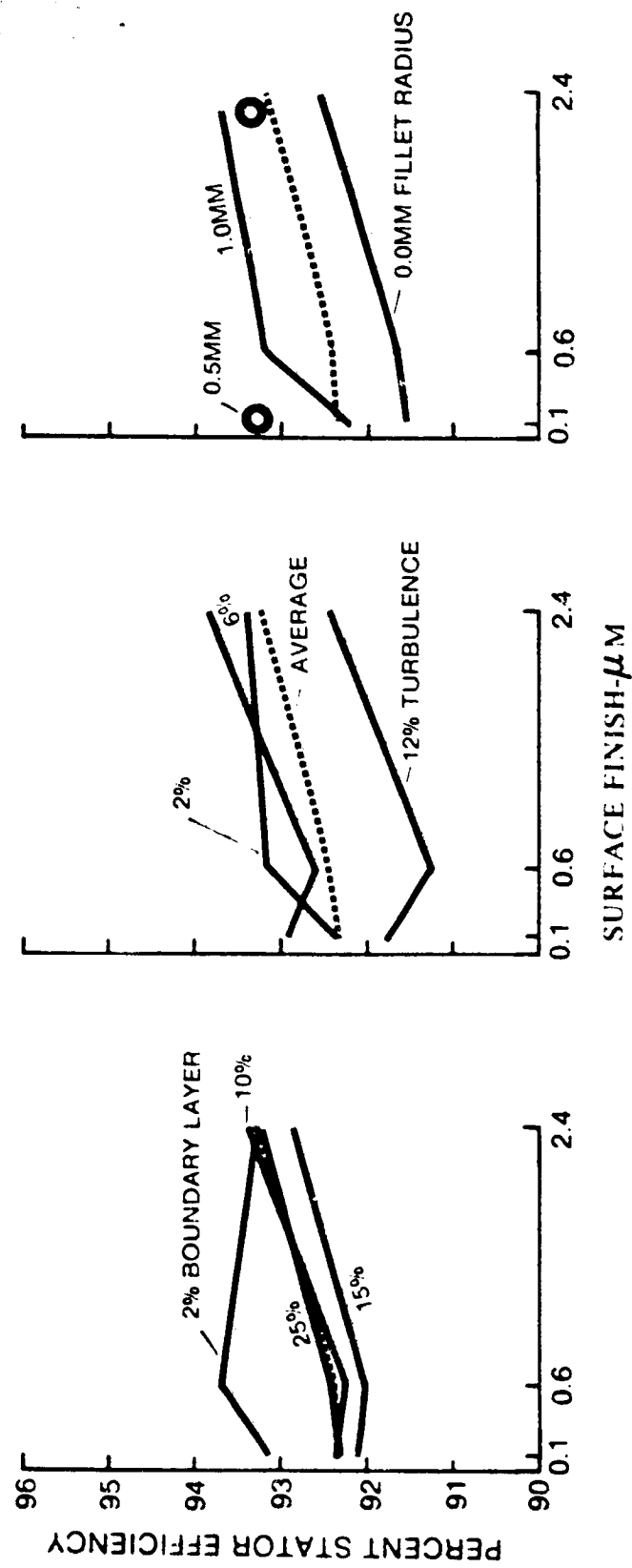


Figure 35. Efficiency Versus Surface Finish at 1.4 Pressure Ratio





BF1108

Figure 36. Efficiency Versus Surface Finish at 1.7 Pressure Ratio

ORIGINAL PAGE IS  
OF POOR QUALITY

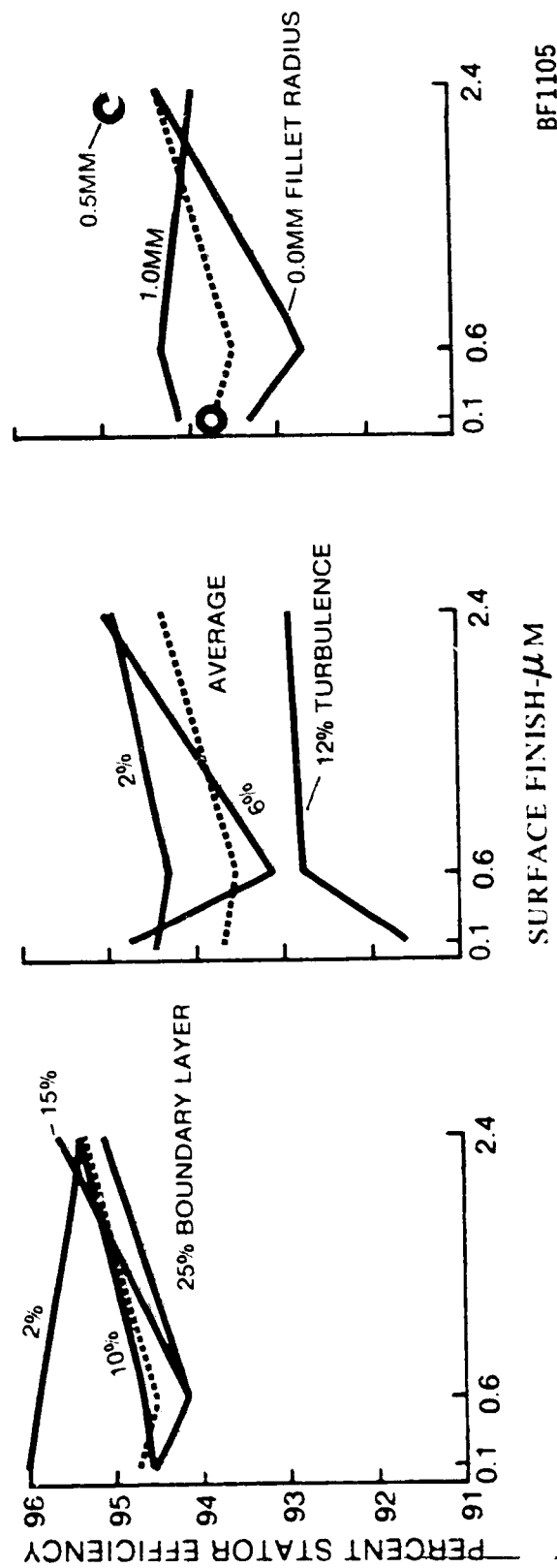


Figure 37. Efficiency Versus Surface Finish at 2.1 Pressure Ratio

ORIGINAL PAGE IS  
OF POOR QUALITY

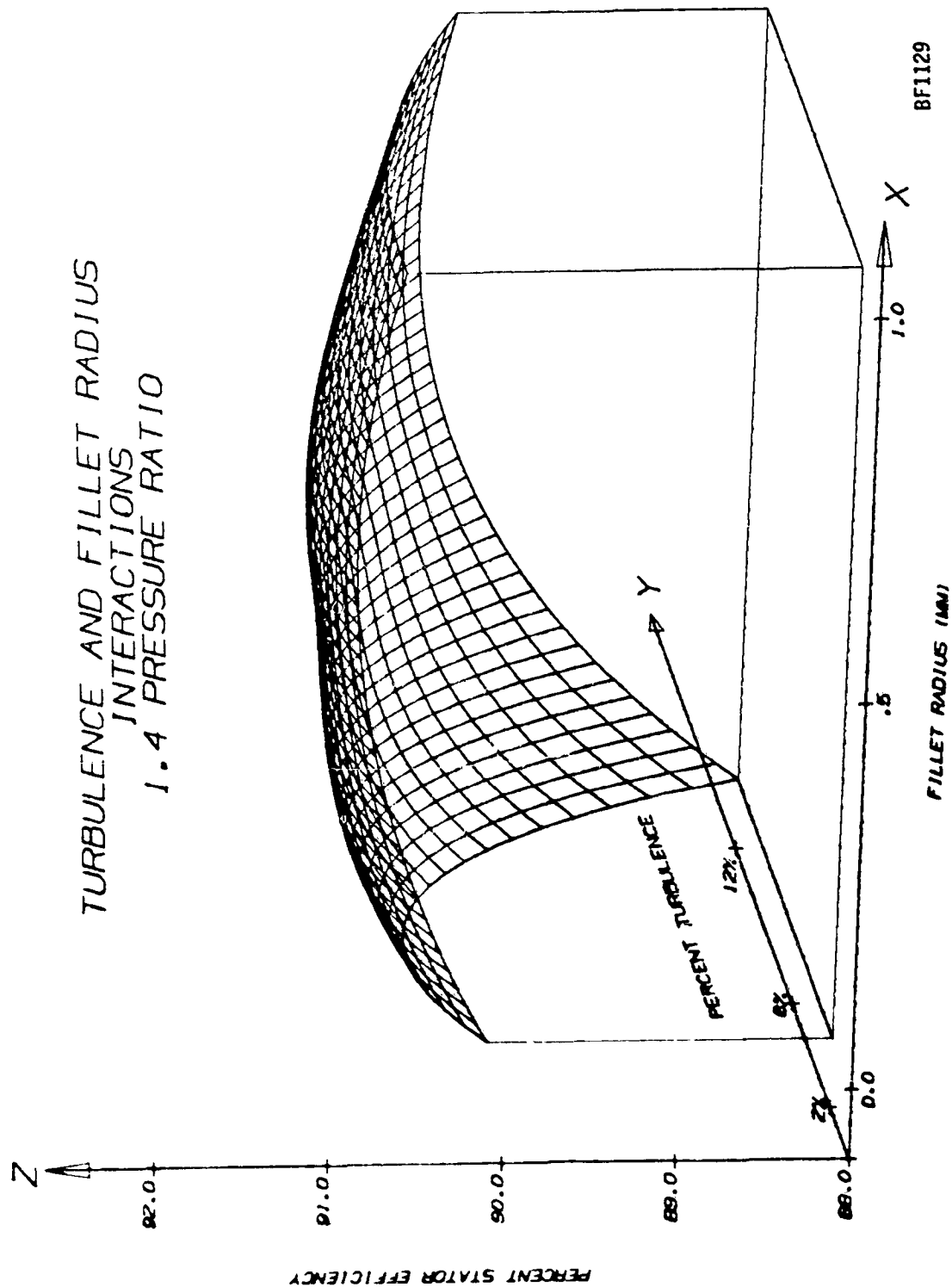


Figure 38. Plot of Turbulence and Fillet Radius Interaction

This strong interaction seems to indicate that the mechanism by which turbulence affects loss in a stator is, to a large extent, involved with the flow near the junction of the vanes with the endwalls. Two of the well known mechanisms of loss that operate near the shroud vane junction are described by Langston (Reference 10). The inlet boundary layer separates and forms a horseshoe (or leading edge) vortex, with one leg of the vortex in one airfoil passage and the other in the adjacent passage. The larger passage vortex migrates from the pressure side of the vane and flows to the suction side. The corner vortex remains in the suction surface end-wall corner and is much smaller than the horseshoe vortex. High levels of turbulence could possibly stimulate local corner separations that would trip an additional vortex formation and tertiary flow which is independent of the secondary flows. L.L. Dubruge (Reference 3) mentions such a separation and vortex formation in a fillet radius investigation. The larger fillet radii could reduce the chances of such a separation or simply delay the separation point and, thereby, reduce the losses.

Fillet radius and surface finish have a weaker interaction than the fillet radius and turbulence interaction as depicted in Figures 23 and 39. The point that differs most from the other data is the 0.0 mm fillet radius and 0.1  $\mu$  m (4  $\mu$  inch) surface finish case. The efficiency level varies from the other fillet radius-surface finish configurations by an average of about 1.5 percent. Even though the very smooth finish at the wall could promote local laminar separations and vortex formations, a rougher surface may tend to create a turbulent boundary layer that could forestall any separation and/or vortex formation.

The turbulence-surface finish interaction is weak, as shown in Figures 27 and 40. This indicates a trend of reduced efficiency at the highest turbulence levels for all surface finishes. The 0.6  $\mu$  m (25  $\mu$  inch) surface finish and 6 percent turbulence level combination show a lower efficiency level than would be expected if the point were extrapolated from the other data. This anomaly is difficult to explain, but a likely candidate is the Reynolds number effects.

The remaining first order interactions are weaker and cannot be clearly identified with certainty. Second order interactions, which require three variables to interact, cannot be readily detected using graphical interpretation. Section 5.5 will discuss second-order interactions determined using statistical means.

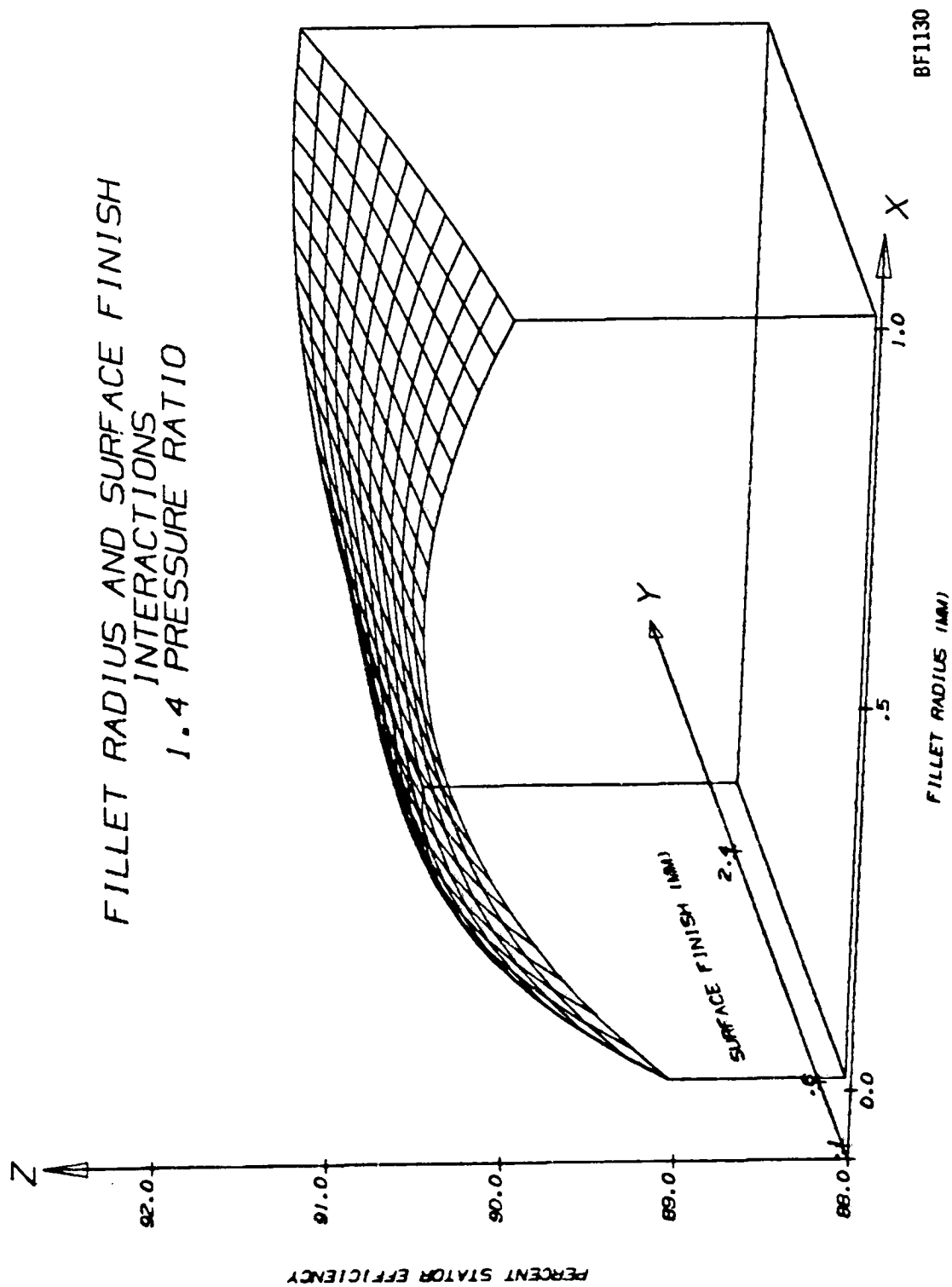
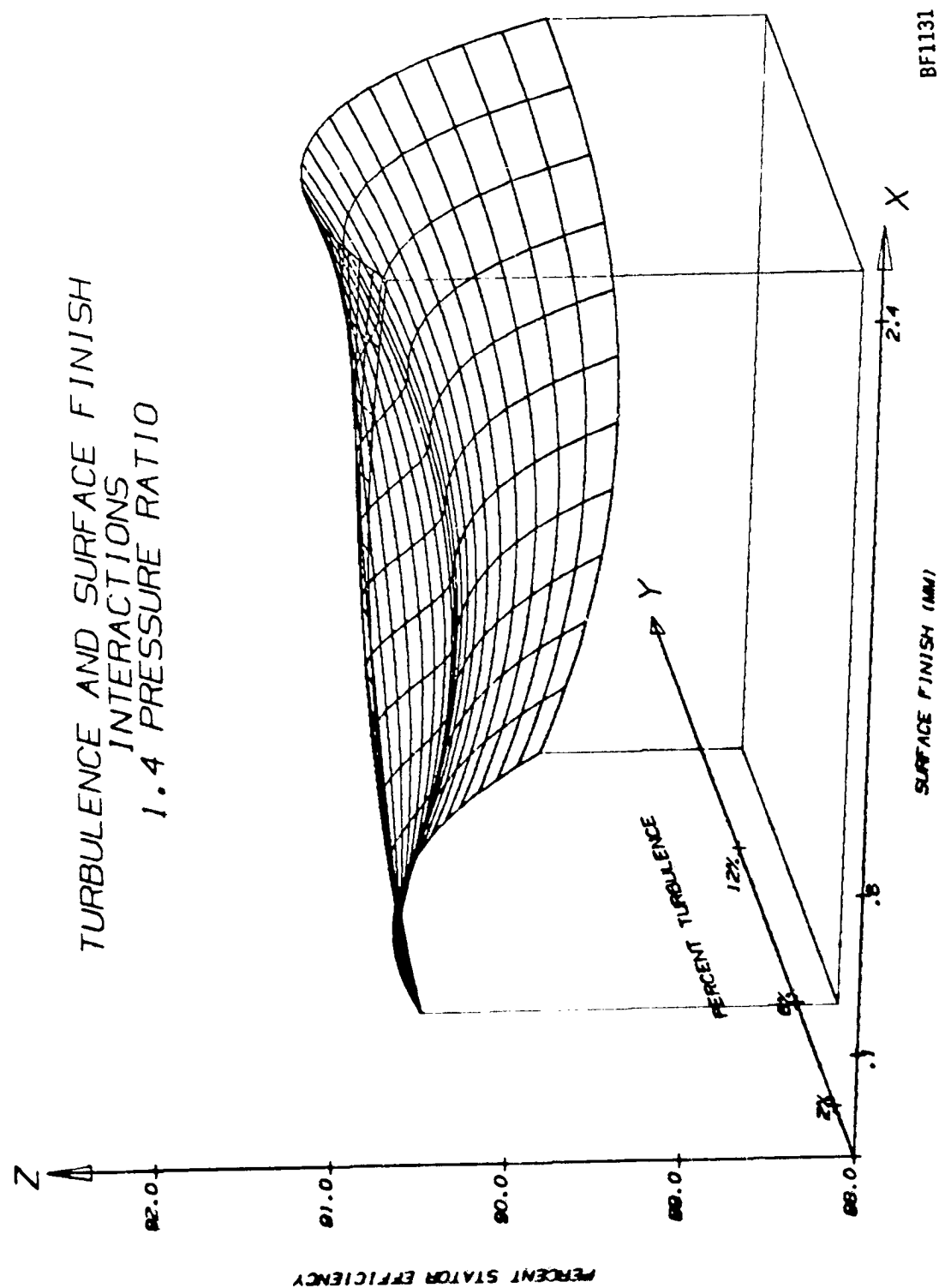


Figure 39. Plot of Fillet Radius and Surface Finish Interaction



ORIGINAL PAGE IS  
OF POOR QUALITY

Figure 40. Plot of Turbulence and Surface Finish Interaction

#### 5.4 COMPARISON WITH FULL-SCALE RESULTS

The full-size stator test (Reference 2) using conventional aerodynamic measurements to determine stator performance was performed with a low loss inlet system and with reasonably smooth surface finish and small fillet radius. This condition was most closely matched by testing the scaled cascade with 2 percent turbulence, 2 percent boundary layer,  $0.1 \mu m$  ( $4 \mu$  inch) surface finish, and zero fillet radius. The overall performance for the full size and one-sixth scale, as well as the predicted one-sixth scale performance, is shown in Figure 41. By definition, the kinetic energy loss coefficient plus the stator efficiency equals unity.

The performance curve for the full-size stator shows values of annular sector blade-exit kinetic energy loss coefficients, which include the loss in kinetic energy caused by surface friction of the blade, pressure loss of the trailing edge, friction of the end walls, and the mixing loss resulting from momentum exchange between the free-stream fluid and the lower velocity fluid from the loss regions.

The loss computed for the scaled cascade is shown. The effects of Reynolds number on the scaled stator losses was estimated from the empirical Soderberg correlation (Reference 5) and applied to the full-scale after-mix kinetic energy loss coefficients. The Reynolds numbers based on throat hydraulic diameter were  $1.8 \times 10^5$  to  $2.5 \times 10^5$  and  $2.9 \times 10^4$  to  $4.0 \times 10^4$  for the full and scaled testing respectively. The measured losses were nearly matched at design pressure ratio, but there was a larger difference at lower pressure ratios. The remaining loss may result from other scaling effects or from the method used to calculate performance using the reaction torque measurement.

Horlock (Reference 5) states that Reynolds number effects are dependent on blade shape which will affect boundary layer growth on the blade surfaces, and hence, the losses. He also maintains that the work of several researchers implies a critical Reynolds number (based on hydraulic diameter  $D_h$ ) around  $10^5$ , which may alter the Soderberg prediction.

Since the testing conducted under this program did not address Reynolds number as a test variable, the effect is uncertain. A Reynolds number investigation would be required to accurately determine its effect.

The equivalent mass flows of the full and one-sixth scale stator test results (Figure 42) were compared. The one-sixth scale stator test referred mass flow was scaled up by a factor of 36, for comparison with the full-scale flow (Reference 2), and this was plotted against pressure ratio. Figure 42 shows that the two referred mass-flow rates are nearly identical. The measured full-scale flow angle from Reference 2 also matched the calculated one-sixth scale stator flow angle. This indicates that the scaled stator was properly manufactured.

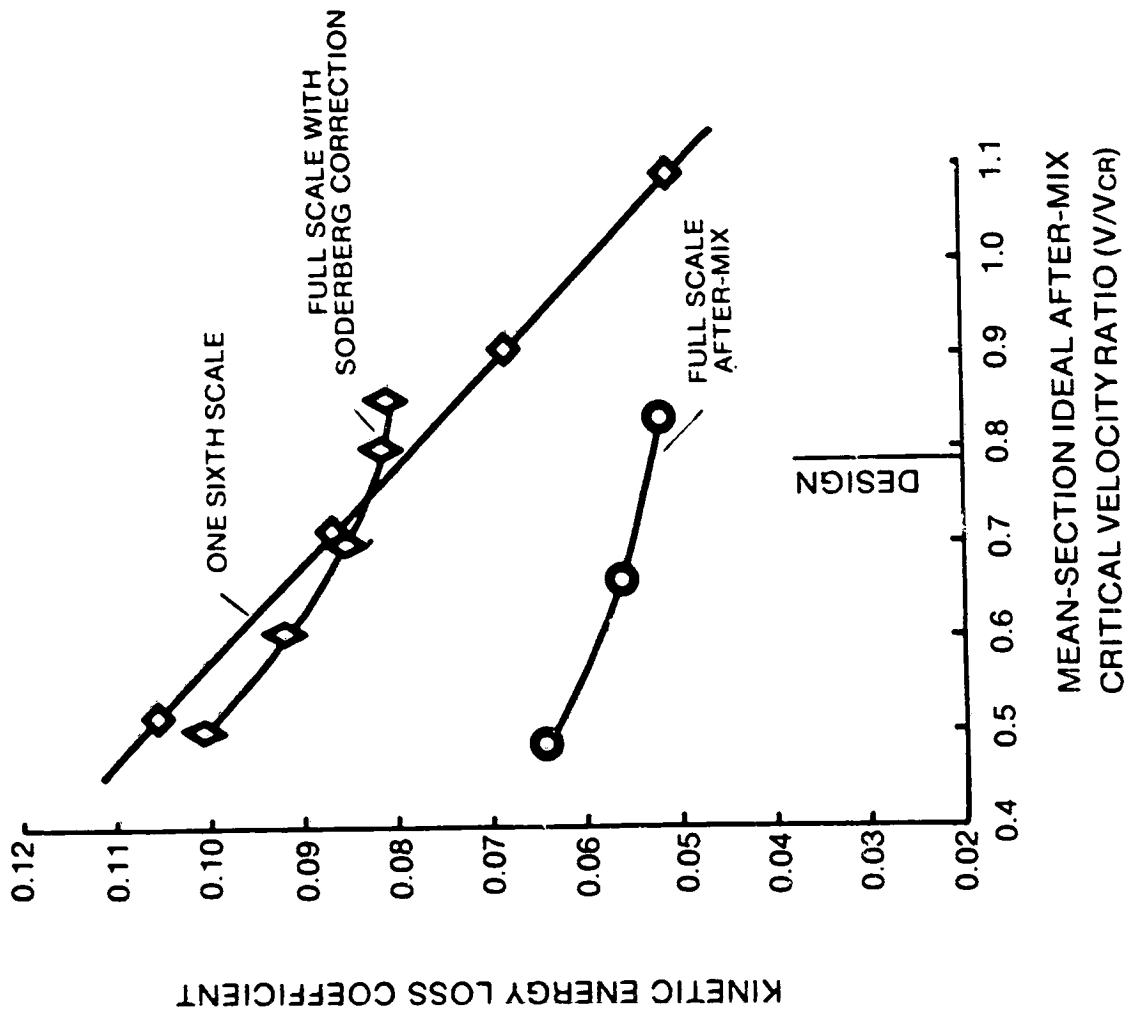


Figure 41. Kinetic Energy Loss Coefficient Versus Critical Velocity Ratio for Full-Scale and One-Sixth Scale Test



ORIGINAL PAGE IS  
OF POOR QUALITY

BF1124

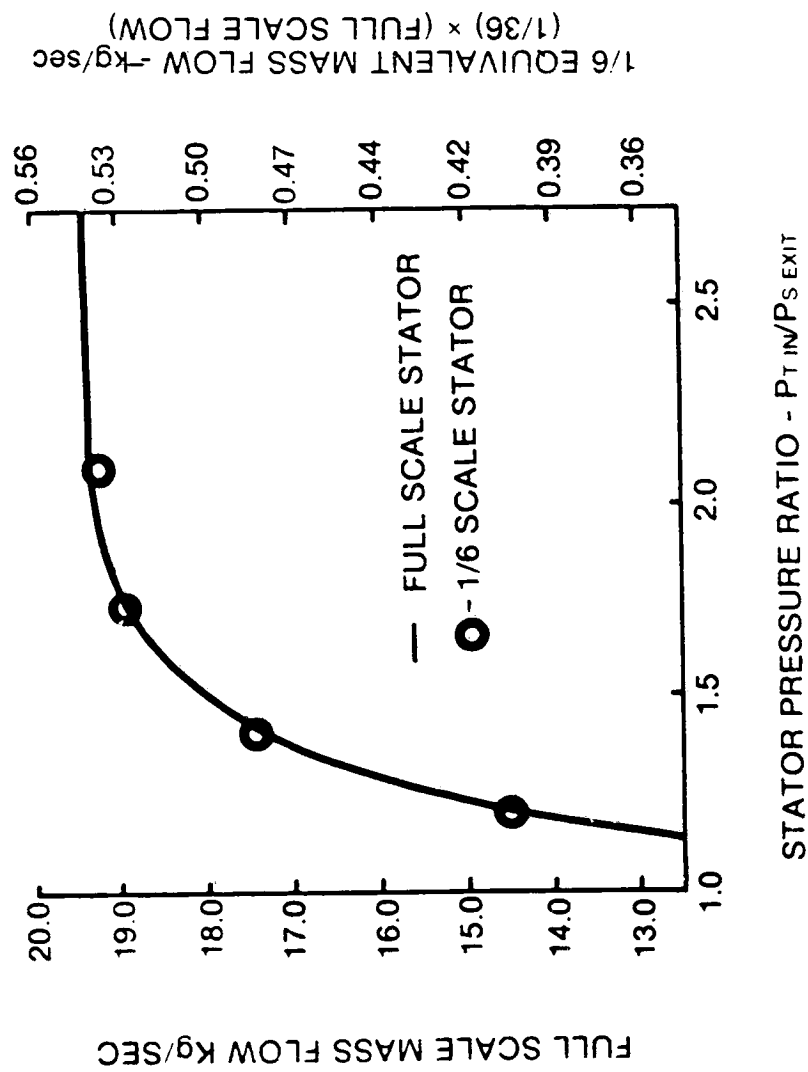


Figure 42. Equivalent Weight Flow Versus Pressure Ratio for Full-Scale and Scaled Stators

## 5.5 STATISTICAL ANALYSIS

Test data were statistically analyzed using the analysis-of-variance (ANOVA) method. This was only performed for the 1.4 pressure ratio since it was the closest to design. These data are in the form of a 3x3x3 matrix. The matrix lacked test data for the 0.6  $\mu$  m (25  $\mu$  inch) surface finish, 0.5 mm (.020 inch) fillet radius case.

The missing test data were estimated by finding values that would minimize the residual variation in standard ANOVA formulae. The degrees of freedom (sample size) were reduced accordingly. This statistical method is basically a way of estimating the missing data by interpolating all of the available test data. This method will give a valid answer if there are no radical fluctuations in the data at the point being estimated.

The above analysis assumed that each level of test variable was of a fixed value throughout the test matrix.

The analysis indicated the relative strength of:

1. Each variable alone which is a direct effect
2. First order interactions that represent the effects produced by combinations of any two variables
3. Second order interactions that are the effects produced by combinations of three variables and,
4. Residuals or error unexplained by the above three.

The results of the statistical analysis are summarized in Table XVI. The relative importance of each variable is determined by the magnitude of the sum of squares term. This is also true of first and second order interactions. However, the relative strength of the direct effect of a variable compared with an interaction cannot be determined by this method. Thus, this significance gives an idea of the order of magnitude of the effects relative to each other. A more in-depth look at the data is needed to establish the relative strengths of the direct effects and interactions.

The direct effect of inlet boundary layer from the 2 to 10 percent level decreased the stator efficiency level up to 2 percent. There was no significant change between the 10, 15, and 25 percent boundary layers. Also, the inlet boundary layer did not interact with any other variable.

The direct effect of turbulence indicates no significant change from the 2 to 6 percent levels, however, there is a 1.5 percent drop in efficiency level in going to the 12 percent turbulent level.

TABLE XVI. STATISCAL RESULTS

## (ANALYSIS OF VARIANCE)

Source	Sum of Squares	Degrees of Freedom	Variance	Significance
Turbulence (T) .....	43.091	2	21.545	**
Finish (F) .....	5.503	2	2.752	**
Radius (R) .....	28.317	2	14.159	**
Boundary Layer (B) .....	0.448	2	0.224	***
TF .....	5.601	4	1.400	*
TR .....	11.731	4	2.933	**
TB .....	1.104	4	0.276	
FR .....	4.117	3	1.392	*
FB .....	0.605	4	0.151	
RB .....	1.345	4		
TFR .....	10.857	6	1.809	**
TFB .....	1.140	8	0.518	
TRB .....	2.493	8	0.312	
FRB .....	2.576	6	0.429	
Residual .....	3.096	12	0.258	
Total		71		

\* Weak indication of presence (95% Conf.)

\*\* Strong indication of presence (95% Conf.)

\*\*\* 2% boundary layer not averaged in analysis. 10%, 15%, and 25% boundary layer show no significant variation. However, the 2% boundary layer does show variation from the other three and there is a 99% confidence that the variation is real.

Definitions of headings in above chart -

Sum of Squares - The sum of the squared deviations of each point or average from the mean value

Degree of Freedom - The number of points averaged minus one

Variance - Sum of Squares divided by Degrees of Freedom

Residual - The Sum of Squares of all data is partitioned into assignable causes; residuals are that part of the Sum of Squares which cannot be explained; therefore, it is considered to be random error.

There is an optimum fillet radius between zero and 1.0 mm (.040 inch) fillets. The 0.0 mm fillet is about 1 percent lower in efficiency level than the other two.

Surface finish has the weakest direct effect with about a one-half percent efficiency drop from the 2.4  $\mu$  m (95  $\mu$  inch) finish to the 0.1  $\mu$  m (4  $\mu$  inch) finish.

The turbulence fillet radius interaction indicates more than a 2 percent reduction in efficiency at 12 percent turbulence and 0.0 mm fillet radius compared with all the lower turbulence level cases.

Generally, second order interactions are rare. The relatively strong effect of turbulence, fillet radius, and surface finish must be questioned, since the experiment was not completely randomized (i.e., surface finish was progressively roughened during the experiment) and other sources of variation are possible such as minor variations in test conditions, etc.

Estimates of experimental error are:

1. Variance is 0.272 with 12 degrees of freedom and,
2. Standard deviation (standard error) of individual efficiency readings is 0.52 percent. This level of standard deviation indicates that individual efficiency measurements are within 0.52 percent of the average-measured efficiency for approximately 67 percent of the data points, assuming a standard distribution of the data scatter.

## 6.0 CONCLUSIONS

The matrix design of the test program provided a high degree of confidence in the direct effects of test variables and identified interaction effects. Multiple test results are averaged to establish the performance effects that tend to minimize random testing scatter which, otherwise, might be interpreted as a real effect.

The direct effects of the four test variables and pressure ratios are summarized below.

Free-Stream Turbulence -	Efficiency was reduced by 1.5 percent as free-stream turbulence levels increased from 2 to 12 percent.
Fillet Radius -	Square corners reduced cascade efficiency by about 1.4 percent compared with the 0.5 mm (.020 inch) fillet tested. A small performance loss resulted with the maximum 1.0 mm (.040 inch) fillet size.
Inlet Boundary Layer -	A small decrease in efficiency level was shown at 15 percent boundary layer thickness compared with 10 and 25 percent; however, with 2 percent boundary layer thickness, a gain of more than 1 percent was measured.
Surface Finish -	Surface finish showed the smallest effect over the tested range. Increased surface roughness improved cascade efficiency.
Pressure Ratio -	Consistent with full-scale testing, a trend of increasing efficiency with pressure ratio was measured.

Interaction effects of two or more variables produce results different from the sum of direct effects of individual variables. Significant variable interactions were:

Fillet Radius - Turbulence -	The performance penalty resulting from no fillet radius was found to be significantly greater at 12 percent turbulence than at 6 or 2 percent turbulence.
Fillet Radius - Surface Finish -	A smaller performance penalty resulting from zero fillet radius was found for the roughest surface finish tested. A progressive trend of reduced performance with reduced roughness was found.

The efficiency measured on the full-size stator, using exit surveys and the one-sixth scale stator using reaction torque measurements, showed the same efficiency level at design stator pressure ratio when the Soderberg empirical Reynolds number correction was applied to data obtained with similar inlet flow conditions and geometry. The correction was about 3 percent in efficiency.

A one-sixth scale stator referred mass flow and flow angle matched the full-scale referred mass flow and flow angle; this indicated that the scaled stator was an accurate scale model of the full-size stator.

The optimum tested configuration for the scaled stator used clean inlet conditions, i.e., 2 percent free-stream turbulence and 2 percent inlet boundary layer. The fillet radius was approximately 0.5 mm (.020 inch), and the surface finish was 2.4  $\mu$  m (95  $\mu$  inch).

## 7.0 RECOMMENDATIONS

The results obtained in this program showed the scaling effects on stator performance. These data should be used to establish key parameters when evaluating scaled turbine stators and to optimize stator design.

Based on published data, the effect of Reynolds number on performance level is significant. The test Reynolds number was relatively low compared with that expected in a gas turbine application. It is, therefore, recommended that a limited test program be conducted at a higher inlet pressure level to establish both the performance level change with Reynolds number and the performance sensitivity of the four test variables to Reynolds number.

The tested stator had a relatively high aspect-ratio design. Since most small gas turbines use lower aspect ratios, an investigation of scaling effects on such a design would produce more realistic data for the designer.

## 8.0 REFERENCES

1. Whitney, Warren J., Szanca, Edward M., Moffit, Thomas P., and Monroe, Daniel E., "Cold-Air Investigation of a Turbine for High-Temperature Engine Application", NASA TN D-3751, Jan 1967.
2. Prust Jr., Herman W., Schum, Harold J., and Behning, Frank P., "Cold Air Investigation of a Turbine for High-Temperature Engine Application". NASA TN D-4418, Feb 1968.
3. Debruge, L.L., "The Aerodynamic Significance of Fillet Geometry in Turbocompressor Blade Rows", ASME Paper Number 80-GT-41.
4. McNally, William D., "Fortran Program for Calculating Compressible Laminar and Turbulent Boundary Layers in Arbitrary Gradients", NASA TN D-5681, May 1970.
5. Schlichting, H., Boundary - Layer Theory, McGraw-Hill Book Company, New York, 1968, P621.
6. Horlock, J.H., Axial Flow Turbines, Robert E. Krieger Publishing Co., Huntington, New York, 1973, P102.
7. Due, H.F., Easterling, A.E., Rogo, C., "Cascade Research on a Small, Axial, High-Work, Cooled Turbine," ASME Paper No. 75-GT-62.
8. Dunham, J., "A Review of Cascade Data on Secondary Losses in Turbines", Journal of Mechanical Science, 1970, Vo. 12 - No. 1.
9. Booth, T.C., "An Analysis of the Turbine Endwall Boundary Layer and Aerodynamic Losses", ASME, Paper No. 75-GT-23.
10. Langston, L.S., "Crossflows in a Turbine Cascade Passage", ASME Paper Number 80-GT-5.



## APPENDIX

### LIST OF SYMBOLS

A	Annulus Area
$\dot{m}$	Mass Flow Rate
P	Pressure - Absolute
$\Delta P$	Differential Pressure
r	Radius
R	Gas Constant
T	Temperature - Absolute
V	Velocity
$\alpha$	Flow Angle Measured From Axial Direction
$\rho$	Density
$\tau$	Torque
$\eta$	Stator Efficiency

#### Subscripts

id	ideal
exit	Stator Exit
in	Stator Inlet
S	Static
T	Total
U	Tangential
X	Axial